

LIBRARY

NAVAL POSTGRADUATE SCHOOL
MONTEREY CALIFORNIA 93943

Special Report 84-22

August 1984



**US Army Corps
of Engineers**

Cold Regions Research &
Engineering Laboratory

Mine detection using non-sinusoidal radar

Part I: Spatial analysis of laboratory test data ADA 150 471

Arnold M. Dean, Jr. and Carl R. Martinson

20100824 263

Unclassified

SECURITY CLASSIFICATION OF THIS PAGE (When Data Entered)

REPORT DOCUMENTATION PAGE		READ INSTRUCTIONS BEFORE COMPLETING FORM								
1. REPORT NUMBER Special Report 84-22	2. GOVT ACCESSION NO.	3. RECIPIENT'S CATALOG NUMBER								
4. TITLE (and Subtitle) MINE DETECTION USING NON-SINUSOIDAL RADAR Part I: Spatial Analysis of Laboratory Test Data		5. TYPE OF REPORT & PERIOD COVERED								
		6. PERFORMING ORG. REPORT NUMBER								
7. AUTHOR(s) Arnold M. Dean, Jr. and Carl R. Martinson		8. CONTRACT OR GRANT NUMBER(s)								
9. PERFORMING ORGANIZATION NAME AND ADDRESS U.S. Army Cold Regions Research and Engineering Laboratory Hanover, New Hampshire 03755		10. PROGRAM ELEMENT, PROJECT, TASK AREA & WORK UNIT NUMBERS DA Project 4A161101A91D								
11. CONTROLLING OFFICE NAME AND ADDRESS U.S. Army Cold Regions Research and Engineering Laboratory Hanover, New Hampshire 03755		12. REPORT DATE August 1984								
14. MONITORING AGENCY NAME & ADDRESS (if different from Controlling Office)		13. NUMBER OF PAGES 101								
		15. SECURITY CLASS. (of this report) Unclassified								
15a. DECLASSIFICATION/DOWNGRADING SCHEDULE										
16. DISTRIBUTION STATEMENT (of this Report) Approved for public release; distribution is unlimited.										
17. DISTRIBUTION STATEMENT (of the abstract entered in Block 20, if different from Report)										
18. SUPPLEMENTARY NOTES										
19. KEY WORDS (Continue on reverse side if necessary and identify by block number)										
<table border="0"> <tr> <td>Mines (ordnance)</td> <td>Mine detectors</td> </tr> <tr> <td>Land mines</td> <td>Radar</td> </tr> <tr> <td>Mine countermeasure</td> <td>Radar cross sections</td> </tr> <tr> <td>Mine detection</td> <td>Radar images</td> </tr> </table>			Mines (ordnance)	Mine detectors	Land mines	Radar	Mine countermeasure	Radar cross sections	Mine detection	Radar images
Mines (ordnance)	Mine detectors									
Land mines	Radar									
Mine countermeasure	Radar cross sections									
Mine detection	Radar images									
20. ABSTRACT (Continue on reverse side if necessary and identify by block number)										
<p>The interaction among UHF radiation, winter roadway conditions and buried mines was investigated in a refrigerated facility. The near-field spatial return from each target was unique. When the target was not in the near field the spatial return was not at all unique. Cobbles in the medium had little effect, but surface-thawed conditions significantly affected the spatial return, and the reflected signal strength and frequency content. The primary frequency content of the returned signal was either spread over a band broader than that of the transmitted primary frequencies, or completely outside of the primary detection</p>										

DD FORM 1 JAN 73 1473

EDITION OF 1 NOV 65 IS OBSOLETE

Unclassified

SECURITY CLASSIFICATION OF THIS PAGE (When Data Entered)

20. Abstract (cont'd)

band. We conclude that the complexity of winter roadway conditions requires 1) a much broader frequency band than is currently being considered, and 2) a more complex and adaptive background-removal, signal-enhancement scheme than is currently used. Further, more data are required describing the interaction of the winter media, UHF radiation, and buried mines so that adequate detection instrumentation can be developed.

PREFACE

This report was prepared by Arnold M. Dean, Jr., Electronics Engineer, and Carl R. Martinson, Civil Engineering Technician, Ice Engineering Research Branch, Experimental Engineering Division, U.S. Army Cold Regions Research and Engineering Laboratory. The work was funded under DA Project 4A161101 A91D, In-House Laboratory Independent Research, Broadband Impulse Radar.

The authors acknowledge with appreciation the technical reviews and suggestions by Steven Arcone and Stephen DenHartog, the construction of the testing box by Calvin Ackerman and Charles Schelewa, the drafting and illustrations by Edward Perkins and Matthew Pacillo, the word processing by Donna Harp, the layout and annotation of radar data by Renee Melendy and Mr. DenHartog, the physical soil characterization by David Carbee, and the photo processing by Robert Demars.

CONTENTS

	Page
Abstract.....	1
Preface.....	iii
Introduction.....	1
Objectives.....	2
Test set-up and procedures.....	2
Results and discussion.....	12
Penetration.....	16
Standoff.....	17
Data processing.....	18
Return pattern.....	20
Non-mine returns.....	20
Frequency content.....	21
Hand-held (portable) detectors.....	25
Conclusions.....	27
Phase reversal.....	28
Unique returns.....	28
Surface return replica.....	28
Early (distant) detection.....	28
Future work.....	29
Literature cited.....	30
Appendix A: Radar scans - non-portable equipment.....	31
Appendix B: Radar scans - portable equipment.....	85
Appendix C: Temperatures in the medium measured by thermocouples.....	91
Appendix D: Frost depth in the medium measured by frost tubes	97

ILLUSTRATIONS

Figure	
1. Test box.....	3
2. Location of items in the test box.....	3
3. Grain size analysis of the silty sand used in the laboratory tests.....	4
4. Orientation of WAX mine for tests.....	5
5. Orientation of RAAM mine for tests.....	5
6. Orientation of ADAM mine for tests in sand without cobbles.....	6
7. Test box covered with plastic and string grid lines....	6
8. Location of stones in the box.....	7
9. Location of stones in the box with RAAM mine in the center.....	8
10. Orientation of ADAM mine for tests in silty sand with cobbles.....	8
11. Range of room air temperature during the test period	9
12. Water content profile of silty sand.....	10
13. Wetting the sand prior to testing.....	10

Figure	Page
14. Temperature of glycol in open containers placed in various areas on the surface of the testing box to evaluate surface cooling.....	11
15. Radar returns.....	12
16. Frequency characteristics of selected background removal programs implemented by the control unit processor.....	18
17. Comparison of wavelet primary frequency range with antenna location and medium condition.....	25
18. Model 3100 antenna being pulled across the test box at a fixed height above the surface.....	26
19. Model 3100 antenna.....	27

MINE DETECTION USING NON-SINUSOIDAL RADAR
Part I: Spatial Analysis of Laboratory Test Data

Arnold M. Dean, Jr. and Carl R. Martinson

INTRODUCTION

Recently questions have been raised about the effectiveness of UHF (ultra high frequency - 300 to 3000 MHz) radar for the detection of mines buried in a complex medium representative of realistic field conditions. To contribute to a better understanding of the interaction among the radar returns, buried mines, and specific elements of the medium, a mine detection project was initiated at CRREL.

Laboratory and field tests were conducted under various conditions to generate a data base for the investigation. This report documents the laboratory tests and is primarily concerned with the spatial (i.e. the physical "hard-copy" picture) variability of the radar returns, although a limited frequency characterization is given. A second report is planned that will cover frequency domain analysis of the radar returns from the laboratory tests (see Future Work). Field tests, covering mines in snow over frozen ground and addressing the problem of mine detection in a stand-off mode, will be subject to similar analysis in a third report.

There is no intent to compare specific equipment. The radar system used provided broadband signal transmission, reception, and manipulation capabilities, and an adequate flexibility for our research needs. For future frequency analysis the subsurface returns will be normalized by comparison of signal frequency and amplitude with the complete return from a reflector on the surface. This will allow development of a direct relationship between medium characteristics and frequency, and of target signatures in the frequency domain.

The components of this impulse radar system, its characteristics, and some non-military applications have been described by Dean (1981).

Appendix A contains representative annotated radar scans made with standard survey equipment, and Appendix B contains similar scans made with a

small, higher-frequency antenna, which represents a more portable mine detection system. Although it is recognized that the inclusion of so many radar scans imposes some inconvenience upon the reader going through the Results and Discussion section, we feel that documentation of the extensive medium conditions and radar returns is essential for this data-base report. Each medium condition could in itself be the subject of extensive analysis, and, when the data are normalized, may be compared with similar conditions and completely different equipment.

OBJECTIVES

The general objective of the overall project is to investigate the effect of a winter environment on broadband UHF radar mine detection.

The specific objectives of the present work are:

1. To simulate and document typical winter roadway conditions.
2. To record the UHF signature of typical mines in the spatial domain under these conditions for use as a data base for future work.
3. To record the effect of these conditions on the attenuation and propagation of UHF radar waves.
4. To record the effect of antenna height on the UHF radar waves.
5. To record the radar returns from typical false targets such as rocks.
6. To perform existing background removal and signal enhancement routines on the data to evaluate their applicability.

TEST SET-UP AND PROCEDURES

The experiments were conducted at the CRREL Ice Engineering Facility in a coldroom about 3.2 m wide by 4.9 m long and 5.5 m high.

A plywood box 3.7 m long by 2.0 m wide by 1.2 m high, insulated on the sides with 15.2 cm of Styrofoam, was built inside the coldroom. The concrete coldroom floor, which is insulated underneath with 12.7 cm of Styrofoam, served as the floor of the box.

Figures 1 and 2 show the box in the test configuration. To aid radar signal strength analysis, three 30.5- x 30.5-cm x 1.6-mm aluminum plates were placed on the floor at 0.9-m intervals along the centerline of the long axis of the box. Screened silty sand, physically characterized in Figure 3, was then added and compacted at about 15-cm depth intervals. Six 22.9-cm-dia-

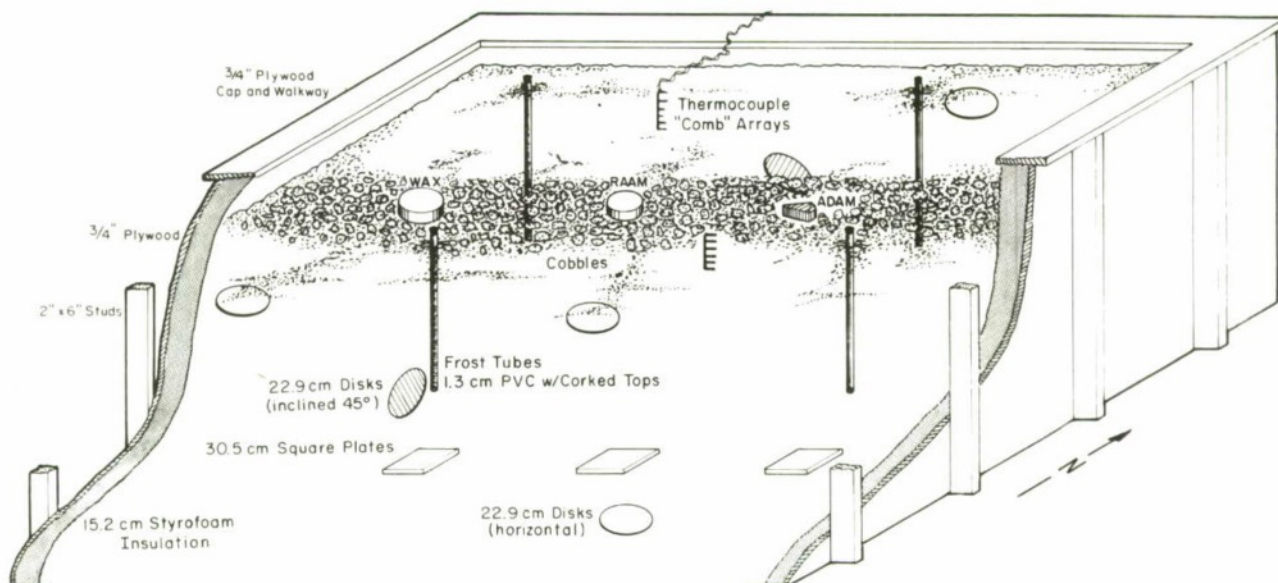


Figure 1. Test box (see also Fig. 2). Along the south line (foreground) circular metal disks were placed at (l. to r.) 0.3-, 0.6- and 0.9-m depths. Along the center line WAX, RAAM and ADAM mines were buried in a typical manner. Along the north line circular metal disks were placed at (l. to r.) 0.9-, 0.6- and 0.3-m depths. Frost depth and thaw layers were monitored by frost tubes and thermocouple arrays.

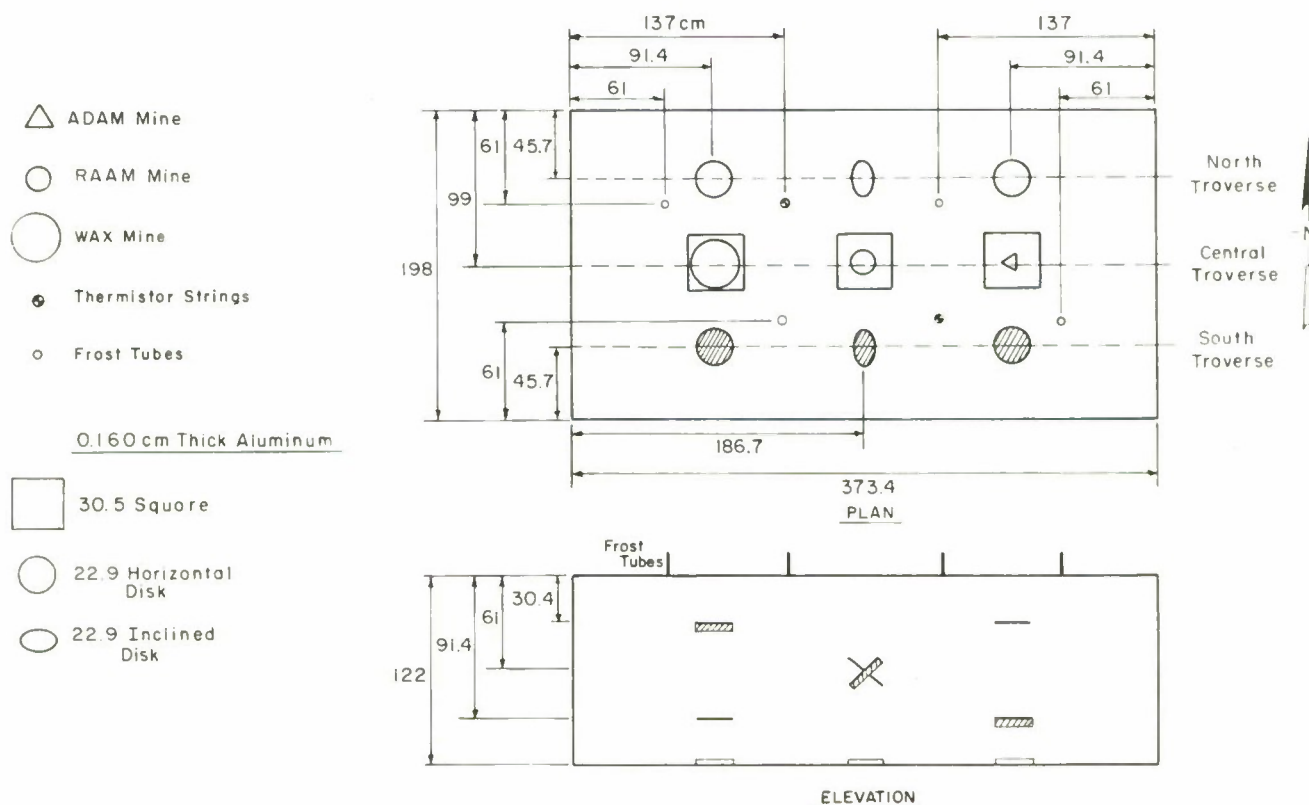


Figure 2. Location of items in the test box.

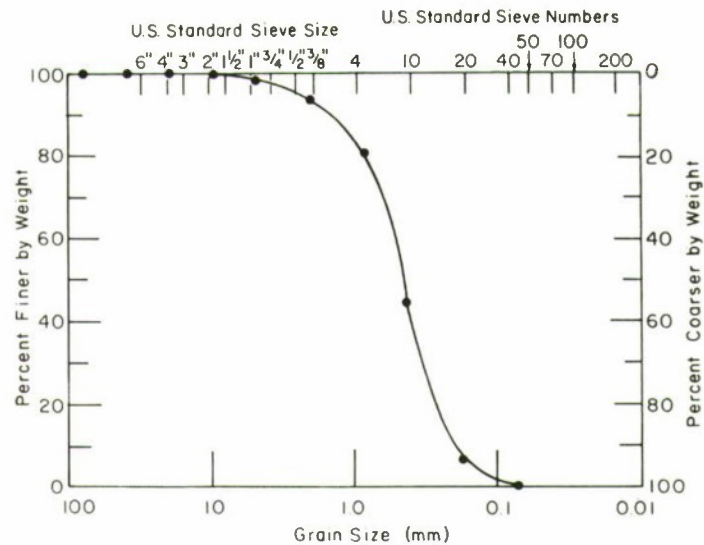


Figure 3. Grain size analysis of the silty sand used in the laboratory tests.

ter by 1.6-mm-thick aluminum disks were placed 46 cm from the edges of the long walls, spaced 0.9 m apart. The disks buried 0.3 m and 0.9 m were horizontal; the disks buried 0.6 m were tilted 45°.

After the sand was in place two strings of six calibrated thermocouples each were positioned in it to determine frost depth. The top thermocouple of each string was positioned just below the surface and the others were at 2-1/2-cm intervals down to a depth of 12-1/2 cm. Four frost tubes measured frost down to 0.58 m. Appendixes C and D contain the data collected from the thermocouples and frost tubes.

Three different types of inert mines (Fig. 4-6) were then placed in the box, following procedures described in U.S. Army Field Manual 20-32, Mine/Countermine Operations at the Company Level. They were buried 1.3 to 2.5 cm below the surface and spaced 0.9 m apart along the centerline of the long axis of the box. The first two mines were cylindrical. One, made of wax, was 27.9 cm in diameter and 15.2 cm thick. The second (RAAM), made of steel, was 12.7 cm in diameter and 70 cm thick. The third (ADAM) was wedge-shaped and was 6.4 cm high and 5.7 cm in radius; it subtended an arc of slightly over 10 cm. After the mines were buried the box was covered with a plastic sheet to prevent moisture from evaporating. String was used to form a grid on top of the plastic to mark the positions of the buried mines and metal plates (Fig. 7).

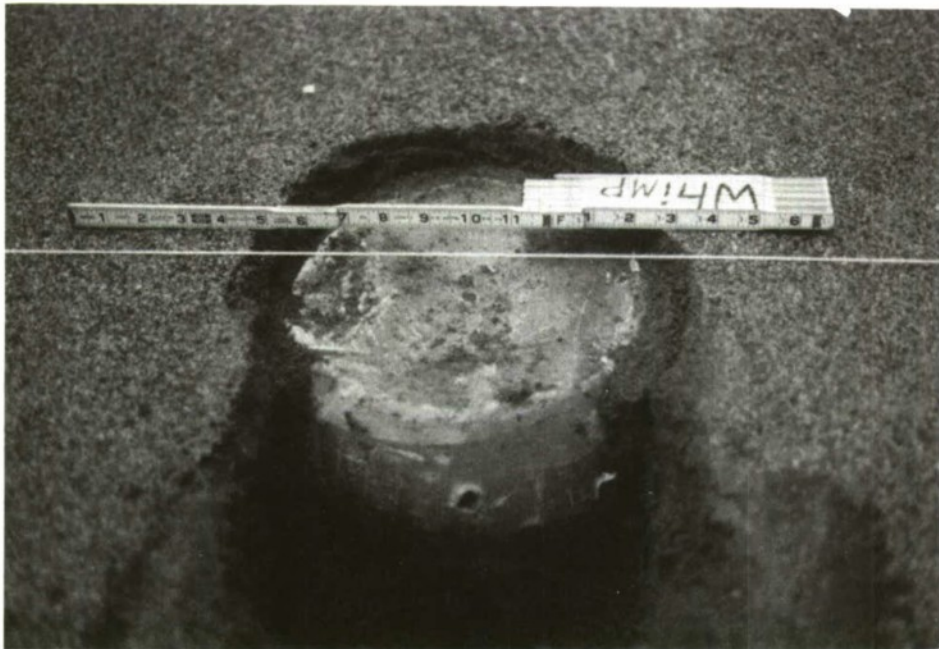


Figure 4. Orientation of WAX mine for tests.

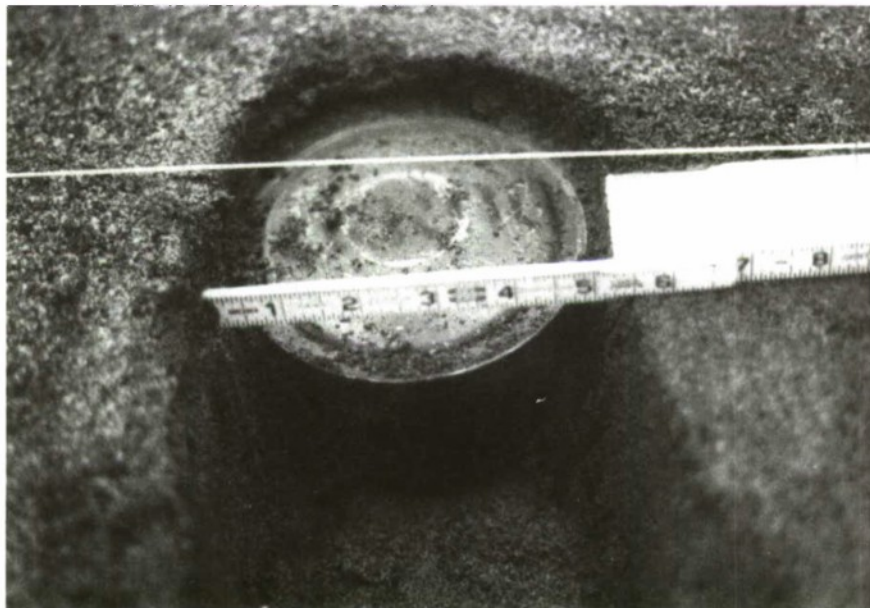


Figure 5. Orientation of RAAM mine for tests.

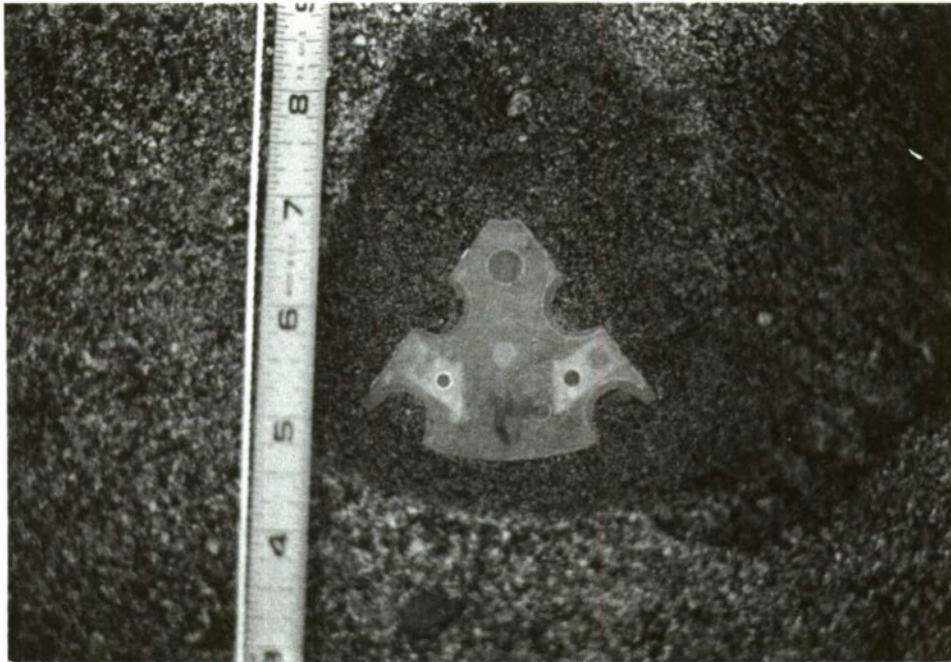


Figure 6. Orientation of ADAM mine for tests in sand without cobbles.

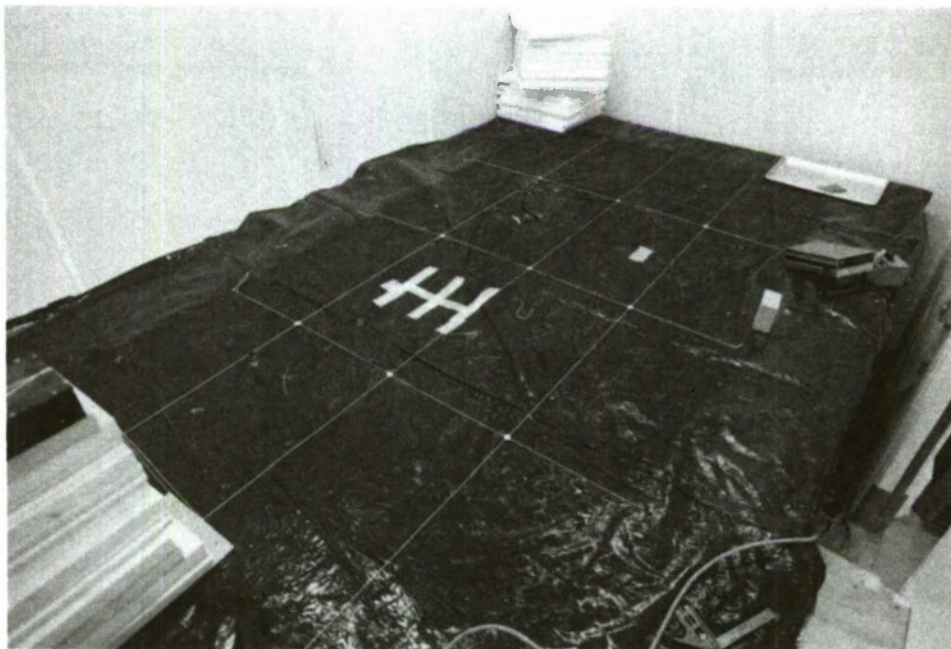


Figure 7. Test box covered with plastic and string grid lines. Mines are beneath the long centerline. Metal plates are beneath the lines on both sides of the centerline.

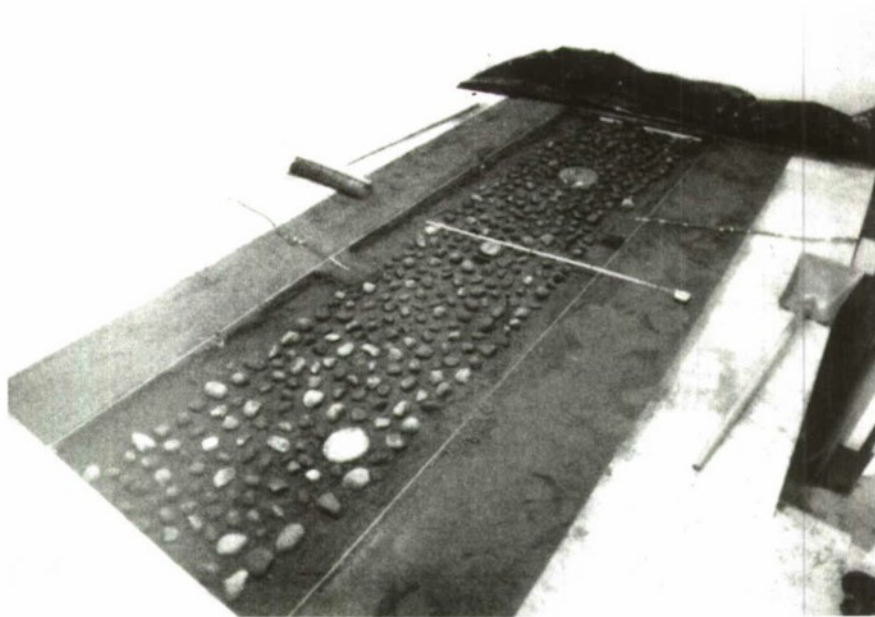


Figure 8. Location of stones in the box. The large rock in the foreground was used as a target for some tests.

After the first set of measurements was made, about 5 cm of sand was removed from the surface along a strip running the entire length of the box and 38 cm to each side of the centerline. Stones ranging from about 4 to 7-1/2 cm in diameter were laid in this section (Fig. 8 and 9). One larger stone about 15 cm in diameter by 7-1/2 cm thick was also positioned off to one side (Fig. 8). The sand was then replaced. The two larger mines were left as they had been but the ADAM mine was reoriented 90° to its previous position at the same location (cf. Fig. 6 and 10).

The room cooling unit, a Krack HG-1610 NH₃ top-feed model located at the ceiling at the west end of the room, can cool the room to -23.3°C. The unit is part of a system used to cool all the coldrooms in the facility.

Air temperature was measured with a mercury thermometer mounted at the midpoint of the south wall, approximately 15 cm above the surface of the sand. The temperature ranges for the test dates are plotted in Figure 11. (The test date of each profile in Appendixes A and B is given in the data block at the lower right of the profile.)

The depth of frozen sand (Appendixes C and D) was determined from the thermocouples (down to 12-1/2 cm) and frost tubes (down to 0.58 m). Thermocouple readings of 0°C or below indicated frost. The frost tubes were made of 0.6-cm vinyl tubing filled with a solution of methylene blue indicator dye



Figure 9. Location of stones in the box with RAAM mine in the center.

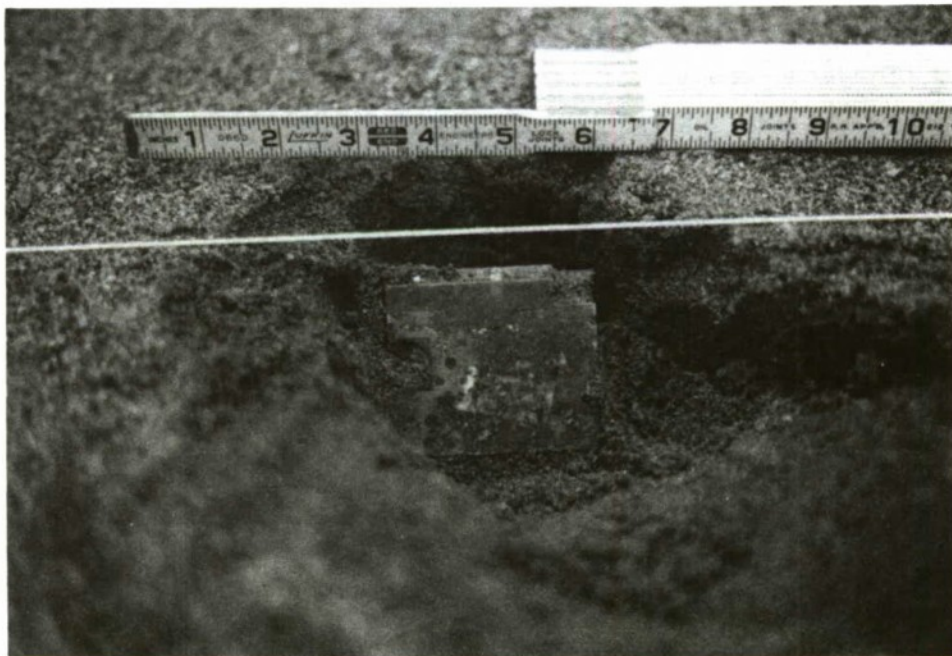


Figure 10. Orientation of ADAM mine for tests in silty sand with cobbles. Note that the narrow edge on top in Figure 6 is now pointing up.

and water. The vinyl tube was inserted into a 1.3-cm PVC (polyvinyl chloride) tube and buried in the sand, leaving about 15 cm of PVC above the surface. As the frost depth increased, the water in the solution froze and expelled the dye. The frost depth was then determined by removing the vinyl tube and measuring the length of the clear ice in the tube from a reference point on the tube. A more detailed discussion of frost tube performance can be found in Ricard et al. (1976).

A sharpened wooden dowel was used twice during thaw cycles to check the thaw depth. The 3-mm-diameter dowel was pushed into the sand until it hit material frozen solid enough to prevent further penetration. The dowel passed through unfrozen and semifrozen layers before reaching the completely frozen material. Because of this, the dowel could not be used to determine the precise frost or thaw depth, but it did confirm the existence of frozen sand where the frost tubes and thermocouples indicated freezing.

The density and water content of the sand in the box were measured on 8 and 16 September (Fig. 12) with a sand cone density apparatus (equipment and procedures described in U.S. Army TM 5-530). This method consists of digging a small hole approximately 15 cm deep and measuring its volume by filling it with a measured quantity of a known material, such as sand. The soil moisture content and density are then determined in the conventional way. The specific gravity of the two samples measured 2.72 and 2.71. For most of the tests the water content in the medium was maintained as shown in the profile for 8 September. For short periods of testing, the top of the frozen medium was wetted (Fig. 13) and the water content increased to the values indicated in the profile for 16 September. When the frozen layer beneath the thawed surface was thawed, the water drained down and the water content again approximated the 8 September profile.

The electrical resistivity of the sand was measured with a Bison Instruments Inc. Model 2350 earth resistivity meter, using the four-probe method.

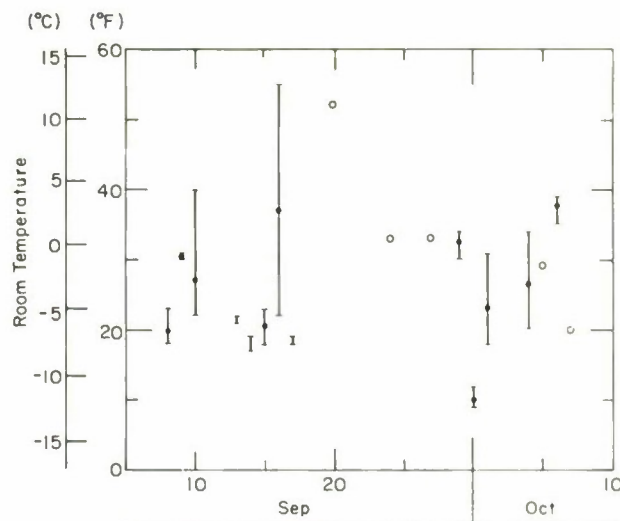


Figure 11. Range of room air temperature during the test period.

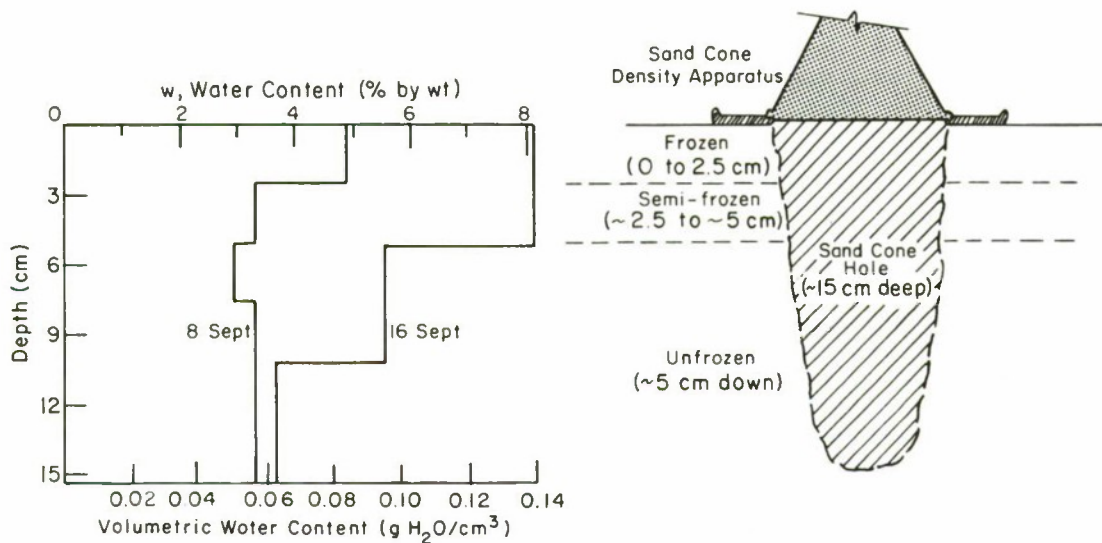


Figure 12. Water content profile of silty sand.



Figure 13. Wetting the sand prior to testing.

The 3.2-mm-diameter probes were inserted about 10 cm into the sand 30 cm apart. This configuration provided a bulk resistivity measurement to a depth of about 20 cm. The unfrozen sand resistivity varied between 1300 and 1700 ohm-meters, and seemed to be unrelated to the length of the wetting period. These readings indicate a relatively clean sand with nearly maximum water adhesion to the particles, and unfilled pore spaces.

During testing it became apparent that the east end of the coldroom was cooling more rapidly than the west end. This discovery was made by inspection of the frost gauges and confirmed by a check of surface temperatures in

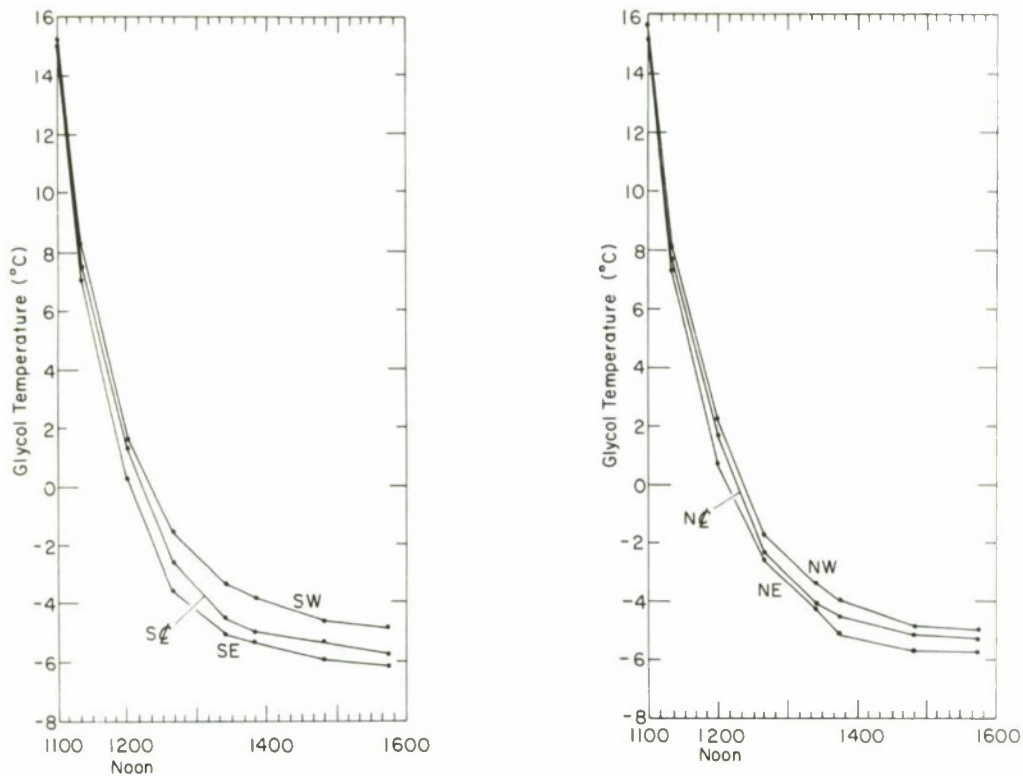


Figure 14. Temperature of glycol in open containers placed in various areas on the surface of the testing box to evaluate surface cooling.

the box at the end of the test period. Analysis of the thermocouple temperatures taken during the test period also showed that frost depths were significantly greater at the east end. To confirm the surface temperatures six open containers of glycol were placed at different points on the sand. The temperature of the glycol was measured before it was brought into the cold-room and was remeasured periodically during a cooling cycle. The cooling pattern was consistent (Fig. 14): the east end was cooling about 1 to 1.5°C more than the west end.

The most likely cause for the differential cooling was the pattern of air circulation in the room. However, exposed valves on pipes leading from the cooling unit may also have had an effect on frost depth in the northwest corner. During defrost cycles they dripped water onto the plastic cover, possibly adding enough heat to retard local frost penetration.

The graphic recorder used with the impulse radar to generate a hard copy facsimile of the radar returns has been used for many years in both sonar and radar work. The radar system transmits energy from the antenna and then waits for a return during a selected time window. In Figure 15 the return on

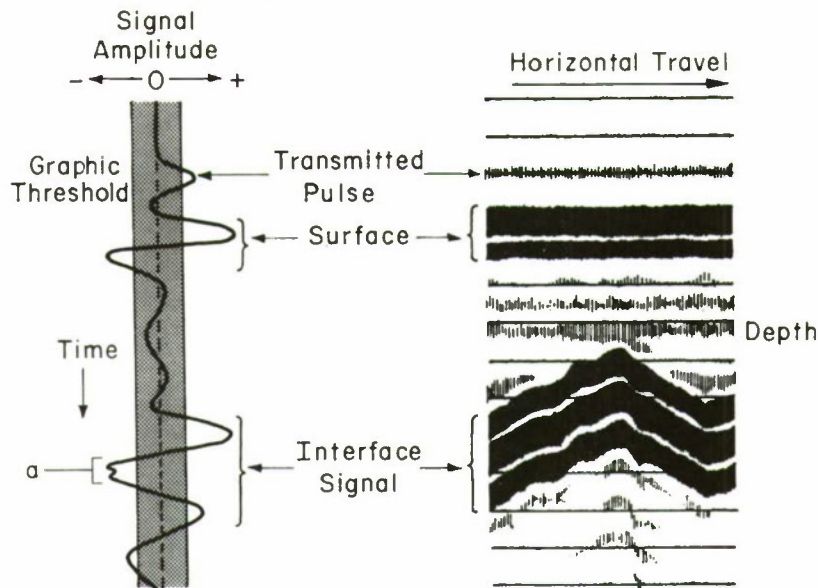


Figure 15. Radar returns. The waveforms of many single returns (left) are combined to make a composite graphic display (right). Small variations in the waveform, such as is indicated at "a," cannot be reproduced well on the composite.

the left represents one vertical line in the graphic facsimile on the right. Depending on the setting of the graphic recorder, such a facsimile may represent 50-200 signal transmissions per inch of graph paper. For each recorded return the graphic performs a threshold function. This function is labeled the graphic threshold, and is indicated by a darkened area about the center-line. The setting of the threshold will obviously affect the representation of the data on the hard copy and may mask certain characteristics of the data, as indicated in the area marked "a" in Figure 15. Although the graphic printer has the capability of differentiating very strong signal excursions and very weak signal excursions, such a small variation in the printed portion of the waveform may not be obvious to the eye. For this reason, various important characteristics of a target return may not be identified. Those characteristics masked by the function of the graphic recorder in the spatial (time) domain may become more obvious in the frequency domain.

RESULTS AND DISCUSSION

When the antenna is operated in the near-field, the medium and any shallow subsurface objects electrically become a part of it. This gives rise to a

diverse spectrum in the target return. When the target is in the far-field of the antenna, a more consistent spectrum is observed.

When the antenna is on the surface and operation is in the near-field:

1. The transmitted frequency and the frequency band containing most of the returned energy are lower than those frequencies generated as the antenna is moved away (up) from the surface.

2. The frost/thaw state of the medium significantly affects the primary energy band, the frequency dispersion, and the strength of the return signal.

When the antenna is above the surface and the operation is in or approaching the far-field:

1. The total energy of the return from a subsurface anomaly is reduced from that available in near-field operation.

2. The frequency content of the return is more restricted than in near-field operation.

3. The transmitted frequency and the frequency band containing most of the return energy (these are not necessarily the same) are higher than those in near-field operation.

Consider how a variation in the electromagnetic characteristics and in the dimensions of a layered medium affect the reflected signal. For simplicity we present two layers. The character of a return from an interface between layers 1 and 2 may be seen in its reflection coefficient, r_2 :

$$r_2 = \frac{z_1 - z_2}{z_1 + z_2} = \frac{\sqrt{\epsilon_1} - \sqrt{\epsilon_2}}{\sqrt{\epsilon_1} + \sqrt{\epsilon_2}} \quad (1)$$

where z_1 and z_2 are complex characteristic impedances of the medium, and ϵ_1 and ϵ_2 are complex dielectric permittivity of each medium. Now ϵ_1 is usually expressed as

$$\epsilon_1 = k_1^* \epsilon_0 \quad (2)$$

where

$k_1^* =$ the complex relative dielectric constant

$\epsilon_0 =$ the dielectric permittivity of free space.

Now,

$$k_1^* = k_1' - jk_1'' \quad (3)$$

where

$k_1' =$ the real, in-phase component

$k_1'' =$ the imaginary, or quadrature phase component.

A frequency-dependent conductivity (σ_1) term adds to the imaginary part, giving

$$\begin{aligned} k_1^* &= k_1' - jk_1'' - j \frac{\sigma_1}{\omega \epsilon_0} \\ &= k_1' - j(k_1'' + \frac{\sigma_1}{\omega \epsilon_0}) \end{aligned} \quad (4)$$

and from eq 2,

$$\epsilon_1 = k_1 \epsilon_0 - j(k_1'' \epsilon_0 + \frac{\sigma_1}{\omega}) \quad (5)$$

The important points here are that these (and, therefore, r_2) are complex variables, and that the travel time and returned signal magnitude and phase are a function of the relative magnitudes of these characteristic parameters. Going from a medium of lower complex dielectric permittivity to one of higher complex permittivity, the phase angle of the reflection will be in an entirely different quadrant of the complex plane than that phase angle obtained going from a medium of higher dielectric permittivity to one of lower permittivity (see eq 1).

Collie et al. (1948) show that the real part of the dielectric constant (eq 3) of liquid water remains reasonably constant at about 80 over the UHF band, and that $0 < k'' < 10$. In comparison, $k' = 3.1$, and k'' stays near zero for ice. Hence, the presence and phase (viz. liquid or frozen) of water in the medium will greatly affect the material conductivity and permittivity and, hence, the nature of the returned signal. Delaney and Arcone (1982) and Arcone et al. (1979) in such investigations have found an order of magnitude change in k' and k'' with a few degrees change about 0°C in sand, silt and clay. Further, reasonable changes in the volumetric water content of the unsaturated, unfrozen medium can at least triple the values of both k' and k'' .

The variation in the dimensions of these layers will also cause interferometric variations in the return signal. Such an effect has already been observed in the "ringing" return from the ADAM mine in the present work.

Other items, in a practical field situation, having a significant effect on the signal are the presence of free ions from road salt and traffic pollutants and non-uniform surface conditions such as water puddles or frozen-mud conditions where the antenna may change its near-field coupling with the medium. Along with the practical mobility aspect of a higher antenna position,

this latter item strengthens the need to pursue a standoff antenna configuration for mine detection.

We will now discuss and compare the radar graphic records in Appendixes A and B. These figures have varying dimensions, and the data have two different vertical (time) scales. The dimensional variation is due to photographic reduction of the figures and data collection speed. In some figures complete time scales (a time window of about 30 ns) are presented to show returns from below the bottom of the box (e.g. Fig. A1-A3). In other figures (e.g. Fig. A4-A8) a time window of about 18 ns is used so that the returns from the near-surface can be observed more closely. The impulse radar system can normally view up to 600 ns. Special component changes can increase this window to over 1 μ s.

The vertical dashed lines on most of the figures are positioning benchmarks which were manually recorded during the tests. Where their location is of importance in understanding the data, a comment is made at the upper end of the set of lines.

Each scan (radar data figure) may be considered to be a side view of the testing box in which, from left to right, one can view the return from the wax mine, the RAAM mine, and the ADAM mine. As the antenna moves from left to right, it moves away from one end of the box, over the three mines, and then on to the other end of the box. With the 30-ns time scale, the bottom of the box and some sub-bottom anomalies can be observed. In both time scales there are significant indicators of the mines over which the antenna is about to travel. In all profiles for which the antenna was directly on the surface of the medium there are unique visual characteristics associated with the returns from each type of mine. Since an effort was made to ensure that the physical characteristics of the medium were consistent throughout the box, these characteristics are apparently associated with the geometry and material of the mines, as opposed to their placement in the box or the material around them. Particularly interesting is the return from the ADAM mine. Although the ADAM is not designed for burial, it was used to determine the capability of the impulse radar to detect its material, shape and size. This mine consistently generates very strong bands, or a "ringing" return. This may be due to some dimensional characteristics of a portion of the mine, i.e. some dimension of the mine may be exciting one of the natural frequencies that is transmitted by the impulse radar.

On most scans the comment "antenna sees side of box" can be observed. This can be better understood if one considers the so-called "footprint," or surface area radiated by the antenna. The footprint is hardly wider than the diameter of the antenna. But in the longitudinal direction (the direction of travel) the footprint may spread out at about a 10° - 25° angle, and thus at depth it may extend several feet beyond the antenna. When the 30-ns time scale is being used, the ends of the box can be observed even when the antenna is at the center of the box.

The antennas were positioned in two different ways: directly in contact with the surface and 15 to 60 cm above the surface. When the antenna is on the surface, the medium and whatever targets or anomalies are within it become electrically a part of the antenna. This increases the sensitivity of the system and makes characterization of each return very straightforward. When the antenna is above the surface of the medium, the characteristics of the return change dramatically. The medium and anomalies within it are no longer electrically a part of the antenna. There is less energy per unit area impinging upon the medium. Mines can still be detected but the results must be further evaluated to determine the practical standoff capability of the impulse radar.

The radar scans in Appendixes A and B were selected from a total of 150 scans. They illustrate seven categories of investigation:

1. Penetration into the medium
2. Antenna standoff above the surface
3. Data processing, i.e. selective background removal and waveform phase (polarity) display
4. Return pattern uniqueness and characteristics
5. Non-mine returns, namely those from cobbles and a mine-size rock
6. Frequency content of the returns
7. Portable operation with a higher-frequency, lightweight antenna

Penetration

Figures A1-A3 demonstrate the first category of investigation. These are scans made along two planes running through the sheet metal targets buried 30, 60 and 90 cm below the surface. The orientation of the targets is indicated on the cross sections. In Figure A1, the center target is tilted toward the left, or the start of the scan. In Figure A2, the center target is tilted away from the start of scan. With proper experience or an interpret-

ing algorithm, the orientation of a target may be determined. These scans indicate that with antennas located on the surface, penetration can be attained to at least 1.2 m in this kind of material. Figure A3, for which the antenna was located 15 cm above the surface, shows deeper penetration. The scans penetrated the bottom of the box, and some sub-bottom anomalies show strong returns.

All three of these scans are raw data. They illustrate the present capabilities of a non-sinusoidal, commercially available system for detection to these depths.

Standoff

This section, comprising Figures A4-A15, covers mine detection in the test facility under freeze/thaw conditions and wetted conditions, and with and without cobbles. Note the more restricted time (vertical) scale. Figures A4-A6 are scans made over the mines in an unfrozen and cobbled medium with the antenna 20 to 60 cm above the surface. There are unique returns from each mine, even though the cobbles were placed at the same depth as the mines.

Figure A7 was taken with the antenna 15 cm off the surface. This antenna had a center frequency lower than that used in most of the tests (see Frequency Content section). The merging of the transmit wavelet with the surface return brought about by the antenna's position and the lower center frequency have not obscured the three target anomalies. Likewise, for Figure A8, the same lower-frequency antenna was used and the target anomalies can still be detected.

Figures A9-A13 illustrate an attempt to simulate conditions where the ground has frozen and then has begun to thaw from the surface downward. The thawing was induced by wetting the surface (Fig. 13). Through this range of conditions target anomalies can still be observed.

Figures A14 and A15 illustrate the utility of an averaging technique implemented with a microprocessor. Figure A14 shows a raw-data profile with the antenna in a standoff condition in an uncobbled silty sand with some surface frost. Target anomalies are indicated as in the previous scans. In Figure A15 a waveform averaging program has removed some of the background noise from the data of Figure A14, making the anomalies much more obvious. If a target return appears to be visually unique, an algorithm can be implemented to detect it.

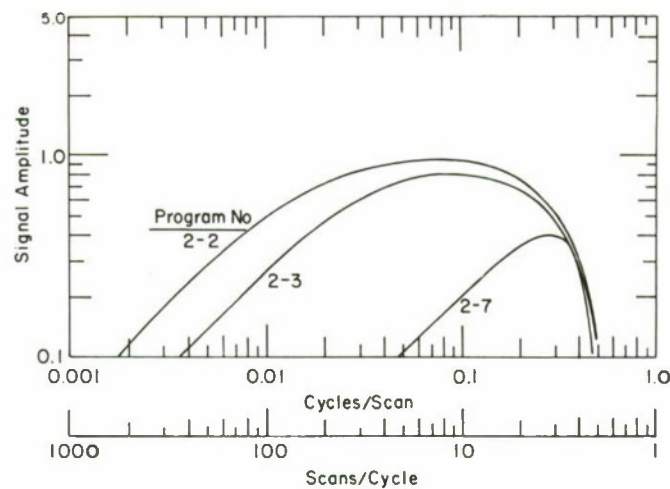


Figure 16. Frequency characteristics of selected background removal programs implemented by the control unit processor.

Data processing

Figure 16 shows the frequency characteristics of the background removal programs mentioned above. The term "frequency" refers to the characteristics among consecutive scans, as opposed to those which are a function of real time. The programs effect no amplification, as seen in the scale of the ordinate. The abscissa ranges from 0.001 to 1 cycle per scan, or 1000 to 1 scans per cycle (the inverse). A "scan" in this case is comparable to a "sample," or a transmit-receive pair. The programs work on a scan-to-scan frequency base, as opposed to the more conventional signal frequency associated with the wavelets in an individual return, such as is seen on the left of Figure 15.

For example, compare digital filter program 2-2 with program 2-7. If there is a target anomaly whose return varies such that 100 scans of the radar see it at about the same point in vertical time (i.e. within one cycle), then program 2-2 will reproduce this return with an attenuation of 0.5. Program 2-7 will not reproduce such a target return. If a return from a target is seen for about 10 scans, program 2-7 will pass it at a 0.2 amplification, and program 2-2 will pass it at about a 0.9 amplification.

From another point of view, program 2-7 has a faster response than program 2-2. Hence, it is representative of a higher pass "frequency" filter.

Figures A16-A28 illustrate a range of frost and thaw conditions and various processing techniques used to enhance the data. In Figure A16 unique return patterns are associated with each of the mine targets, and similar

patterns (which will be called surface return replicas) are repeated far below the surface at each mine location. These may be investigated in the future to enhance target detection.

In several of the processed data scans the terms "positive phase" or "negative phase" appear. These refer to the side of the signal that is being printed by the hard-copy recording device, the graphic. On the left-hand side of Figure 15, where signal amplitude is indicated, a graphic positive phase would depict only that portion of the signal above the graphic threshold and to the right of the centerline of the waveform indicated. Likewise, negative phase would print only that portion of the signal above the graphic threshold and to the left of the centerline of the waveform indicated. Figures A17 and A18 (a positive phase and a negative phase) compare the target return phase with the initially transmitted wavelet phase. There is a consistent phase reversal between the transmitted wavelet and the first return from the metal mine (RAAM). In these figures (and in others) unique patterns can be noted in the returns from the three different mines.

Figures A16-A18 were taken with a shallow surface frost, and Figures A19 and A20 with much deeper frost. The returns from the same mine under both conditions are similar, and, after processing, the returns from the three different mines in Figure A20 are unique. In Figures A16 and A19 there is significant "ringing" (multiple banding) from the ADAM mine in comparison with the returns from the other two mines. This is also observed with deeper frost in Figures A21 and A22, taken in a clean silty sand and a cobbled silty sand, respectively. The background removal process illustrated in Figure A21 enhances the returns from all three of the mines, making the ADAM mine more obvious and the wax mine detectable (in comparison to its not being detectable in Figure A22). This illustrates the sensitivity of target identification to the selection of the processing algorithm. The standoff capability of the system is also illustrated with a 0.3-m elevated antenna position in these figures.

With even deeper frost, Figures A23-A25 illustrate the system detection capabilities, phase comparison, the processing algorithms, and the consistent similarity in pattern associated with each of the three mines.

Figures A26-A28 document the radar response during a rapid surface thaw period over a deep frost with cobbles. Background removal programs significantly enhance the data in Figures A27 and A28. The capability of early detection may be a significant and exploitable characteristic. It is illus-

trated by the long trails of the returns from the RAAM and ADAM mines in Figure A26 and from all three mines, whose returns are enhanced by the program, in Figure A28. The returns are detectable and visually unique with respect to one another.

Return pattern

There appears to be a consistent pattern associated with each of the three mines, which were chosen for their differences. Figures A29-A41 include scans made after freezing periods, surface thawing, and surface wetting in a silty sand with and without cobbles. Figures A29, A30, A32 and A33 were made during progressive frost penetration, while Figures A31 and A34 were made with a surface thaw layer over frost. In each of these cases the return from each type of mine is unique. In Figure A29 the surface return replica is again observed. Figure A35 was taken after intense wetting of the surface, as illustrated by the soil cross section. The frost extended down to 35 cm. Even with these conditions the visual uniqueness of the returns from each mine is observed. Figure A36 was taken immediately after a thorough wetting of an unfrozen medium. Early detection trails from the three mines are quite obvious.

Figures A37-A41 represent a sequence of freezing followed by surface thawing. Layer returns can be observed below the return from each of the mines. Each mine has a unique return characteristic and is detectable within the band of frequencies associated with the antennas used in Figures A38-A41.

Non-mine returns

A large fine-grained granitic rock about the size of the RAAM mine was placed in the test facility and scans were taken in conjunction with the mine scans. In the laboratory the rock was determined to hold a maximum of 1% water by weight.

Figures A42-A45 illustrate the various returns from the rock under freezing and thawing conditions, with the antenna on the surface as well as in a standoff position. A definite pattern anomaly is associated with the rock. This anomaly is not as nearly unique as that associated with a surface return over the mines. These data will enable a later frequency evaluation of the returns associated with the rock and the various mines that were used.

Figures A46 and A47 were made with the antenna in a standoff mode 30 cm above the surface and in a deeply frozen medium. In Figure A46 there is an unfrozen layer with cobbles, and in Figure A47 the medium is completely fro-

zen with cobbles. A visually detectable return from the rock is questionable using the conventional graphic record. Under these conditions the mines can still be detected. Using frequency domain analysis, the rock may be more detectable and the difference in response between rock and mine more obvious. This will be the subject of later analysis.

In Figures A48-A50 a return from a rock under deep frost conditions is illustrated. Figure A50 is processed data (see Fig. 16 for program characteristics). The return from the rock can probably not be discriminated on the basis of signal intensity from the return from a mine. At present, signal intensity, or threshold detection, is used to determine the existence of a target. Current background removal algorithms, one of which is used for Figure A50, are not acceptable discriminators. This problem will be pursued with frequency-domain analysis. The phase of the return from the rock in Figure A49 is different from the return phase from a metallic mine. This gives a starting point in discriminating between metallic mines and rocks which, heretofore, have been false targets under such detection schemes.

Figures A51-A53 illustrate the returns from the rock under deep frost conditions where a strong surface reflection exists. There is an anomaly in the returns (Fig. A53) which can be enhanced by a background removal algorithm (Fig. A51, A52). The intensity of the return from the rock is greatly diminished when there is layering such as the surface thaw illustrated in these figures. The return signal strength is greater when the area in which the rock is located is frozen (Figure A48). This may be associated with the permeability of the rock, the availability of liquid water in the soil, and the temperature of the frozen soil.

Frequency content

Although no systematic analysis in the frequency domain was attempted in this phase of the program, it is interesting to note the dominant frequency characteristics of some of the returns.

The primary frequency bands for the antennas used in this work when operating above the surface are as follows:

<u>Antenna model</u>	<u>Approximate primary frequency (MHz)</u>	<u>Approximate antenna (fan aperture) length, D (m)</u>
3102	250-500	0.290-0.310
101C	600-800	0.155-0.180
3100	800-1250	0.065-0.075

These antennas transmit and are sensitive to a broad frequency spectrum which has been found empirically to include those primary frequencies in the mine returns.

The frequency analysis described in this report is a result of manually measuring the half wavelet times of the transmitted signal, the return from the surface, and the return from a target of interest. These measurements are not so precise as those made by a spectrum analyzer, but approximate the primary frequency band of the returned signals. Only trends and comparisons will be discussed.

Apart from the basic antenna design, significant parameters affecting the frequency content of the return signal are the interface proximity and the distance between the antenna and the target. If a conductive medium is very close to the antenna, it can affect the propagating characteristics of the antenna. This makes the antenna electromagnetically larger, broadening and lowering its primary frequency band. Inhomogeneities in the medium provide discontinuities at which other frequencies are also generated.

Characterizing the spatial energy distribution as a function of distance from the antenna is classically a discussion of the near-field, or Fresnel, region and the far-field, or Fraunhofer, region. The former ends at about $0.4 D^2/\lambda$ and the latter begins at about $2 D^2/\lambda$ (D is the antenna aperture dimension and λ is the wavelength). The region between the two is a transition zone. The wavefront in the near-field is not formed and generally unpredictable, and in the far-field it has become perpendicular to the antenna direction. Significantly, the theory was developed for narrow frequency bands. Frequency spectra differences between these two regions are beyond the scope of this work.

Since the energy is distributed over a broad frequency band in the transmitted and received signals of a non-sinusoidal radar, the application of the classic definitions, above, is difficult. It is particularly complicated in the near-field, since both surface proximity and antenna-to-target distance affect the frequency content of the return signal. This explains the broad frequency dispersion which is encountered under field conditions, and emphasizes the need for a broad-banded detection scheme.

In the present work, the far-field is that region from which the directivity is reasonably restricted and consistent and individual wavelets can be selected for frequency analysis. Clearly, a mine is in the near-field when the antenna is on the surface of the medium, but at the same time the surface

proximity effect is strongest. As the antenna is raised, a return becomes more nearly in the far-field as its frequency content becomes more nearly restricted and consistent. Illustrations of these effects are discussed below.

Surface proximity effect. In Figure B3 the 3100 antenna is about 10 cm above the surface, and the frequency variation in the return from the RAAM mine was between 590 and 910 MHz, a difference of 320 MHz. In Figure B1, with the antenna on the surface, the center frequency of the return signal varied between 560 and 1250 MHz, a difference of 690 MHz.

Near-field/far-field effect. As an example of the effect of the near-field/far-field on the frequency content of the returned signals with the 101C antenna, compare Figures A2 and A3. With the antenna operating directly on the surface (Fig. A2) the surface/transmit return varies between 500 and 560 MHz. The frequency content of the return from the buried metal disks at about 0.9 m varies between 670 and 710 MHz. This return is about 14 nanoseconds below the surface and is in the far-field of the antenna. The bottom of the box also has a reasonably consistent return at about 630 MHz. In Figure A3, where the antenna is located about 15 cm above the surface, the operation is in a transitional zone between the near-field and the far-field. In this case the frequency band of the transmitted signal is between 500 and 710 MHz and the surface return is about 910 MHz. At 14 ns from the surface, the return from the buried metal disk is about 910 MHz. At 20 ns below the surface, the bottom return is also about 910 MHz.

The frequency content of these target returns was measured directly over the target. If one observes the frequency content of the return on the "tails" of the target the frequency dispersion is significantly greater. Nevertheless, Figures A2 and A3 illustrate that once a target is in the far-field of this type of antenna, the frequency content of the return is much more restricted. In both cases, the medium has about 4 cm of frost; therefore, variation in the medium may be discounted.

The near-field/far-field effect on the frequency content of the transmitted signal and the surface return can be compared in Figures A36, A5 and A6. In these three figures the same antenna is used and the medium is unfrozen. In Figure A36, the 101C antenna is on the surface and the transmit/surface frequency band ranges from 420 MHz to 540 MHz. When the antenna is 0.3 m off the surface (Fig. A5) the transmitted frequency band ranges from 630 MHz to 830 MHz and the surface return ranges from 690 MHz to 1 GHz. When the antenna is located 0.6 m off the surface, clearly in the far-field, the

transmitted wavelet frequency content is between 630 MHz and 740 MHz, while the surface return ranges between 710 MHz and 830 MHz.

In Figures A19 and A10 the 101C antenna is on the surface and 0.3 m off the surface, respectively. The transmitted surface return in Figure A19 measured away from the influence of a mine has a frequency content ranging between 570 MHz and 670 MHz. When the antenna is 0.3 m off the surface (Fig. A10) the transmitted frequency band ranges from 630 MHz to 770 MHz and the surface return spectrum ranges from 710 MHz to 870 MHz. In both of these cases, the soil is frozen down to 17-26 cm; hence, only the near-field/far-field condition is affecting the frequency content.

For near-field operation, a comparison of the frequency content from the transmit/surface return under various freeze/thaw conditions can be made when considering Figures A36, A19 and A34. When the medium is unfrozen (Fig. A36) the frequency range is between 420 and 540 MHz. When there is 17 to 26 cm of frost (Fig. A19) the frequency of the transmit/surface return is from 570 to 670 MHz; and when there is thaw over deep frost (Fig. A34), the frequency content is from 440 to 570 MHz. The center frequency of the transmit/surface return under these conditions ranges from 480 MHz up to 630 MHz, a difference of 150 MHz.

With this coarse analysis, the most significant point to be observed in the frequency domain is the variation in frequency of the return from the mine itself. Figure 17 illustrates the variation in the frequency content of the return signals from the RAAM mine corresponding to those variations previously discussed for Figures A5, A6, A10, A19, A34 and A36. The variation and dispersion are quite extreme. Consider the return from the RAAM mine in Figure A5 and the return in Figure A36. In Figure A5 the return is reasonably consistent at 830 MHz, whereas in Figure A36 the center frequency ranges in a band between 310 MHz and 1.85 GHz.

A frequency shift in the primary energy returned from the mine can be observed in both Figures A19 and A34. In both cases the antenna is on the surface. Medium conditions are frost and thaw over frost, respectively. In Figure A19 the primary frequency of the return signal from the RAAM varies from 370 to 540 MHz.

The frequency ranges from 300 to 500 MHz. The significance is that the frequency band between 600 and 800 MHz has typically been considered the optimum band for mine detection. This is valid in Figure A36, for instance, when the medium is unfrozen. However, when the medium is frozen, particular-

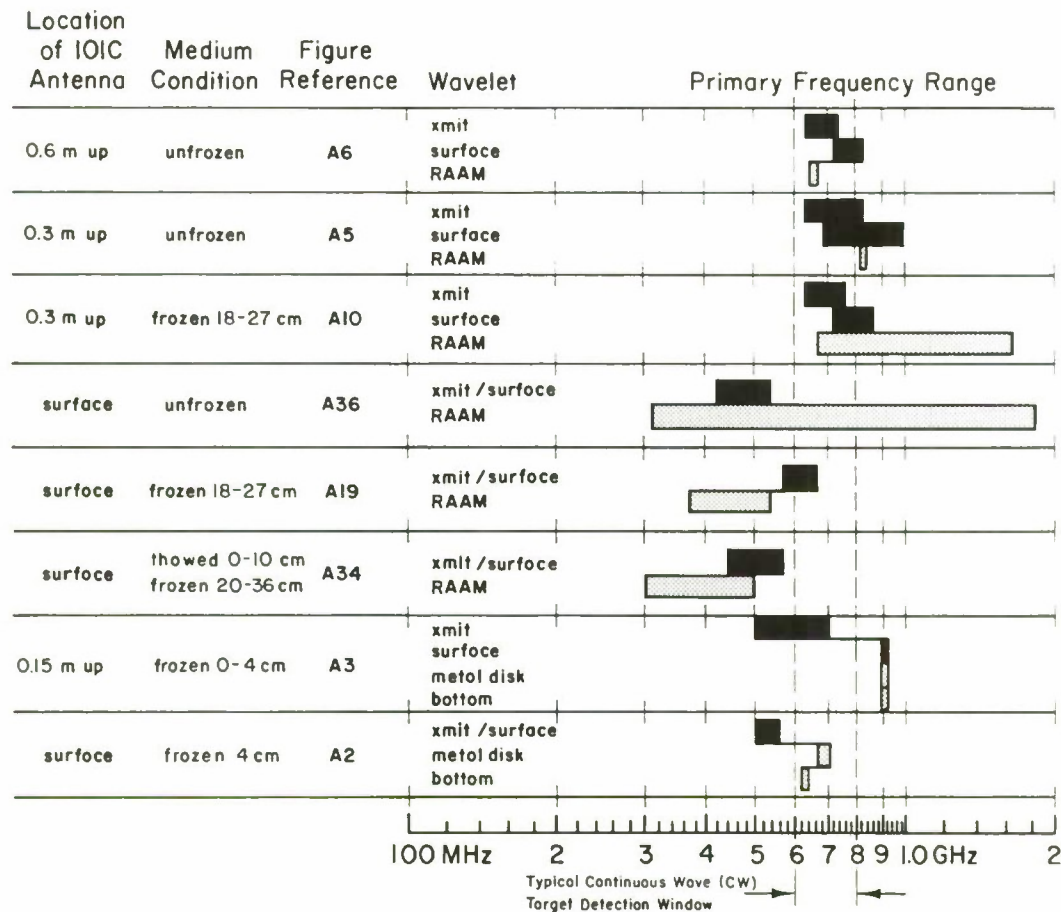


Figure 17. Comparison of wavelet primary frequency range with antenna location and medium condition.

ly when thaw exists over frost, this is no longer an optimum band. A broader frequency window appears to be necessary.

In light of the strong variation in frequency content of returns from the mines as a function of antenna position and medium conditions, it appears reasonable to assume that the investigations planned for background removal and frequency analysis (see Future Work) may provide significant data leading to the characterization of mine returns.

Hand-held (portable) detectors

To investigate non-sinusoidal radar for hand-held mine detectors and to evaluate a higher frequency antenna, tests were conducted using a "1-GHz" antenna, provided by Geophysical Survey Systems, Inc. Selected results of these tests are illustrated in Figures B1-B5. The tests were done in a direct print mode and conducted in real time; that is, the hard copy facsimile was made as the data were taken. The horizontal dimension is significantly



Figure 18. Model 3100 antenna being pulled across the test box at a fixed height above the surface. Scan data for these tests appear in Figures B1-B4.

shorter than in previous figures, as there were fewer samples per unit length along the survey line.

Figure B1 represents a profile made along the centerline with the antenna at the surface of the medium. In the direct print mode the graphic recorder is highlighting, by way of vertical lines in place of a continuous tone, the negative phase excursion of the return waveform. The location of the mines is obvious and the mine returns are unique in comparison with one another. Figure B2 represents another scan similar to Figure B1. The data of Figure B2 were processed in real time with program 2-7. For Figures B1 and B2 the antenna was in the near-field. For Figures B3 and B4 the antenna was located approximately 10 cm above the surface. The uniqueness of the mine returns is less evident, the signal strength is reduced, but the detection of the mines is still reliable. Detection is particularly obvious in Figure B4, where the background has been removed under real-time program 2-2.

In Figures B1-B4 the antenna was moved along the survey line in a manner similar to other tests discussed in this report. An example of this may be seen in Figure 18 where the antenna is being pulled with its cable. To attempt simulation of a more operational mode for a hand-held device, the antenna was attached to the end of a rod and moved back and forth in front of the surveyor (Fig. 19). The real-time results of this survey, with the nega-



Figure 19. Model 3100 antenna, attached to a rod, is being swept across the path of the surveyor. Scan data for this operation appear in Figure B5.

tive phase of the return highlighted, are presented in Figure B5. These returns are distinct and illustrate the capability of detection under these conditions.

CONCLUSIONS

We find that the detection of mines in the frequency band between 600 and 800 MHz in unfrozen homogeneous ground is achievable. When the medium is frozen, however (particularly when thaw exists over frost), a broader frequency window is at least required for more realistic field conditions (see Figure 17 and the accompanying discussion).

Our findings and the previous discussion of the medium and antenna effects put in question the effectiveness of the approach of band-limiting the signal return and keying simply on the intensity of the weighted return.

Such a detecting algorithm is very susceptible to medium inhomogeneity and will miss legitimate targets in an unstable-background, high-noise environment, e.g. a wet, surface-thawed road.

Phase reversal

The phase of the returns from metallic mines and background targets such as rocks was compared and found to exhibit directly opposite characteristics. This is due to the dielectric difference and is a strong characteristic which should be further investigated for real-time mine detection.

Unique returns

Among all three of the mines in this test, and under these conditions, unique returns were observed when the antenna was in the near-field configuration. The uniqueness of returns in a far-field configuration has not yet been determined. In the spatial domain the three mines are consistently distinctive. Due to the dielectric change from the medium to the target, the phase of the radar return from the natural rock about the size of a mine was found to be opposite to that of the metallic mine. It is significant to note that these characteristics are those not only of individual returns (as on the left side of Figure 15), but of many consecutive returns. The pattern representing the influence of the mine on the radar signal, which one sees in the radar profiles in this report, is constructed with several hundred returns. Although this implies a more sophisticated data analysis, it provides credibility to the technology's capability to detect mines and to discriminate among ordnance and background returns.

Surface return replica

In the near-field mode of operation, surface return replicas (echoes of the near-surface radar reflection) were observed in several deeper profiles. In cases where the transmit waveform overshadows the return from anomalies directly below the surface of the medium, a surface return replica found further down the (vertical) time scale may provide those significant spatial characteristics necessary for mine detection. This characteristic should also be considered when the impulse radar is being evaluated for standoff detection capability.

Early (distant) detection

In some profiles significant early returns (i.e. returns received well before the antenna was directly over the mine) were detectable from all three

of the mines. This presently appears to be a characteristic of medium layering and water content because it was observed after wetting and during a surface thaw period. With proper background removal (high-pass filtering), these early "skirts" of the target return may be detectable in other medium conditions.

We conclude that because of the extreme variations in the electromagnetic characteristics of media encountered in a typical winter regime, a broad-banded system with more sophisticated detection capability than is currently being used is required for reliable mine detection. We suggest 1) that the non-sinusoidal radar technology can provide the system capability in the near- and far-field, 2) that detection schemes based upon digital signal processing appear promising, 3) that a standoff antenna configuration is practically required, and 4) that the state-of-the-art in non-sinusoidal antenna design can provide a significant increase in power and beam focusing for enhanced performance in the standoff configuration.

FUTURE WORK

The objectives of the planned frequency domain analysis are:

1. To develop a hardware/software system which will aid in the analysis of the radar returns.
2. To analyze the mine signature in the frequency domain as a function of the antenna position with respect to the target.
3. To evaluate the electromagnetic characteristics of the medium so that the results of these tests may be compared with other field conditions.
4. To normalize the radar transmission/reception characteristics so that the results of this work can be directly compared with other tests and systems.
5. To develop a limited model, or an algorithm, for UHF radar mine detection based upon frequency, spatial, and signal intensity characteristics of both the target and the background.

Some limited spatial domain evaluation (i.e. radar hard-copy analysis) will proceed on the data which have been obtained from these series of tests. However, a majority of the work will now be focused on the frequency content of the returns. The selected returns will be converted to a digital format and analyzed in the frequency domain on a 3-dimensional color graphic comput-

er (to display time, signal amplitude, signal frequency content and consecutive profiles). The output will be a color display showing characteristics in the frequency domain, displayed in a form similar to the current spatial display. Catalogs may be constructed of various mine returns and some unique characteristics may be identified which can be used specifically to locate mines within a noisy background. It is hoped that characteristic signatures of the various mines can be determined. In addition, characteristic signatures of the background may be identified, thereby allowing an exclusion of certain frequency bands. A more sophisticated frequency characterization will also be attempted which deals with the change, or the rate of change, among frequency bands. This identification scheme may also aid in the early warning capability of the impulse radar system. Far-field operation will particularly be investigated.

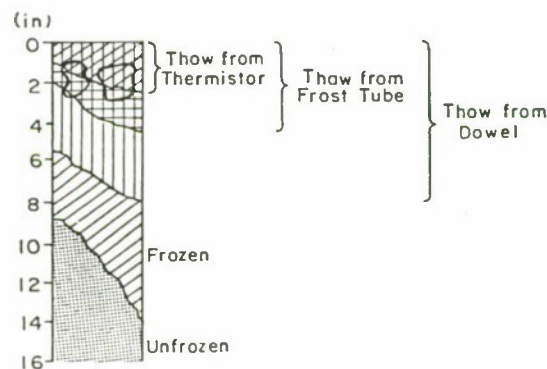
LITERATURE CITED

- Arcone, S.A. and A.J. Delaney (1982) Measurement of ground dielectric properties using wide-angle reflection and refraction. USA Cold Regions Research and Engineering Laboratory, CRREL Report 82-6, 11 p.
- Arcone, S.A., A.J. Delaney and P.V. Sellmann (1979) Detection of arctic water supplies with geophysical techniques. USA Cold Regions Research and Engineering Laboratory, CRREL Report 79-15.
- Collie, C.H., J.B. Hasted and D.C. Ritson (1948) Dielectric measurements of water at centimeter wavelength. Proceedings of the Philosophical Society, 60, p. 145.
- Dean, A. (1981) Electromagnetic subsurface measurements. USA Cold Regions Research and Engineering Laboratory, Special Report 81-23.
- Delaney, A.J. and S.A. Arcone (1982) Laboratory measurements of soil electric properties between 0.1 and 5 GHz. USA Cold Regions Research and Engineering Laboratory, CRREL Report 82-10.
- Dept. of the Army (1966) Sand cone density determination. Materials Testing, U.S. Army Technical Manual 5-530.
- Dept. of the Army (1976) Mine characteristics and installation procedures. Appendix C to Mine/Countermining Operations at the Company Level, FM 20-32, 30 Nov, p. 139-152.
- Ricard, J., W. Tobiasson and A. Grestorex (1976) The field assembled frost gage. USA Cold Regions Research and Engineering Laboratory, Technical Note (unpublished).

APPENDIX A: RADAR SCANS - NON-PORTABLE EQUIPMENT

Two information blocks accompany each figure in Appendixes A and B: a graphic representation of the medium and the scan information.

The graphic representation (see below) summarizes the condition of the medium at the time of the test, i.e. thawed, frozen or unfrozen and with or without cobbles. It facilitates comparison of the scans. The presence of irregular shapes between 2.5 and 6 cm indicates that the silty sand contained a layer of cobbles (see Fig. 8 and 9). The upper and lower bounds of frozen and unfrozen material are given by the left and right extremes of its line, i.e. in the example below the frozen/unfrozen boundary ranges between about 22 and 35 cm. The line itself has no significance. Note that the soil depth scales in these blocks are not the same as the scales on the figures.



The scan information block is explained below:

- Date:** Of test (used to correlate temperature and frost curves).
- Time:**
- Tape Number:**
- Tape Channel(s):** Location of recorded data.
- Approx. Tape Count:**
- Test Location:** All tests reported here were done in the small Ice Engineering Facility coldroom (see *Test Set-up and Procedures*).
- Media Conditions:** Abbreviated description (see graphic representation on each scan).
- Antenna Location:** On the medium surface or a measured distance above.
- Antenna Model:** Three different models, having different frequency bands (see text).
- Line of Survey:** Line traversed during test (see Fig. 1 and 2).
- Data:** Unprocessed (raw), processed (using a specified program), or printed (using a specified waveform polarity).

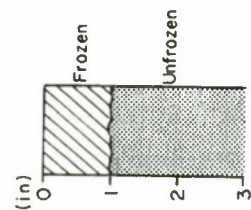
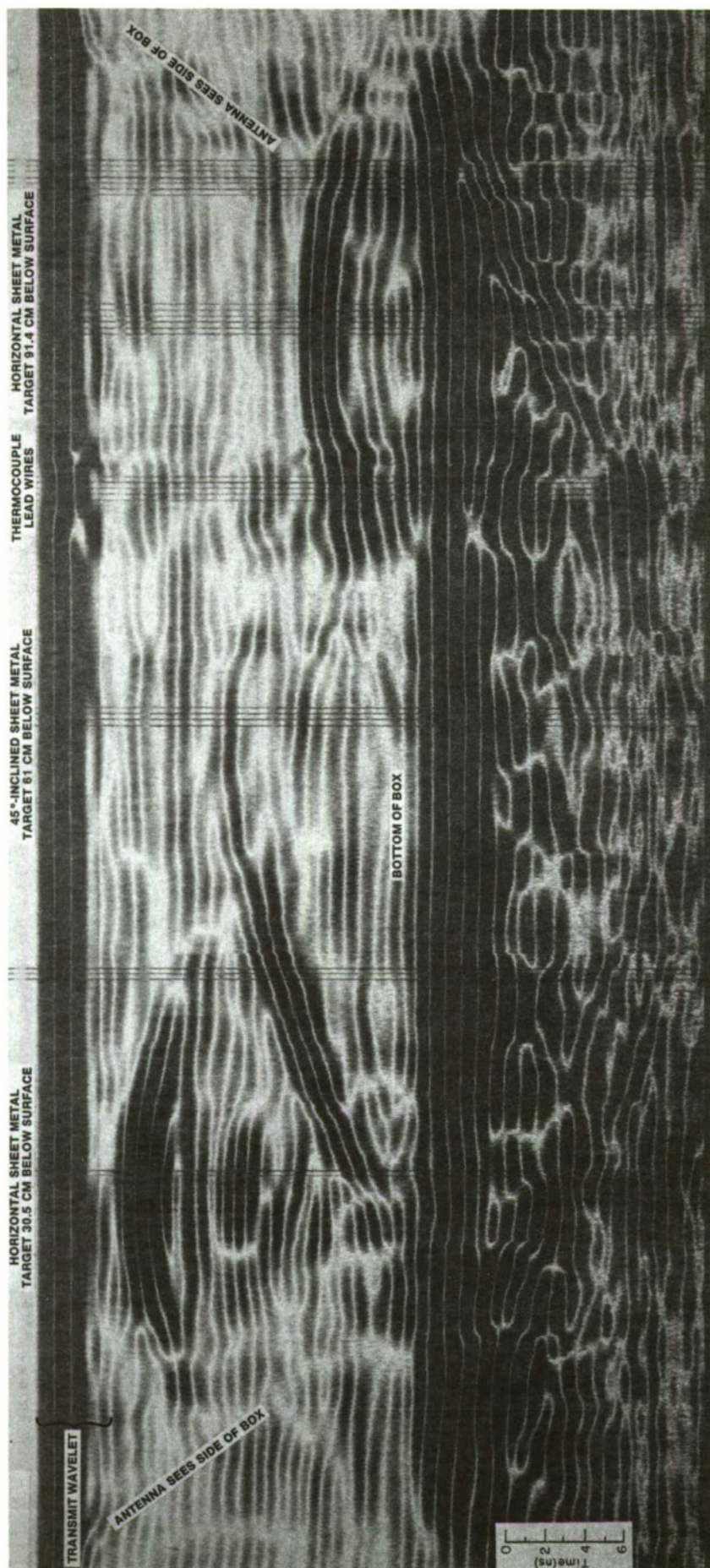


Figure A1.

Date: 7 Sept 82
 Time: 1405
 Tape Number: MB2
 Tape Channel(s): 1
 Approx. Tape Count: 1138-1311
 Test Location: IEF cold storage room
 Media Conditions: 1 in. frozen sand
 Antenna Location: Surface
 Antenna Model: 101C
 Line of Survey: South traverse
 Data: Unprocessed

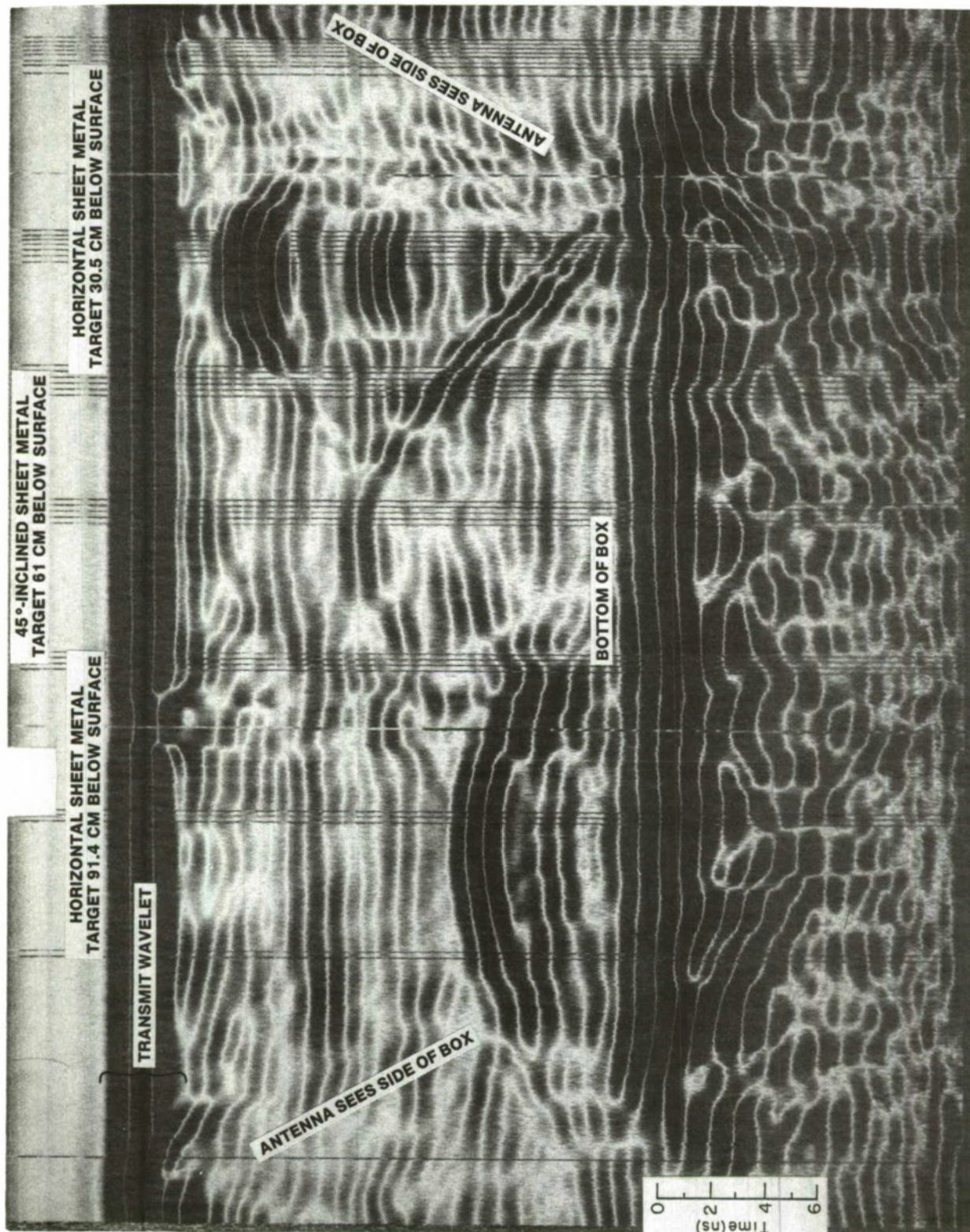
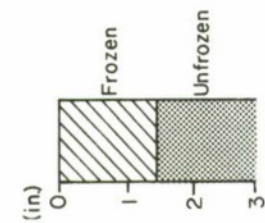


Figure A2.

Date: 8 Sept 82
 Time: 0900
 Tape Number: MB2
 Tape Channel(s): 1
 Approx. Tape Count: 1801-1871
 Test Location: IEF cold storage room
 Media Conditions: 1/2 in. frozen sand
 Antenna Location: Surface
 Antenna Model: 101C
 Line of Survey: North profile
 Data: Unprocessed

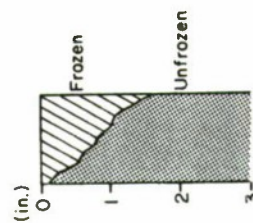
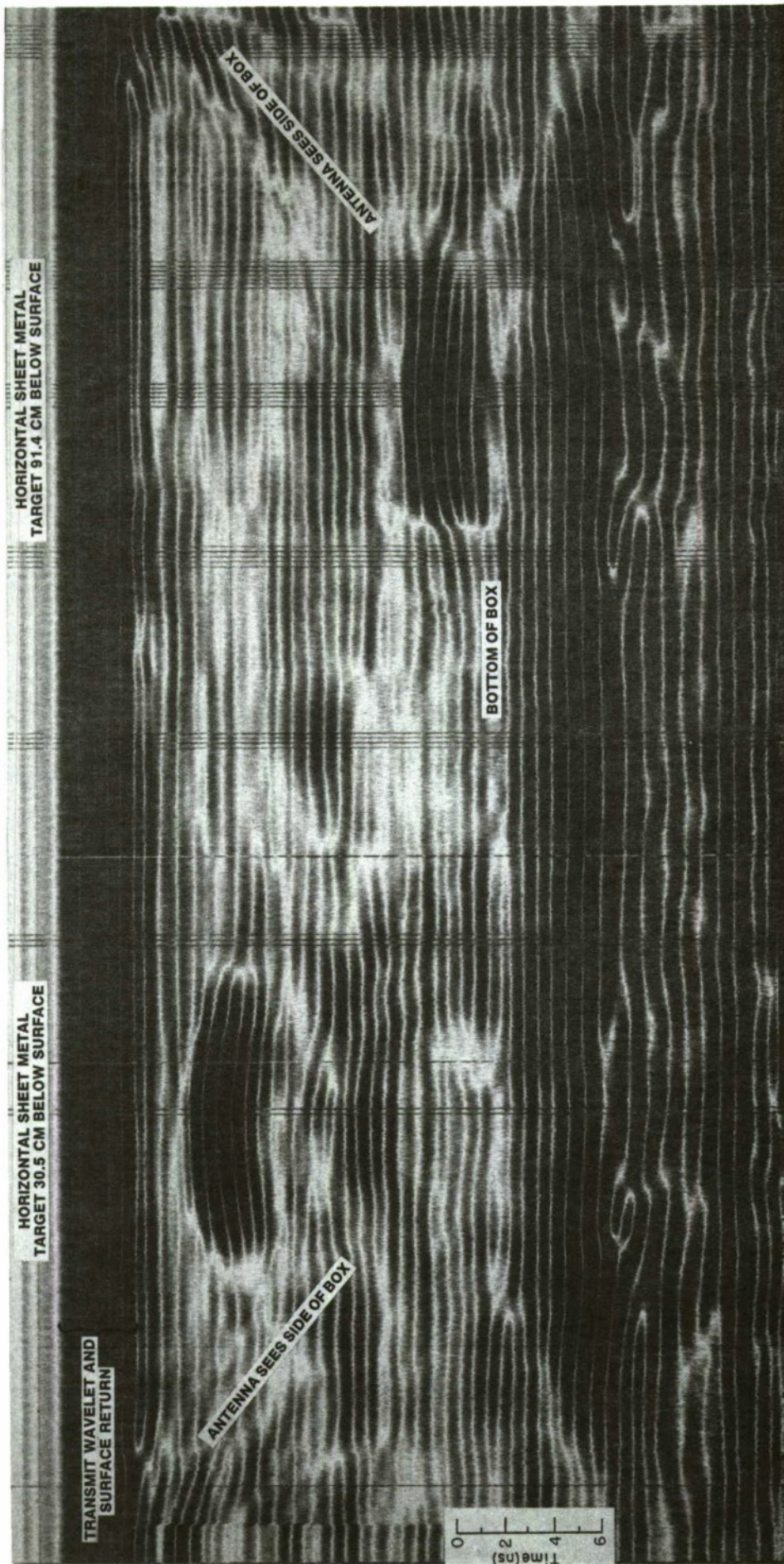


Figure A3.

Date: 8 Sept 82
 Time: 1148
 Tape Number: MB3
 Tape Channels: 0
 Approx. Tape Count: 9798-0888
 Test Location: IEF cold storage room
 Media Conditions: 0.1 1/2 in. frozen silty sand
 Antenna Location: 8 in. off surface
 Antenna Model: 101C
 Line of Survey: South traverse
 Data: Unprocessed

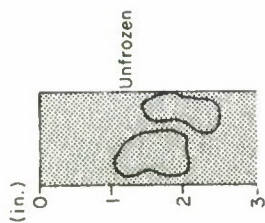
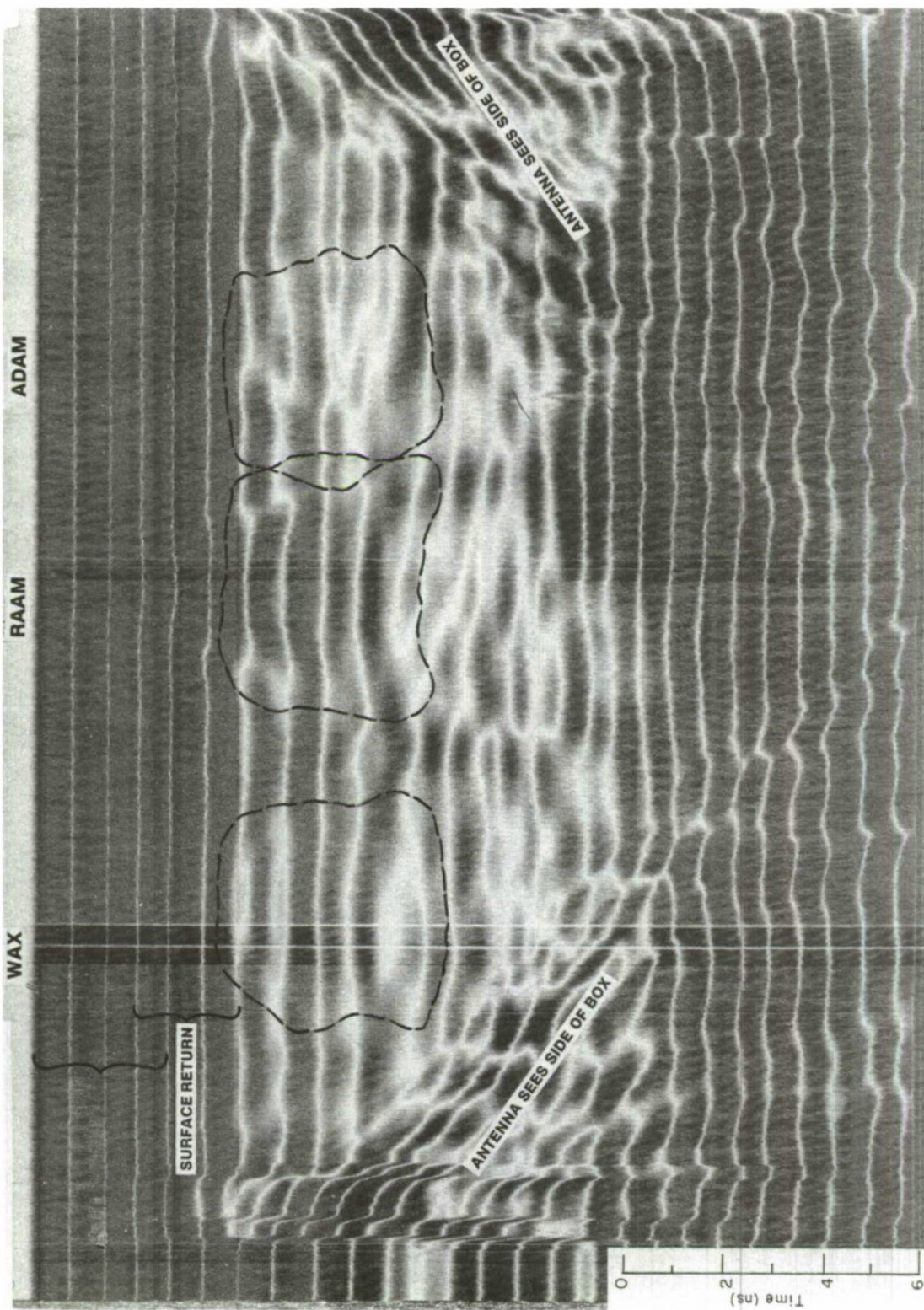


Figure A4.

Date: 24 Jan 83
 Time: 1104
 Tape Number: MB12
 Tape Channel(s): 1, 4
 Approx. Tape Count: 1423-1522
 Test Location: IEF cold storage room
 Media Conditions: Unfrozen silty sand w/cobbles
 Antenna Location: 8 in. off surface
 Antenna Model: 101C
 Line of Survey: Centerline
 Data: Unprocessed

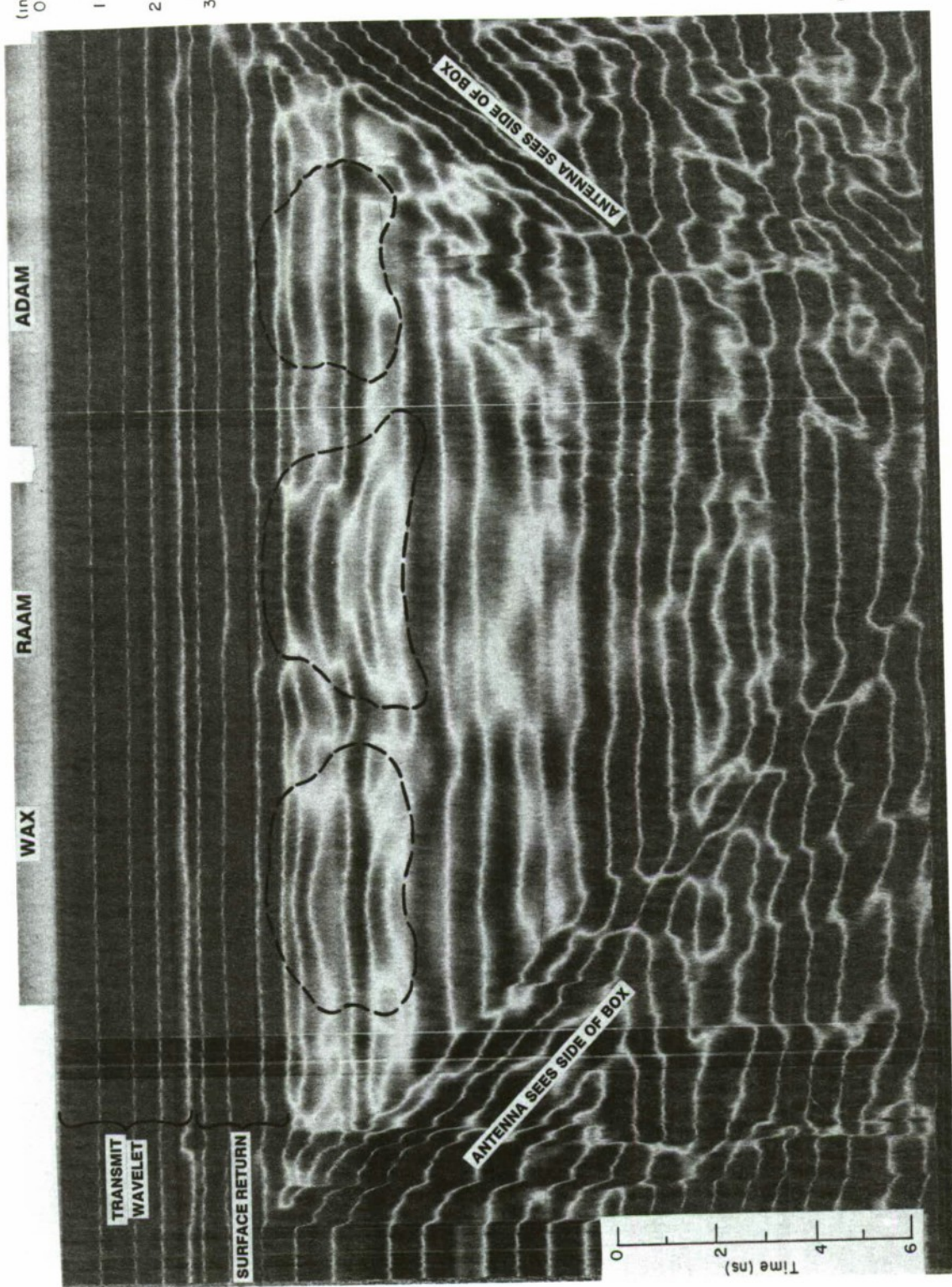
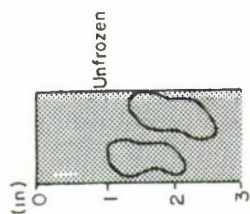


Figure A5.
 Date: 24 Jan 63
 Time: 1111
 Tape Number: MB12
 Approx. Tape Count: 1, 4
 Test Location: EF cold storage room
 Media Conditions: Unfrozen silty sand w/cobbles
 Antenna Location: 12 in. off surface
 Antenna Model: 101C
 Line of Survey: Centerline
 Date: Unprocessed

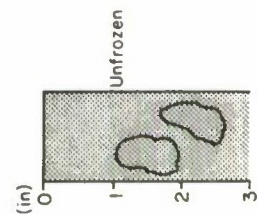
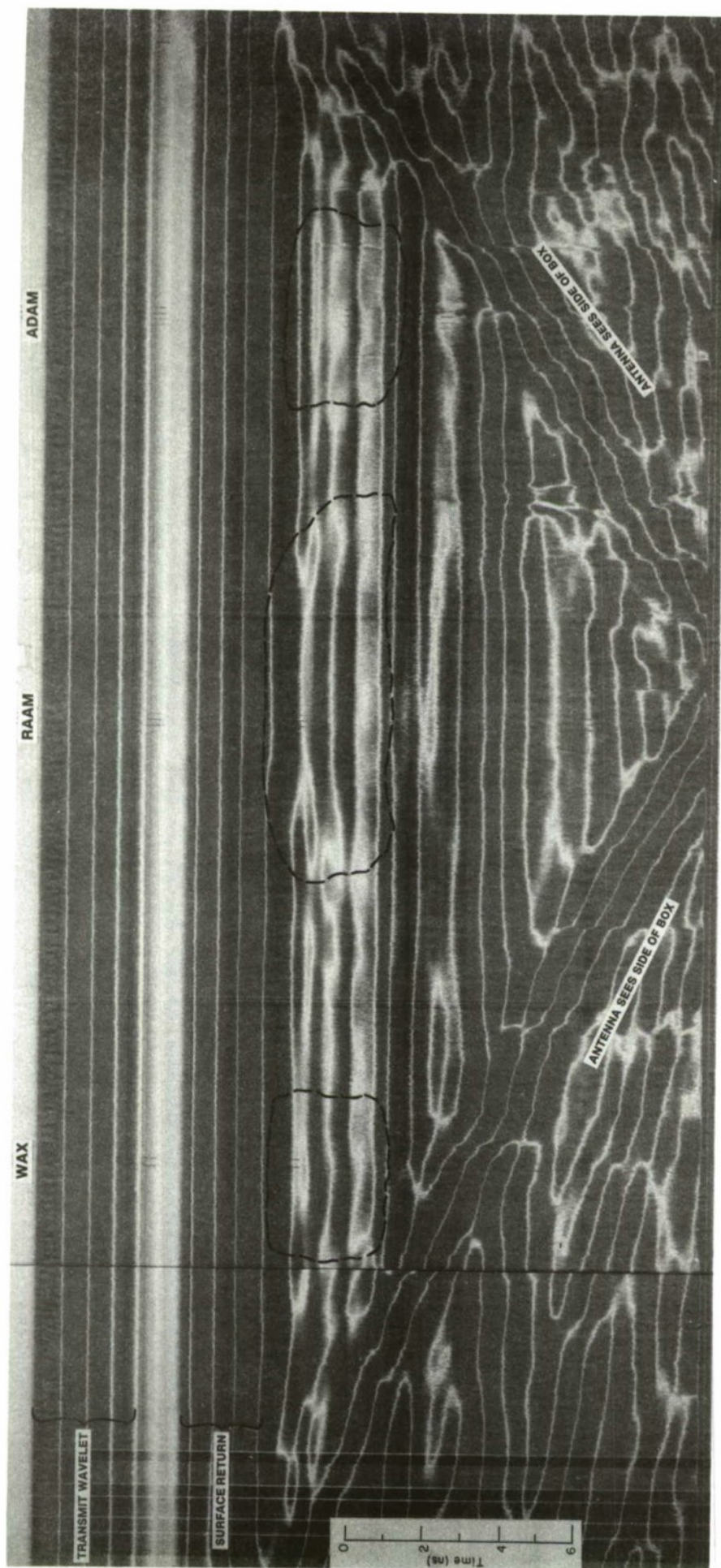


Figure A6.

Date: 28 Sept 82
 Time: 1540
 Tape Number: MB8
 Tape Channels: 1, 4
 Approx. Tape Count: 1010, 1203
 Test Location: IEP cold storage room
 Media Conditions: Unfrozen silty sand w/cobbles
 Antenna Location: 24 in. above surface
 Antenna Model: 101C
 Line of Survey: Centaline
 Data: Unprocessed

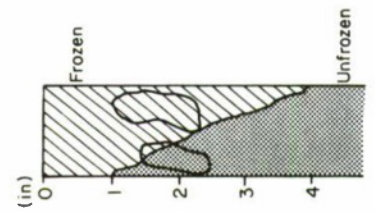
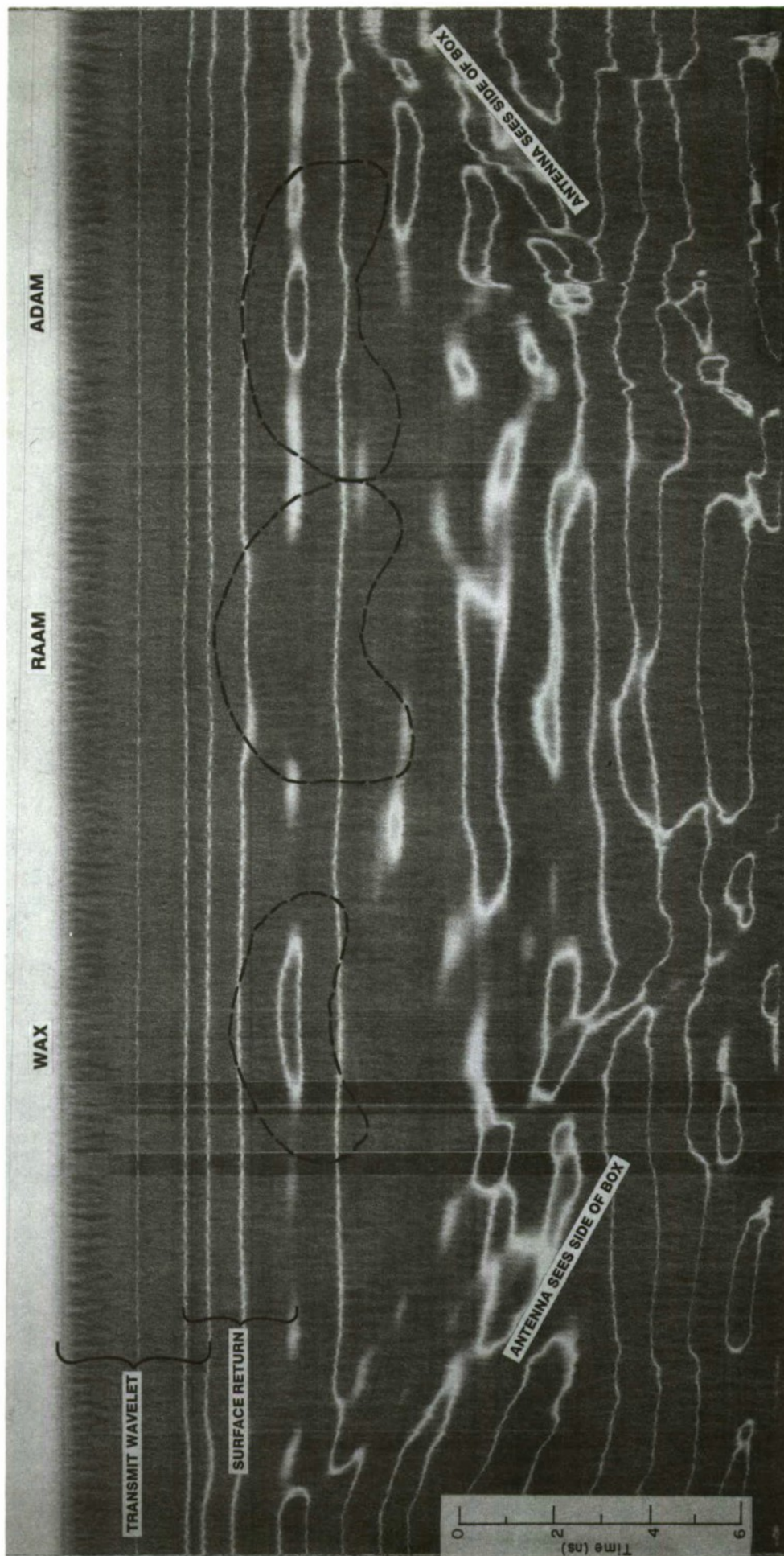


Figure A7.

Date: 2 Nov 82
 Time: 1024
 Tape Number: MB11
 Tape Channel: 1, 4
 Approx. Tape Count: 1483, 1803
 Approx. Location: IEF solid storage room
 Media Condition: Silty sand w/cobbles
 Antenna Location: 6 in. off surface
 Antenna Model: 3102
 Line of Survey: Centerline
 Data: Unprocessed

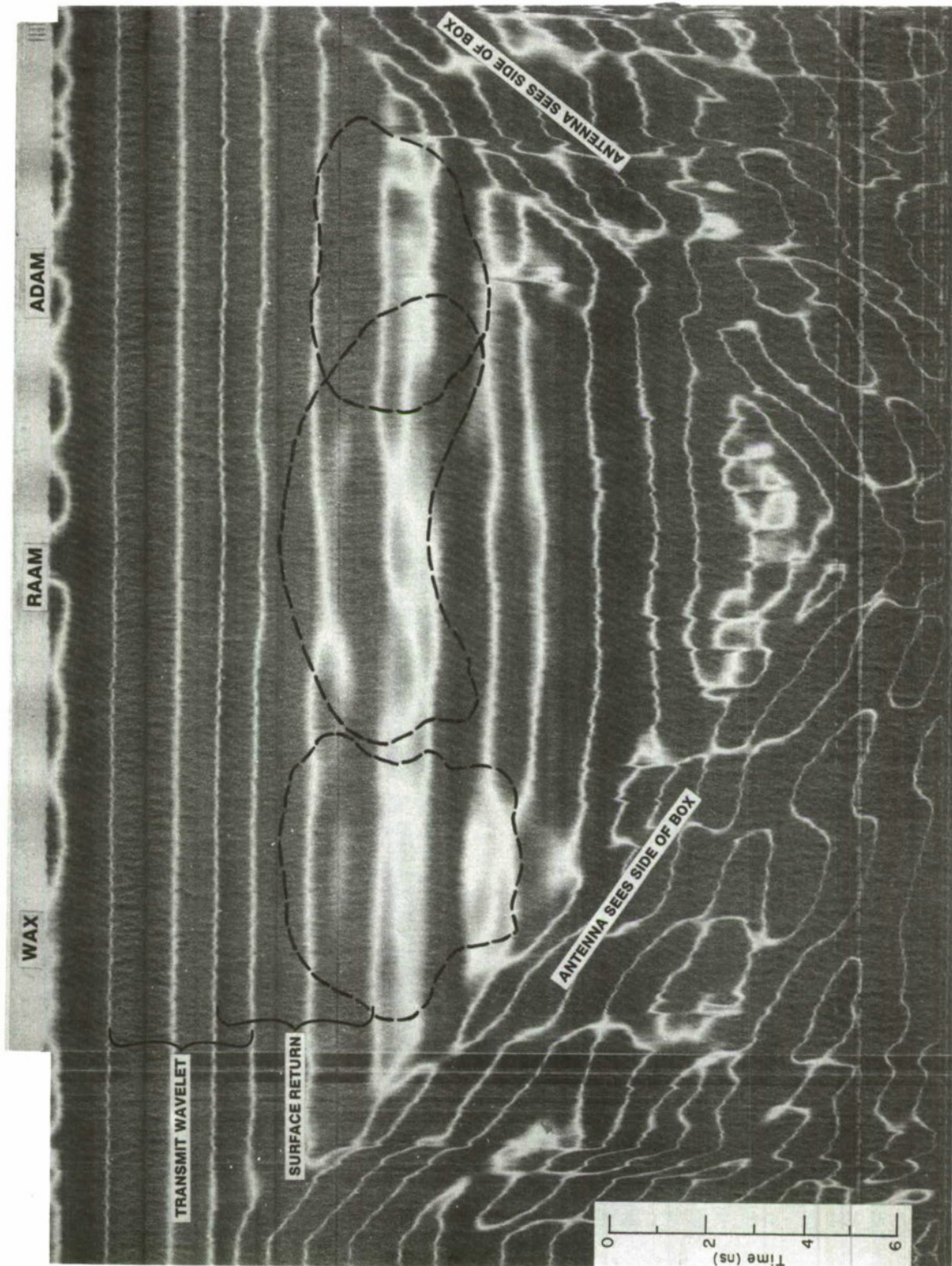


Figure A8.

Date: 5 Nov 82

Time: 1526

Tape Number: MB12

Tape Channel(s): 1, 4

Approx. Tape Count: 0921-1045

Test Location: IEF cold storage room

Media Conditions: Surface thawed silty sand

w/cobbles

Antenna Location: 12 in. off surface

Antenna Model: 3102

Line of Survey: Centerline

Data: Unprocessed

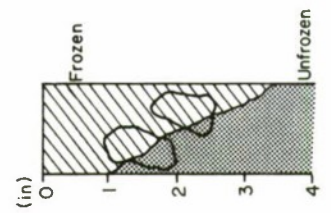
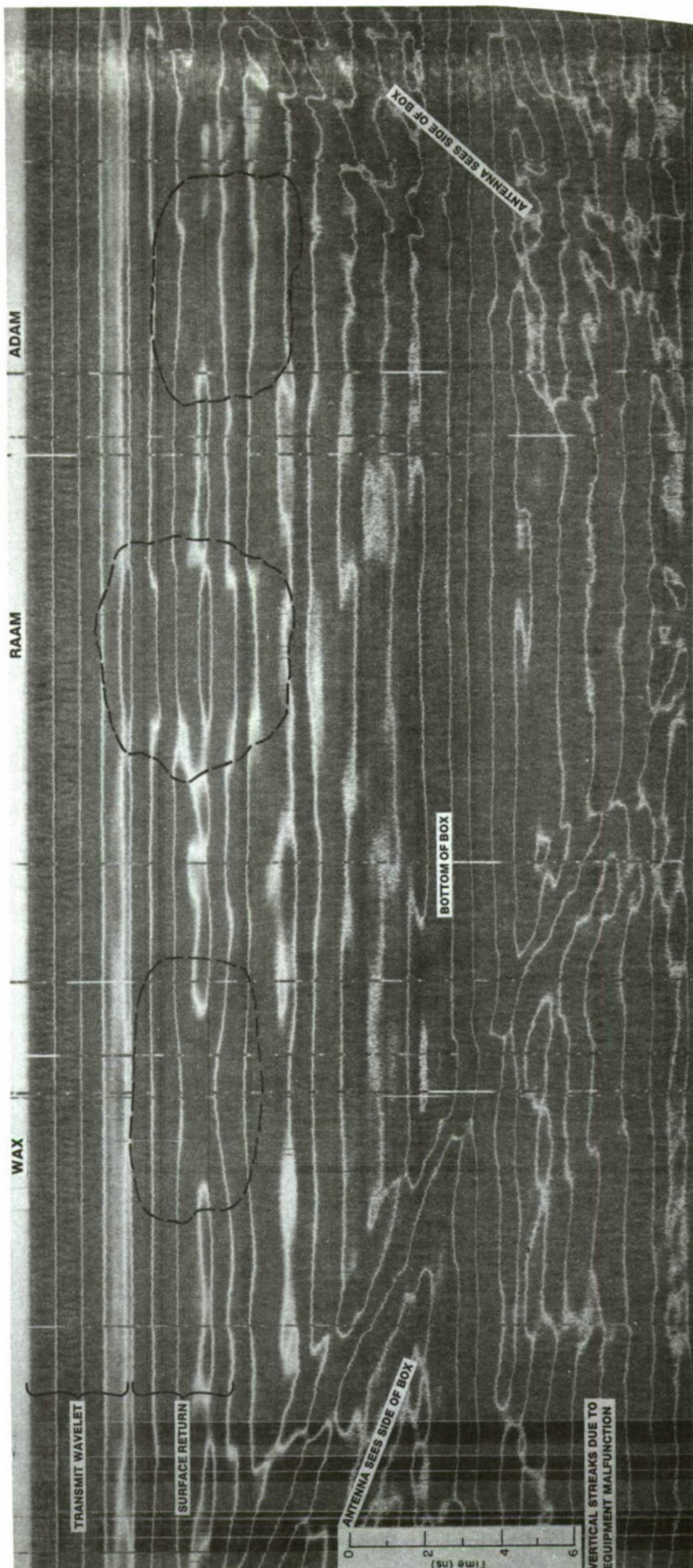


Figure A9.

Date: 30 Sept 82
 Time: -0840
 Tape Number: M85
 Tape Channel(s): 1, 4
 Approx. Tape Count: 1487-1627
 Test Location: JEP cold storage room
 Media Conditions: 1 to 3 in. frozen silty sand
 w/cobbles
 Antenna Location: 12 in. off surface
 Antenna Model: 101C
 Line of Survey: Centerline
 Data: Unprocessed

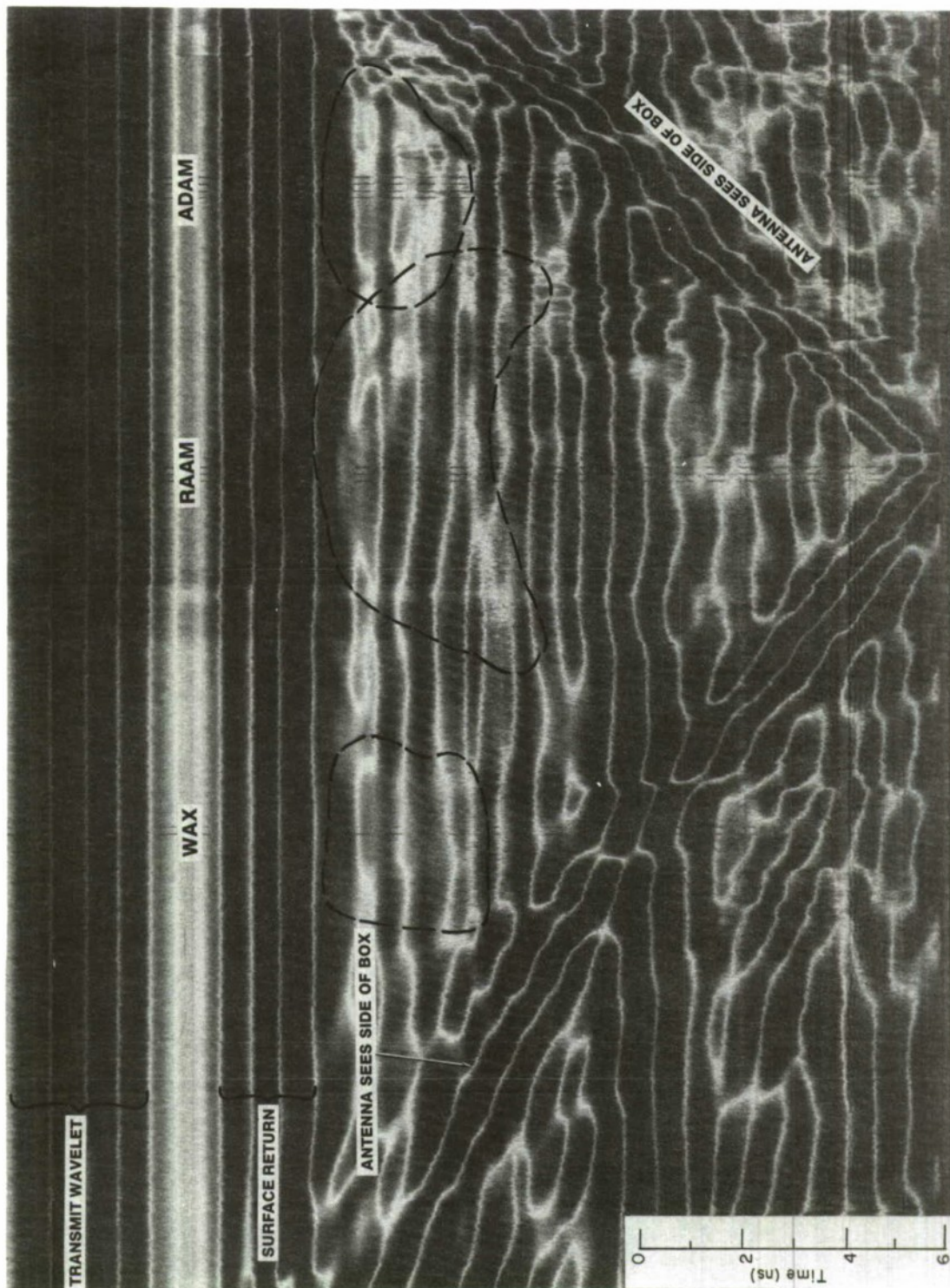
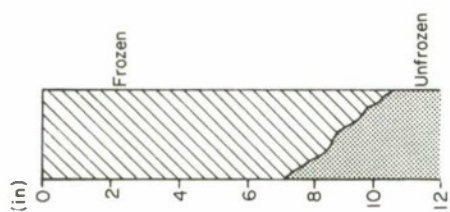


Figure A10.

Date: 14 Sept 82
 Time: 1130
 Tape Number: MB4
 Tape Channel(s): 1
 Approx. Tape Count: 1181-1300
 Test Location: IEF cold storage room
 Media Conditions: 7 to 10 in. frozen silty sand
 Antenna Location: 12 in. off surface
 Antenna Model: 101C
 Line of Survey: Centerline
 Data: Unprocessed

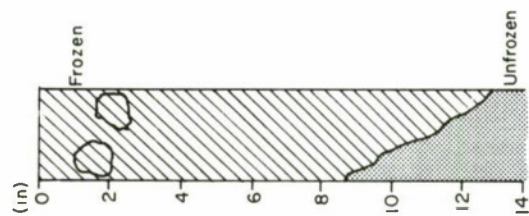
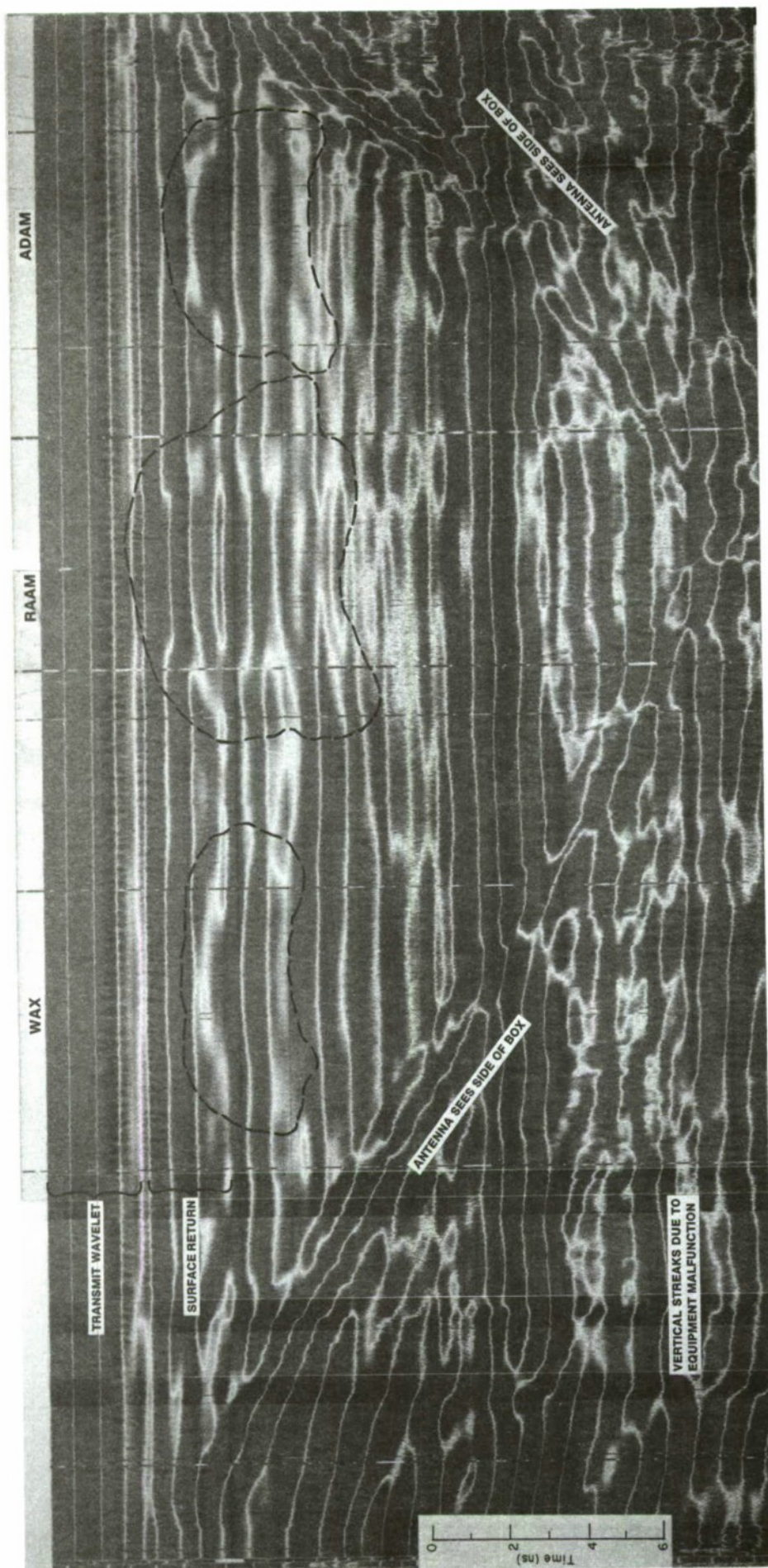


Figure A11.

Date: 4 Oct 82
 Time: 1248
 Tape Number: MB8
 Tape Channel(s): 1, 4
 Approx. Tape Count: 0450-0662
 Test Location: IEF cold storage room
 Media Conditions: 9 to 13 in. frozen silty sand
 w/cobbles
 Antenna Location: 12 in. above surface
 Antenna Model: 101C
 Line of Survey: Centerline
 Date: Unprocessed

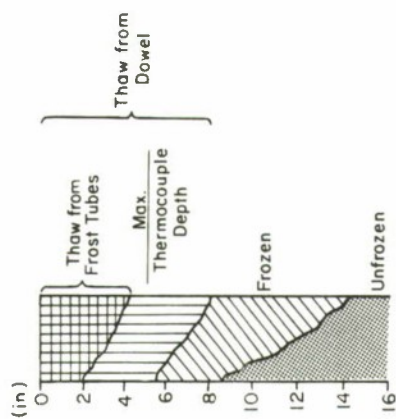
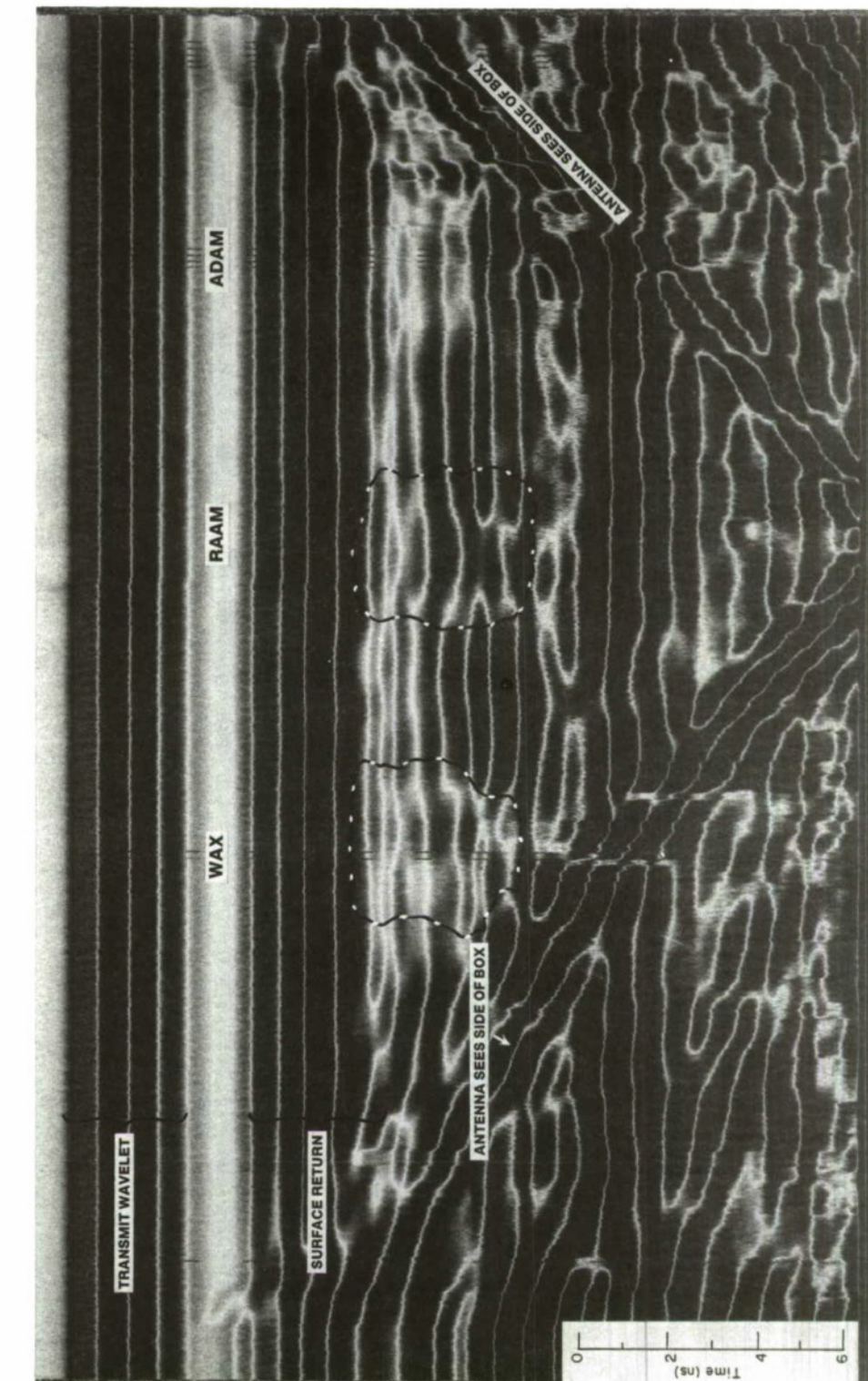


Figure A12.

Date: 16 Sept 82
 Time: - 1610
 Tape Number: MBS
 Tape Channel(s): 1
 Test Count: 1318-1432
 Approx. Tape Location: IEF cold storage room
 Media Conditions: 9 to 14 in. frozen silty
 sand—after wetting
 Antenna Location: 24 in. off surface
 Antenna Model: 101C
 Line of Survey: Centerline
 Data: Unprocessed

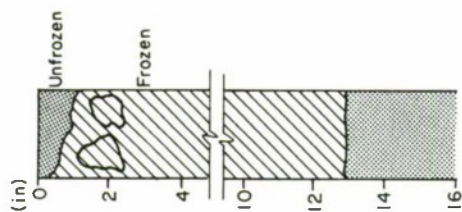
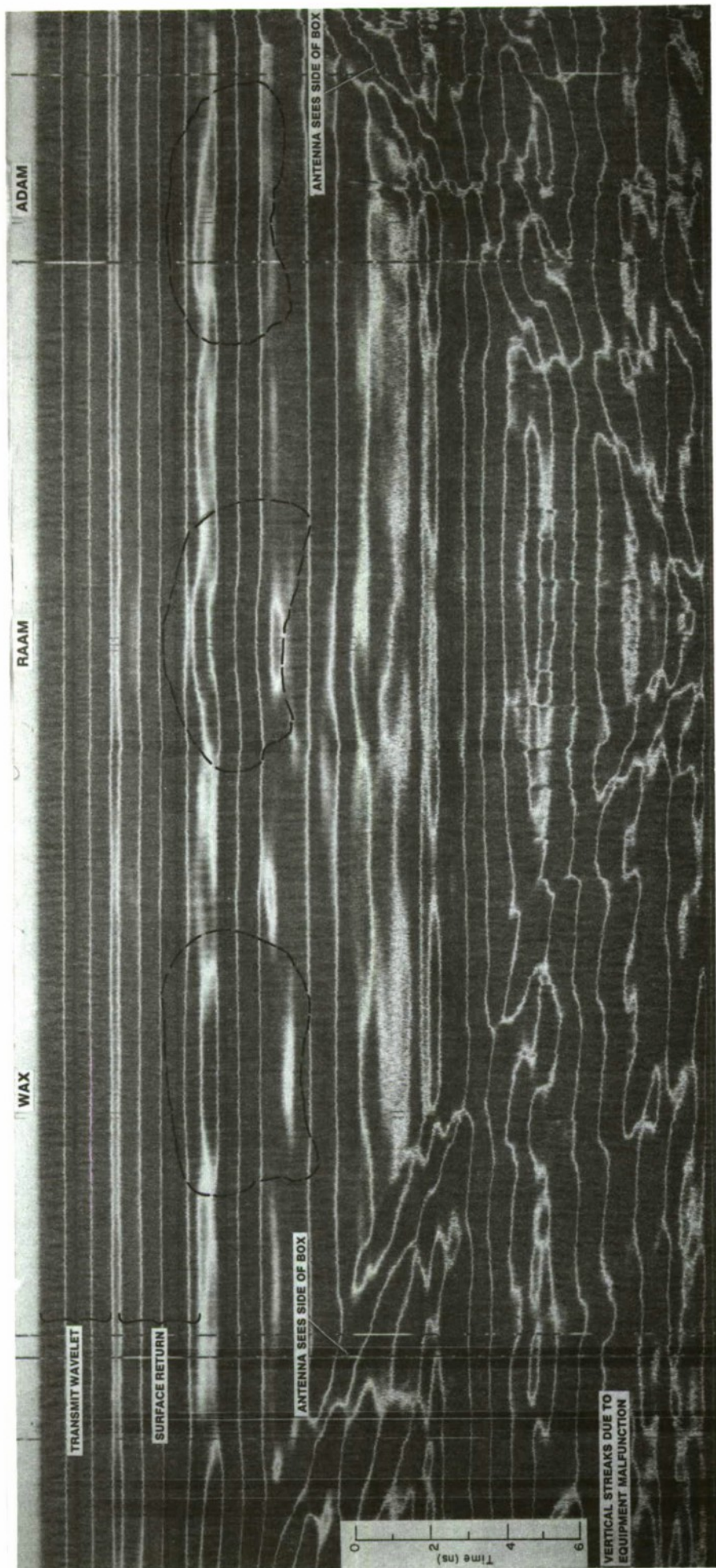


Figure A13.

Date: 6 Oct 82
 Time: 1327
 Tape Number: W89
 Tape Channel(s): 1, 2, 4
 Approx. Tape Count: 0552-0792
 Text Location: IEF cold storage room
 Media Conditions: Frozen silty sand w/cobbles.
 Antenna Location: 12 in. off surface
 Antenna Model: 101C
 Line of Survey: Centerline
 Data: Unprocessed

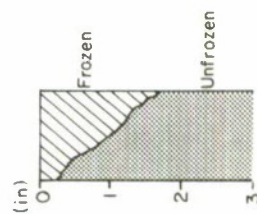
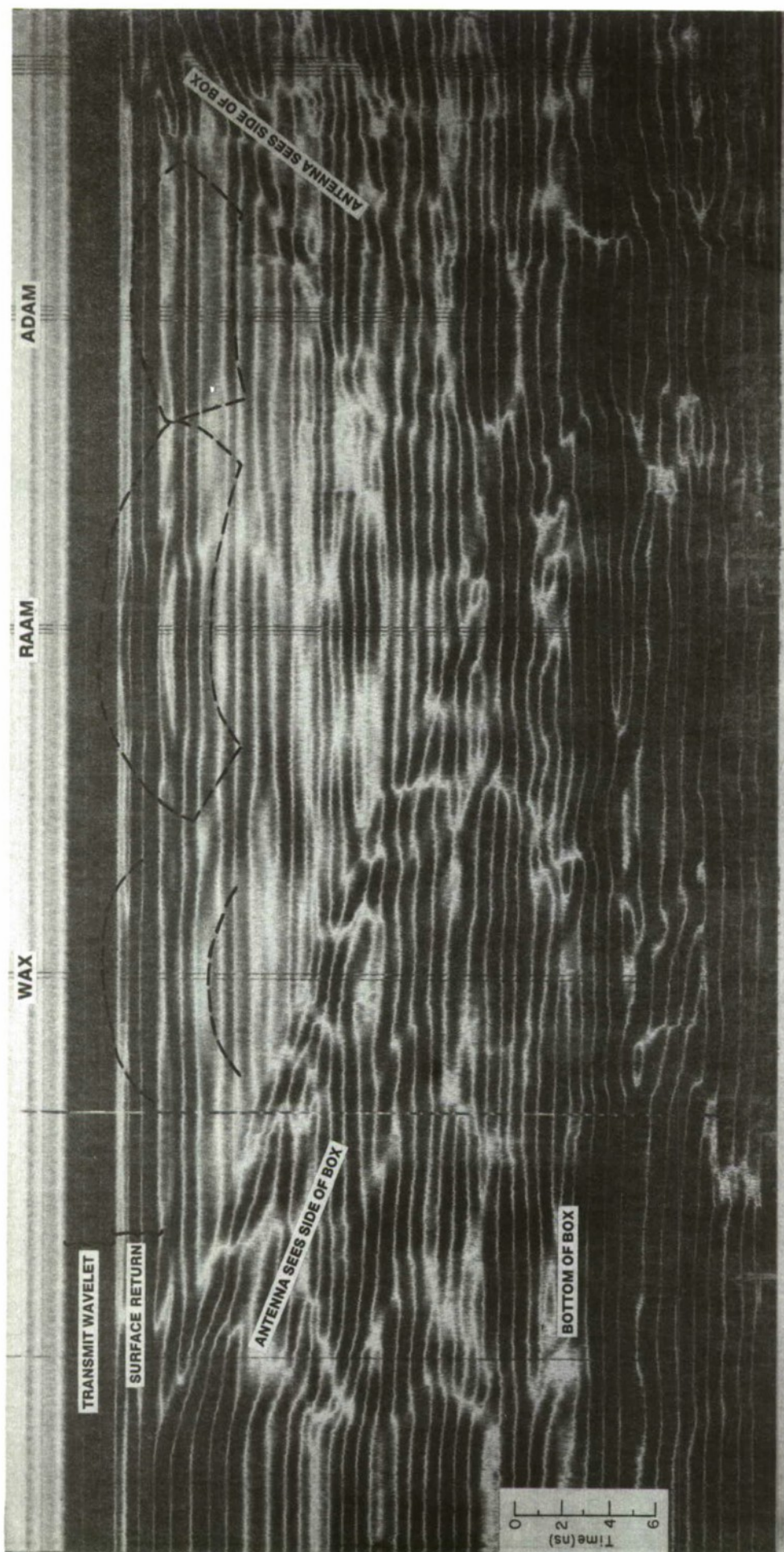


Figure A14.

Date: 8 Sept 82
 Time: 1210
 Tape Number: MB3
 Tape Channel(s):
 Approx. Tape Count: 0870-1035
 Test Location: IEF cold storage room
 Media Conditions: $\frac{1}{2}$ to $1\frac{1}{2}$ in. frozen silty sand
 Antenna Location: 12 in. off surface
 Antenna Model: 101C
 Line of Survey: Centerline
 Data: Unprocessed

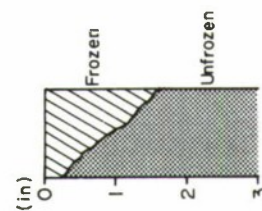
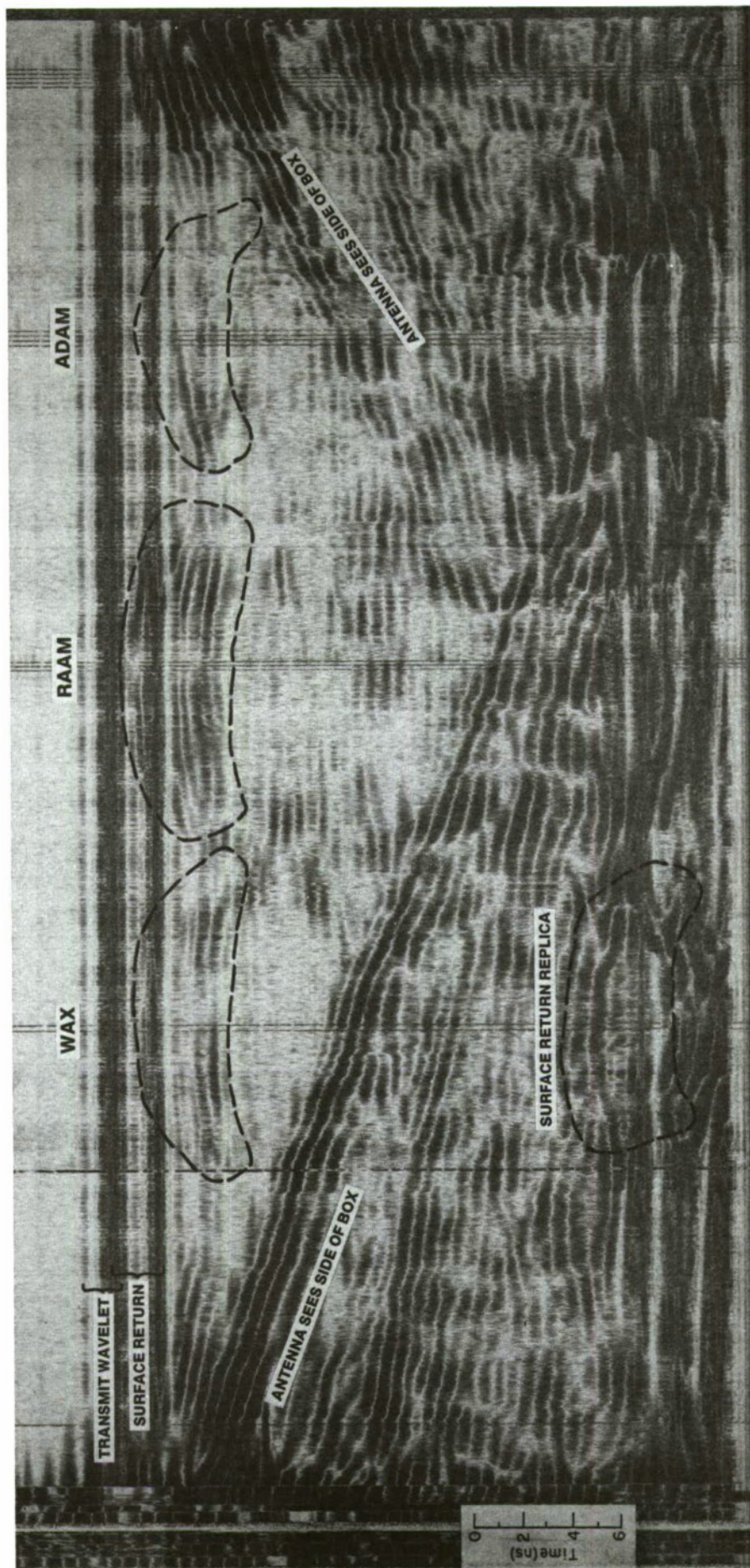


Figure A15.

Date: 8 Sept 82
Time: 1210

Tape Number: MB3
Tape Channel(s):

Approx. Tape Count: 0890-1035
Test Location: IEF cold storage room

Media Conditions: $\frac{1}{2}$ to 1 $\frac{1}{2}$ in. frozen silty sand
Antenna Location: 12 in. off surface

Antenna Model: 101C
Line of Survey: Centerline
Date: Program 2-4

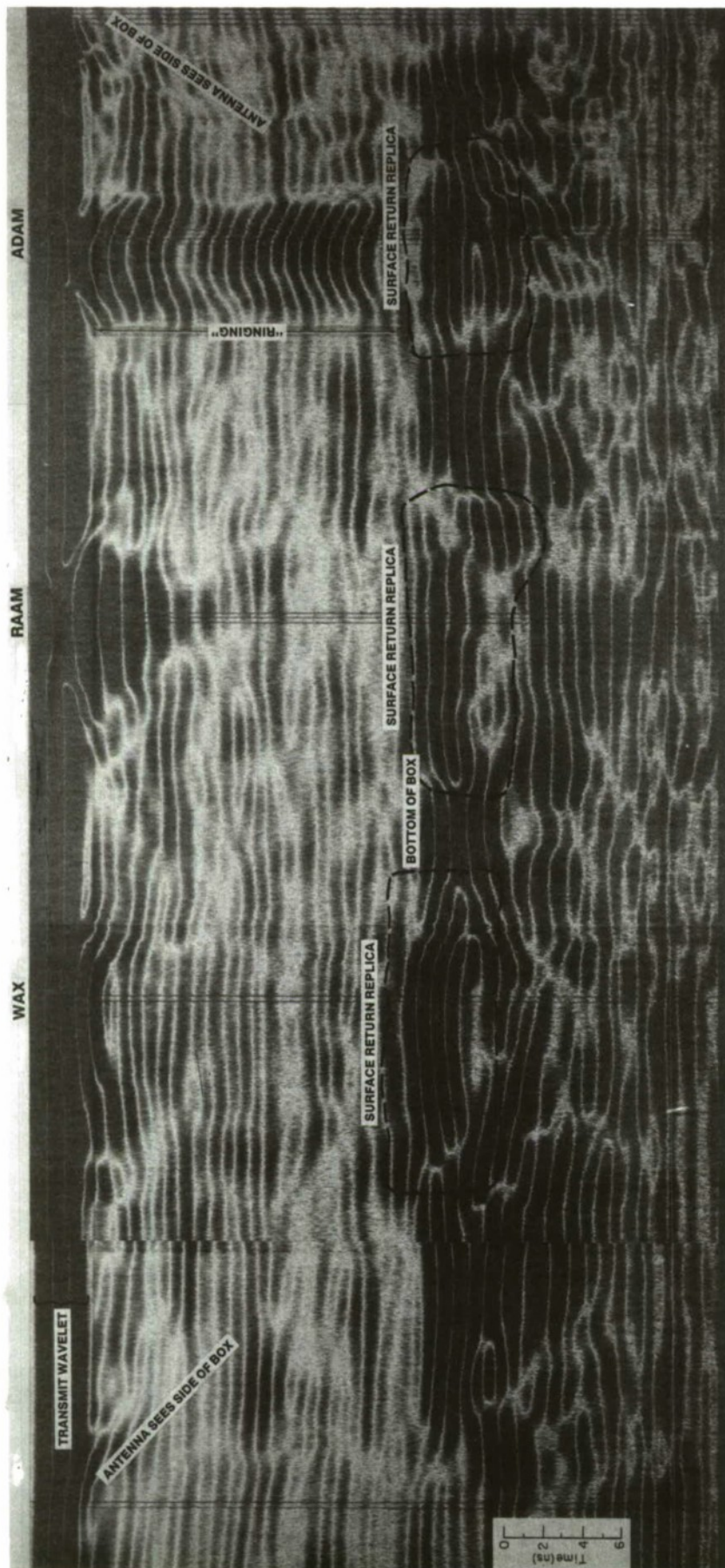
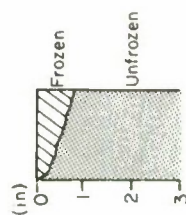


Figure A16.

Date: 7 Sept 82
 Time: - 1200
 Tape Number: MB2
 Tape Channel(s): 1
 Approx. Tape Count: 0735-0940
 Test Location: IEF cold storage room
 Media Conditions: 0 to 1/2 in. frozen silty sand
 Antenna Location: Surface
 Antenna Model: 101C
 Line of Survey: Centerline
 Data: Unprocessed



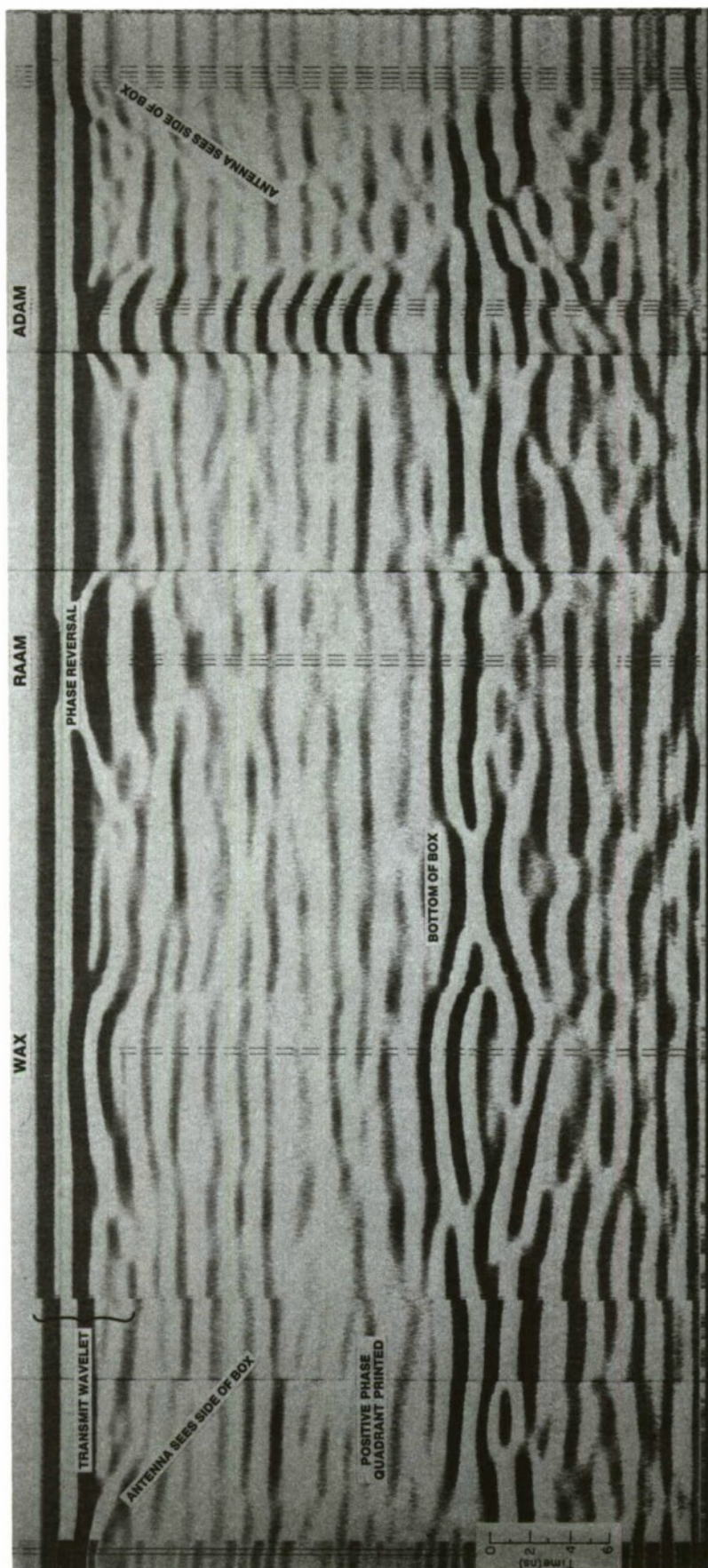
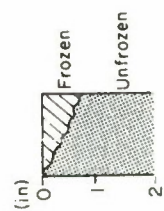


Figure A17.

Date: 7 Sept 82
 Time: 1200
 Tape Number: MB2
 Tape Channel: 1
 Approx. Tape Count: 0735.9940
 Test Location: IEF cold storage room
 Media Condition: 0 to 10 in. frozen silty sand
 Antenna Location: Surface
 Antenna Model: 101C
 Line of Survey: Centerline
 Date: Print



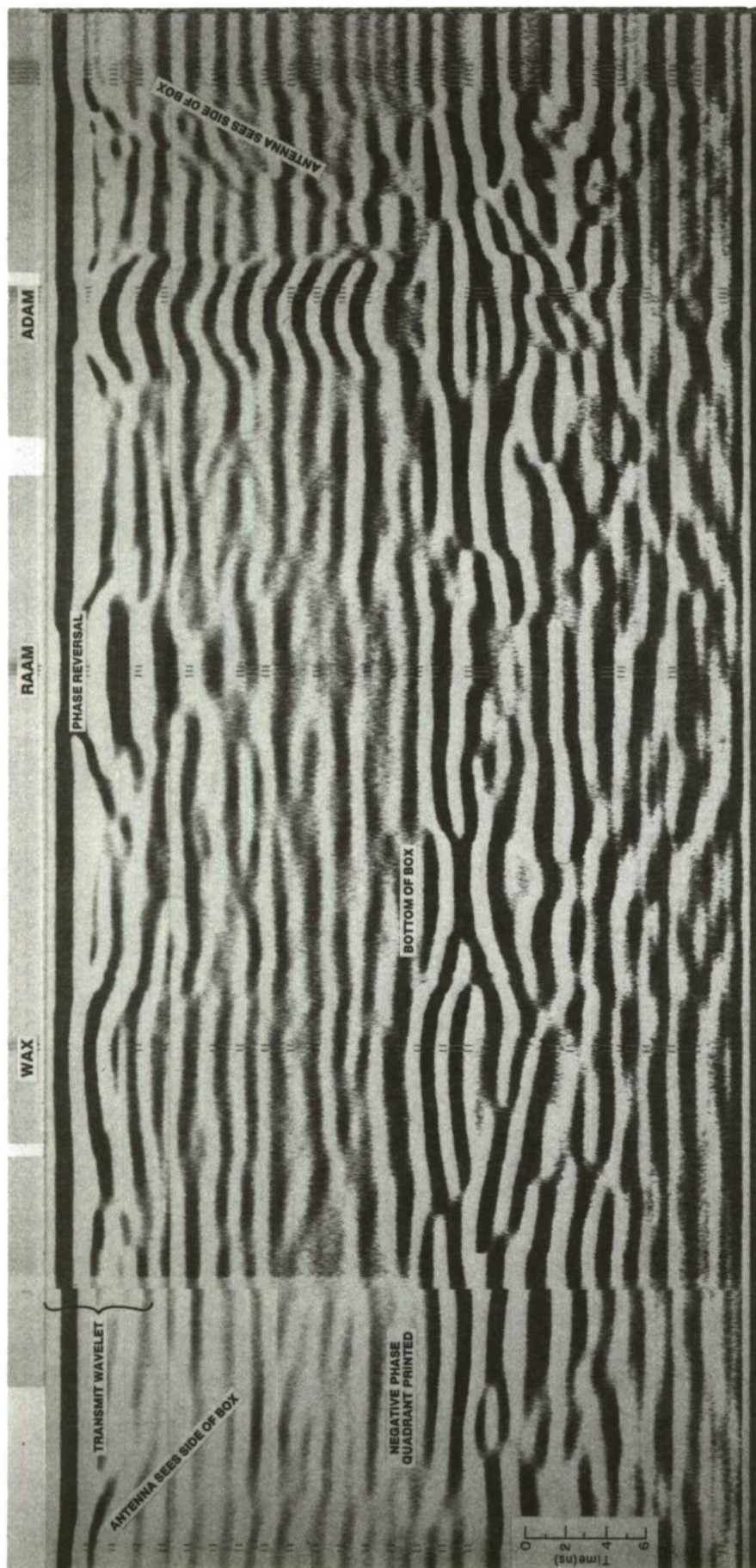


Figure A18.

Date: 7 Sept 82
Time: 1200

Type Number: MB2

Type Channel(s): t

Approx. Tape Count: 0735-0940

Test Location: IEF solid storage room

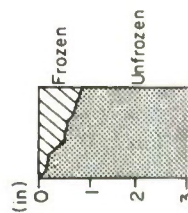
Media Conditions: 0 to 1 in. frozen silty sand

Antenna Location: Surface

Antenna Model: 101C

Line of Survey: Cantarlina

Data: Print: "..."



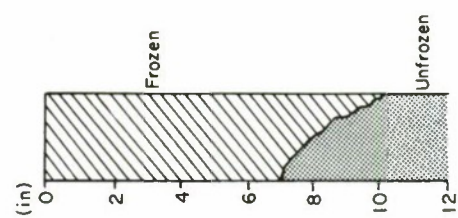
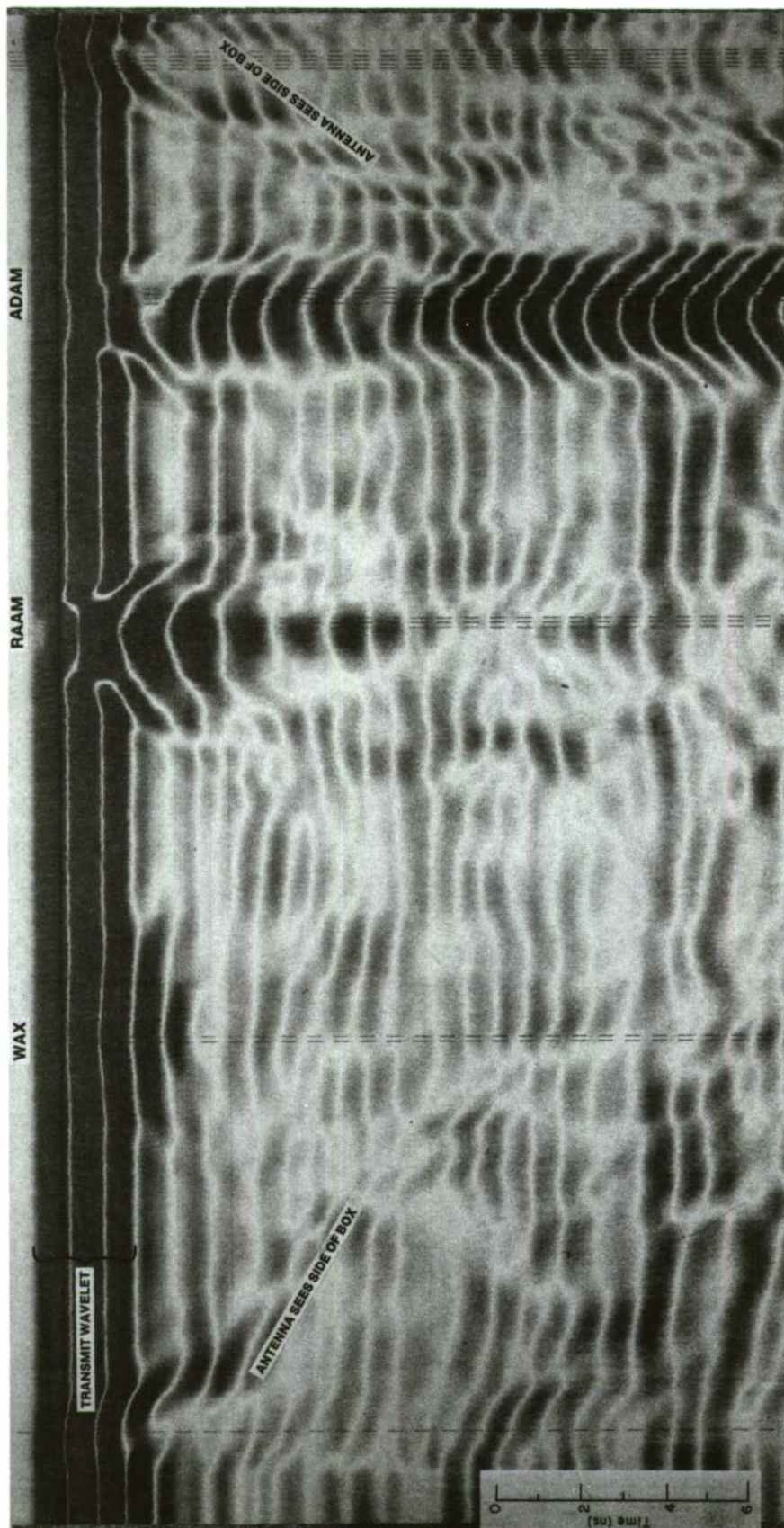


Figure A19.

Date: 14 Sept 82
 Time: 1200
 Tape Number: MB4
 Tape Channel(s): 1
 Approx. Tape Count: 1425-1554
 Test Location: IEF cold storage room
 Media Conditions: 7 to 10 in. frozen silty sand
 Antenna Location: On surface
 Antenna Model: 101C
 Line of Survey: Centerline
 Date: Unprocessed

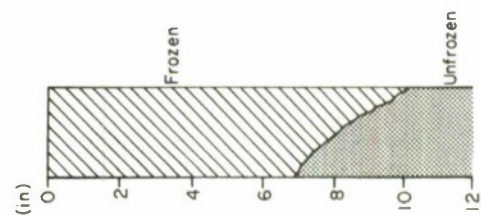
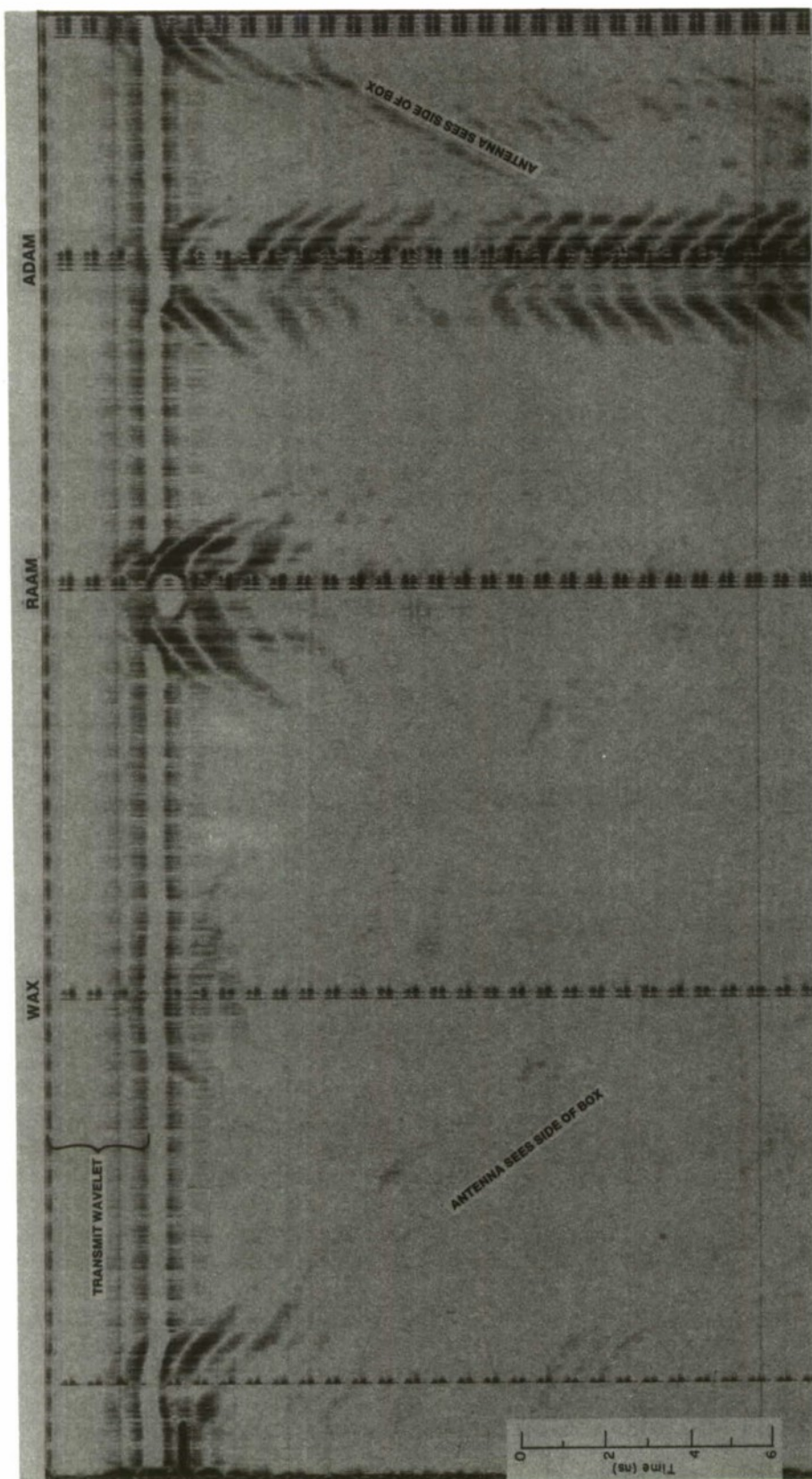


Figure A20.
 Date: 14 Sept 82
 Time: 1200
 Tape Number: MB4
 Tape Channels: 1
 Approx. Tape Count: 1425-1554
 Test Location: IEF cold storage room
 Media Conditions: 7 to 10 in. frozen silty sand
 Antenna Location: On surface
 Antenna Model: 101C
 Line of Survey: Centerline
 Data: Program 2.7

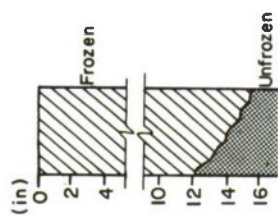
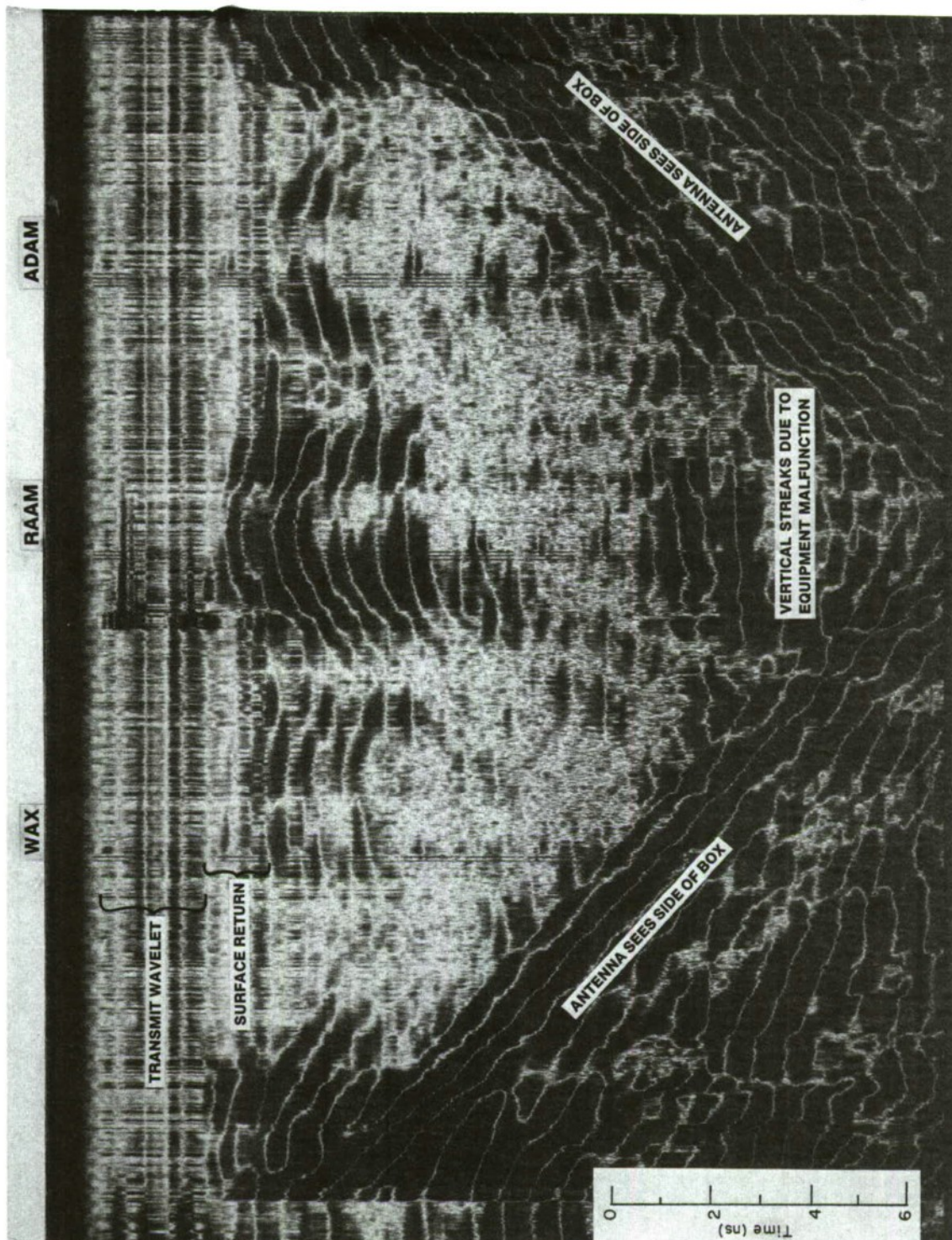


Figure A21.

Date: 7 Oct 92
Time:

Tape Number: MB10

Tape Channel(s): 1, 2, 4

Approx. Tape Count: 9420-0767

Test Location: IEF cold storage room

Media Conditions: 12 to 15 in. frozen silty sand

wicobbles

Antenna Location: 12 in. off surface

Antenna Model: 101C

Line of Survey: Centerline

Data: Program 2-3

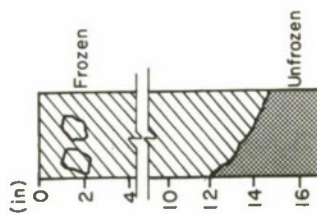
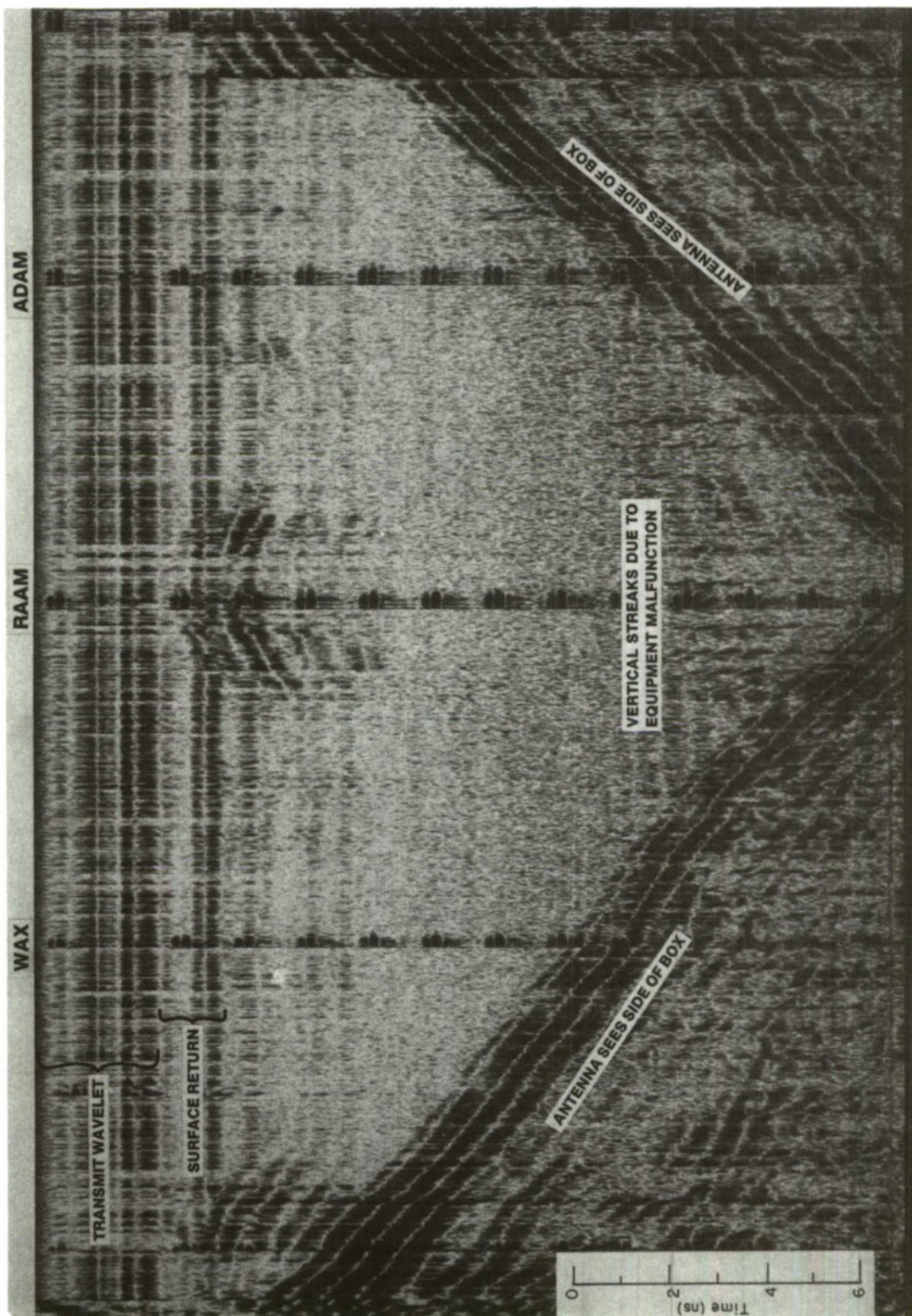


Figure A22.

Date: 7 Oct 82
 Time:
 Tape Number: MB10
 Tape Channel(s): 1, 2, 4
 Approx. Tape Count: 0045-0420
 Test Location: IEF cold storage room
 Media Conditions: 12 to 14 in. frozen silty sand
 w/cobbles
 Antenna Location: 12 in. off surface
 Antenna Model: 101C
 Line of Survey: Centerline
 Data: Program 2-7

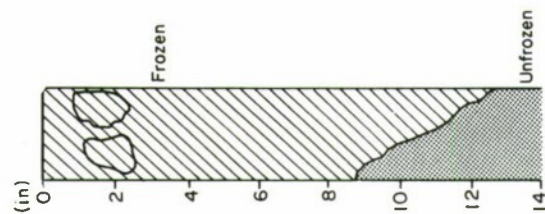
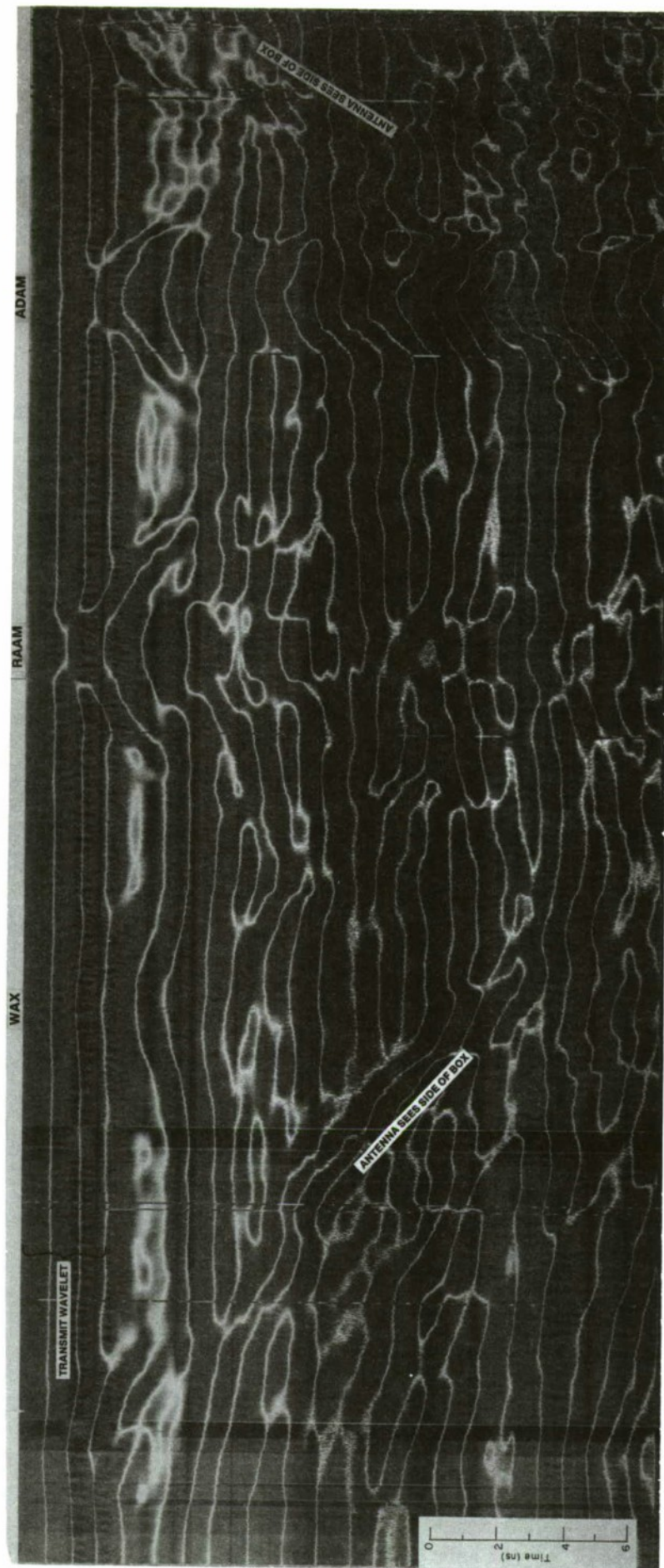


Figure A23.

Date: 4 Oct 82
 Time: 1255
 Tape Number: MB8
 Tape Channels: 1, 4
 Approx. Tape Count: 0765-0961
 Test Location: IEF cold storage room
 Media Conditions: 9 to 12 in. frozen silty sand
 w/cobbles
 Antenna Location: Surface
 Antenna Model: 101C
 Line of Survey: Centerline
 Data: Unprocessed

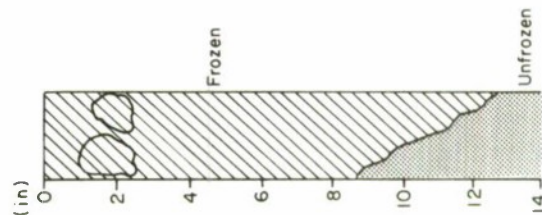


Figure A24.

Date: 4 Oct 82
 Time: 1255
 Tape Number: MB8
 Tape Channel(s): 1, 4
 Approx. Tape Count: 0765-0961
 Test Location: IEF cold storage room
 Media Conditions: 9 to 13 in. frozen silty sand
 w/cobbles
 Antenna Location: Surface
 Antenna Model: 101C
 Line of Survey: Centerline
 Des.: Print

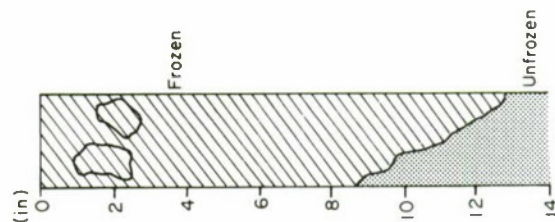
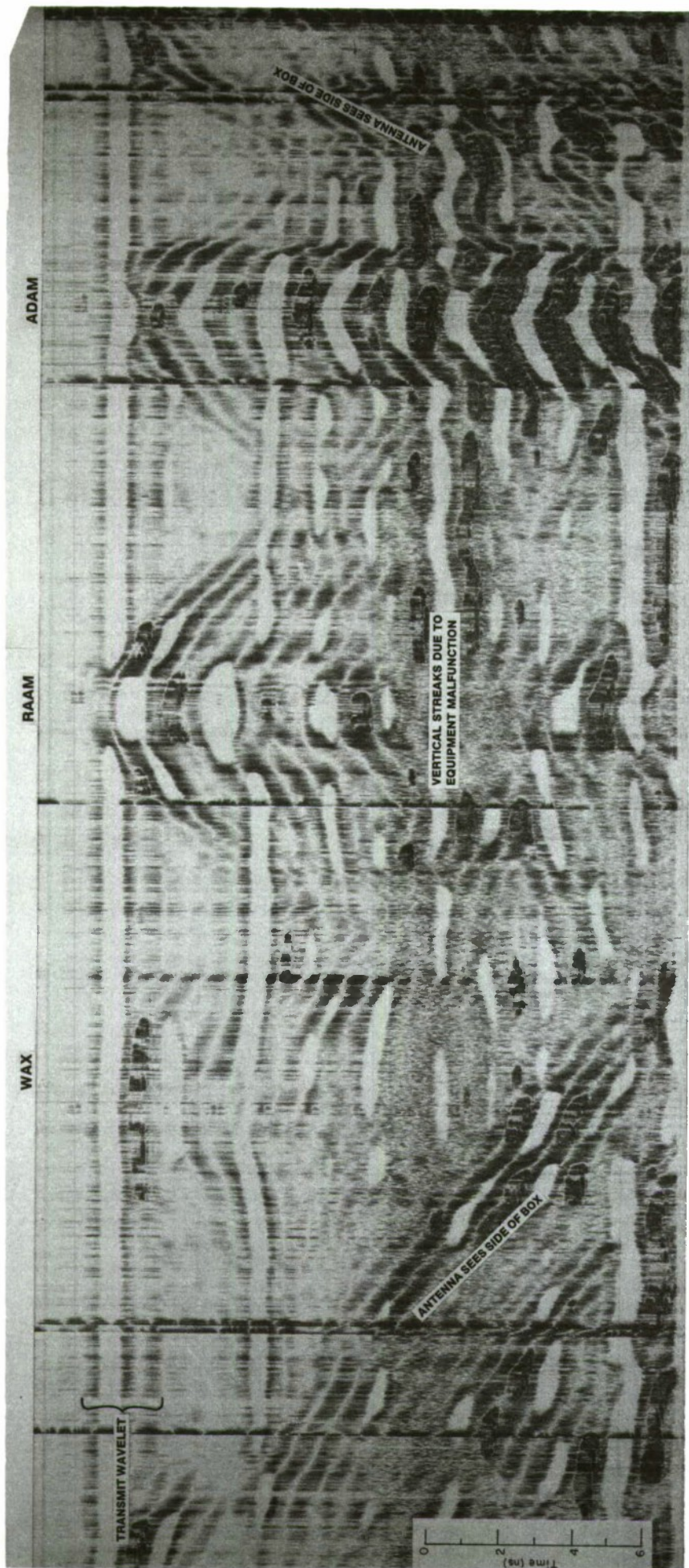


Figure A25.

Date: 4 Oct 82
 Time: 1255
 Tape Number: MB8
 Tape Channel(s): 1, 4
 Approx. Tape Count: 0765-0961
 Test Location: IEF cold storage room
 Media Conditions: 9 to 13 in. frozen silty sand
 w/cobbles
 Antenna Location: Surface
 Antenna Model: 101C
 Line of Survey: Centerline
 Data Program: 2.3

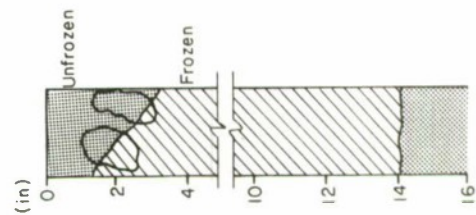
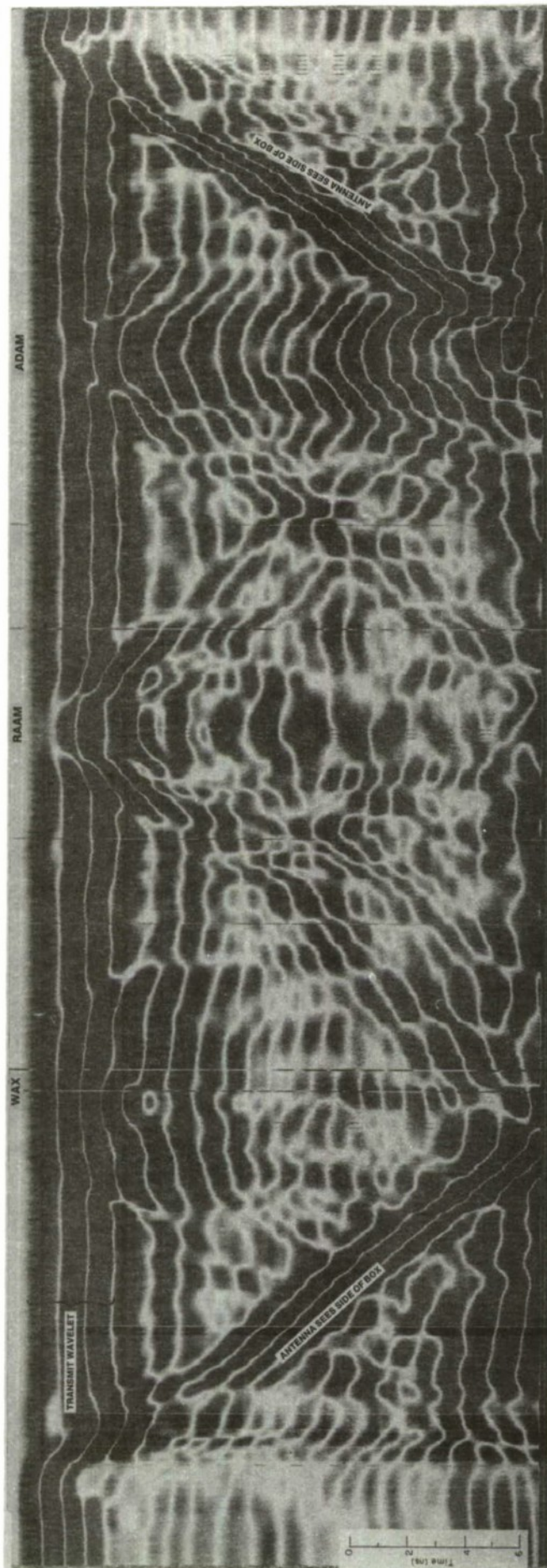


Figure A26.

Date: 8 Oct 82
 Time: 1356
 Tape Number: MB9
 Tape Channels: 1, 2, 4
 Approx. Tape Count: 0866-1085
 Test Location: IEF cold storage room
 Media Conditions: 14 in. frozen silty sand w/cob-
 blis. w/surface thaw
 Antenna Location: Surface
 Antenna Model: 101C
 Line of Survey: Centerline
 Data: Unprocessed

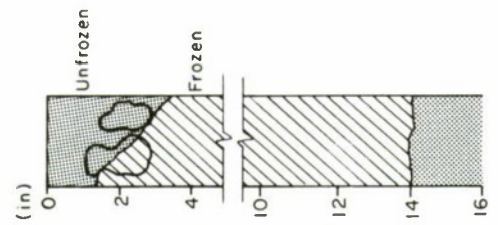
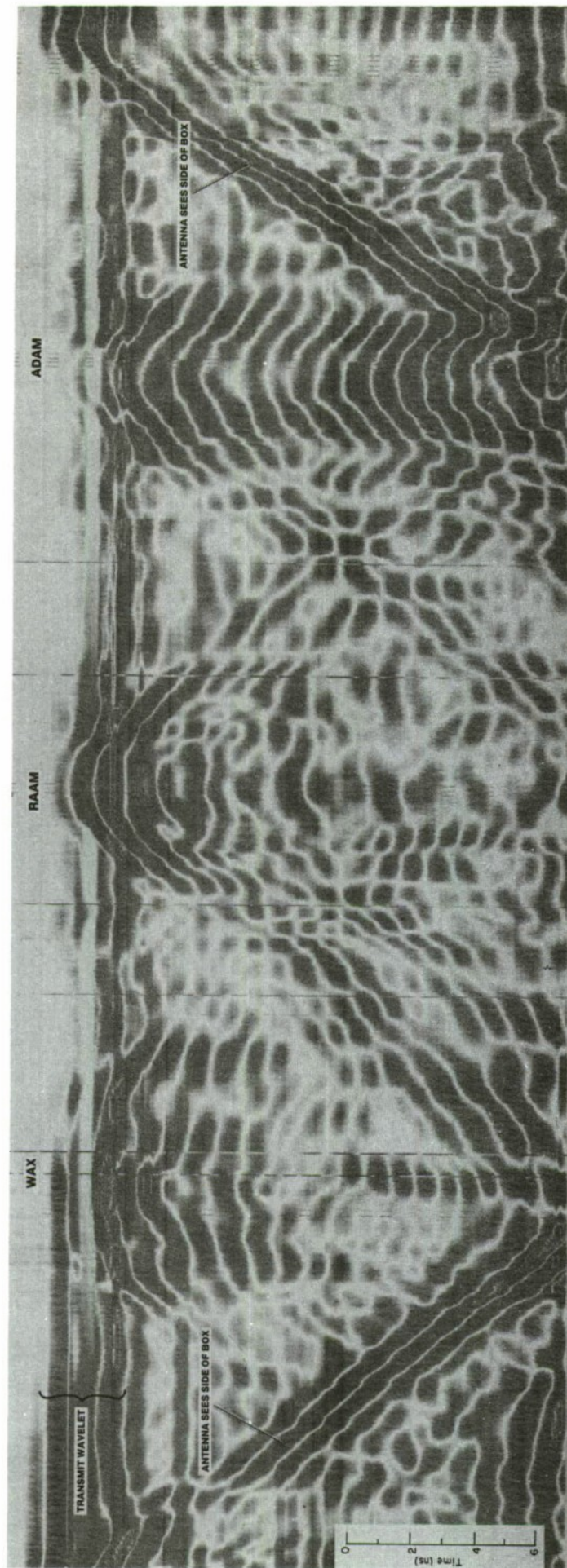


Figure A27.

Date: 6 Oct 82
 Time: 1356
 Tape Number: MB9
 Tape Channel(s): 1, 2, 4
 Approx. Tape Count: 0866 - 1085
 Test Location: IEF cold storage room
 Media Conditions: 14 in. frozen silty sand w/cob-
 bles, w/surface thew
 Antenna Location: On surface
 Antenna Model: 101C
 Line of Survey: Centerline
 Date: Program 2.1

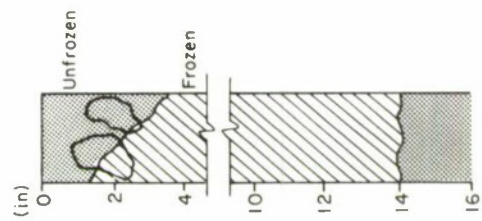


Figure A28.

Date: 6 Oct 1982
 Time: 1356
 Tape Number: M89
 Tape Channel(s): 1, 2, 4
 Approx. Tape Count: 0865-1085
 Test Location: IEF cold storage room
 Media Conditions: 14 in. frozen silty sand w/cob-
 bles; 1 to 3 in. surface thaw
 Antenna Location: Surface
 Antenna Model: 101C
 Line of Survey: Centerline
 Data: Program 2.3

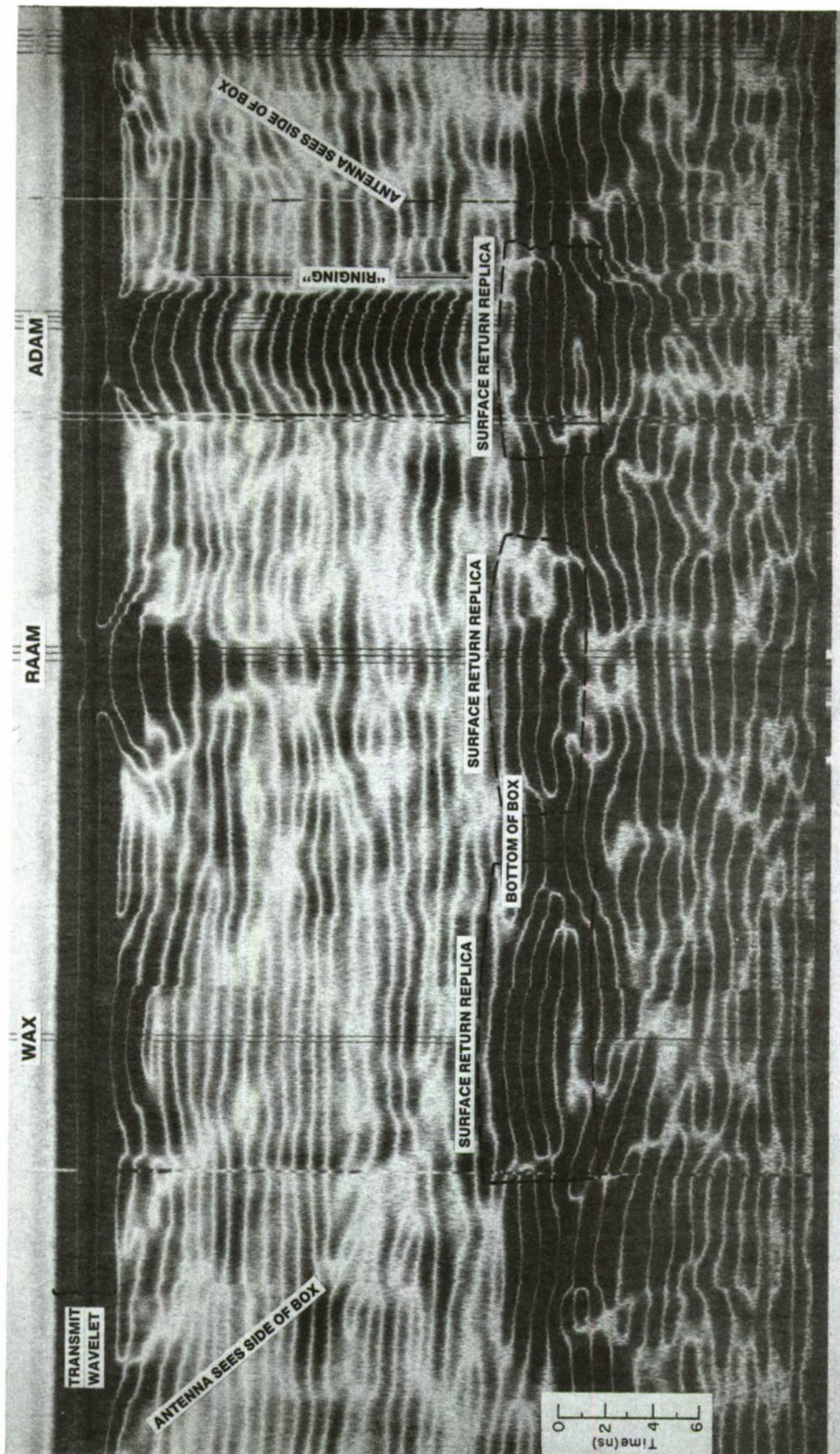
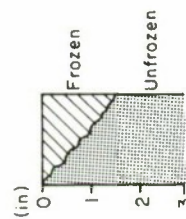


Figure A29.

Date: 8 Sept 82
 Time: 0900
 Tape Number: 482
 Tape Channel(s):
 Approx. Tape Count: 1698-1801
 Test Location: IEF cold storage room
 Media Conditions: 1 to 1 in. frozen silty sand
 Antenna Location: Surface
 Antenna Model: 101C
 Line of Survey: Centerline
 Data: Unprocessed



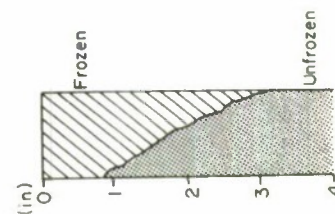
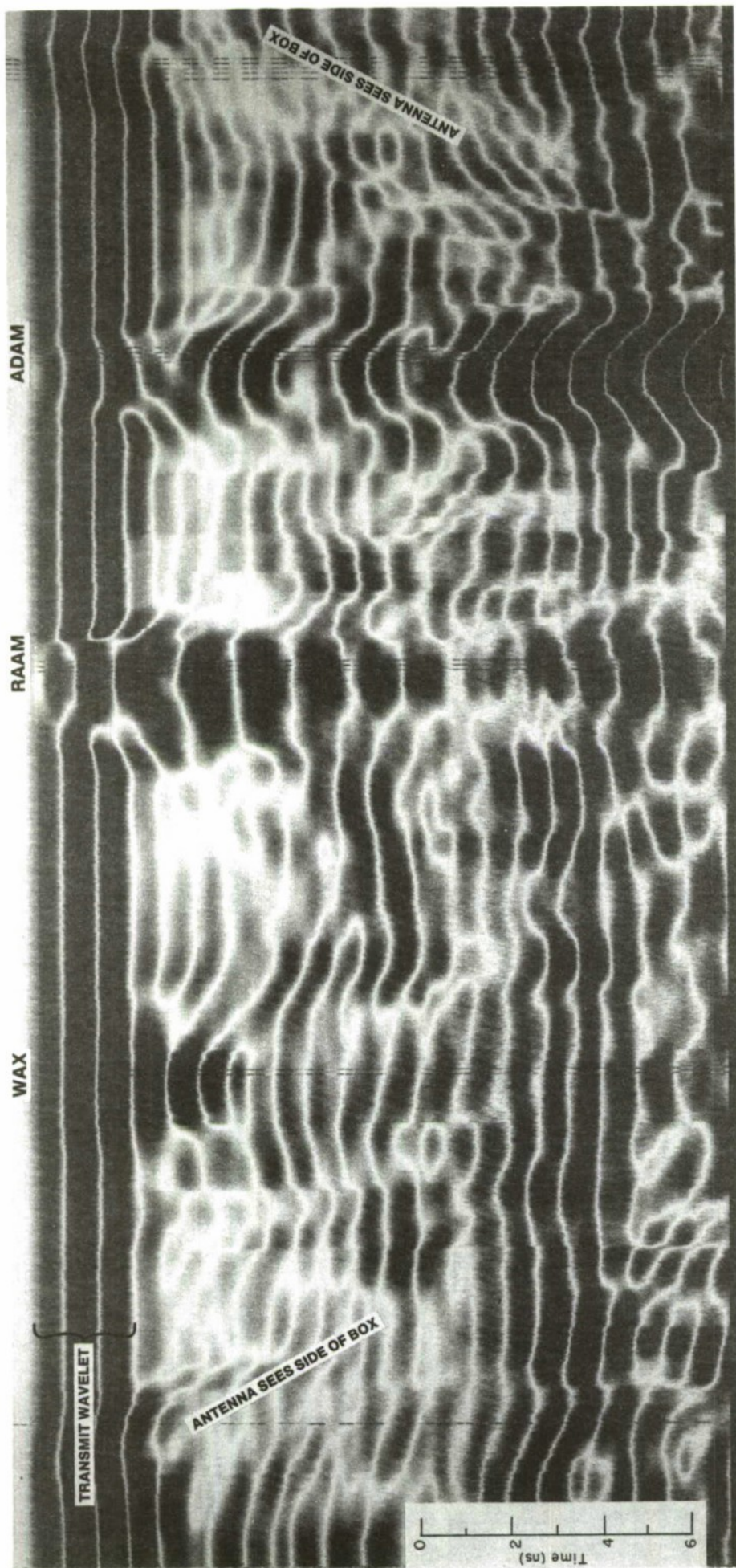


Figure A30.

Date: 8 Sept 82
 Time: 1530
 Tape Number: MB3
 Tape Channel(s):
 Approx. Tape Count: 1498-1512
 Test Location: IEF cold storage room
 Media Conditions: 1 to 3 in. frozen silty sand
 Antenna Location: Surface
 Antenna Model: 101C
 Line of Survey: Centerline
 Data: Unprocessed

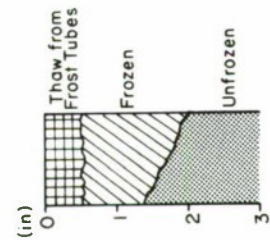
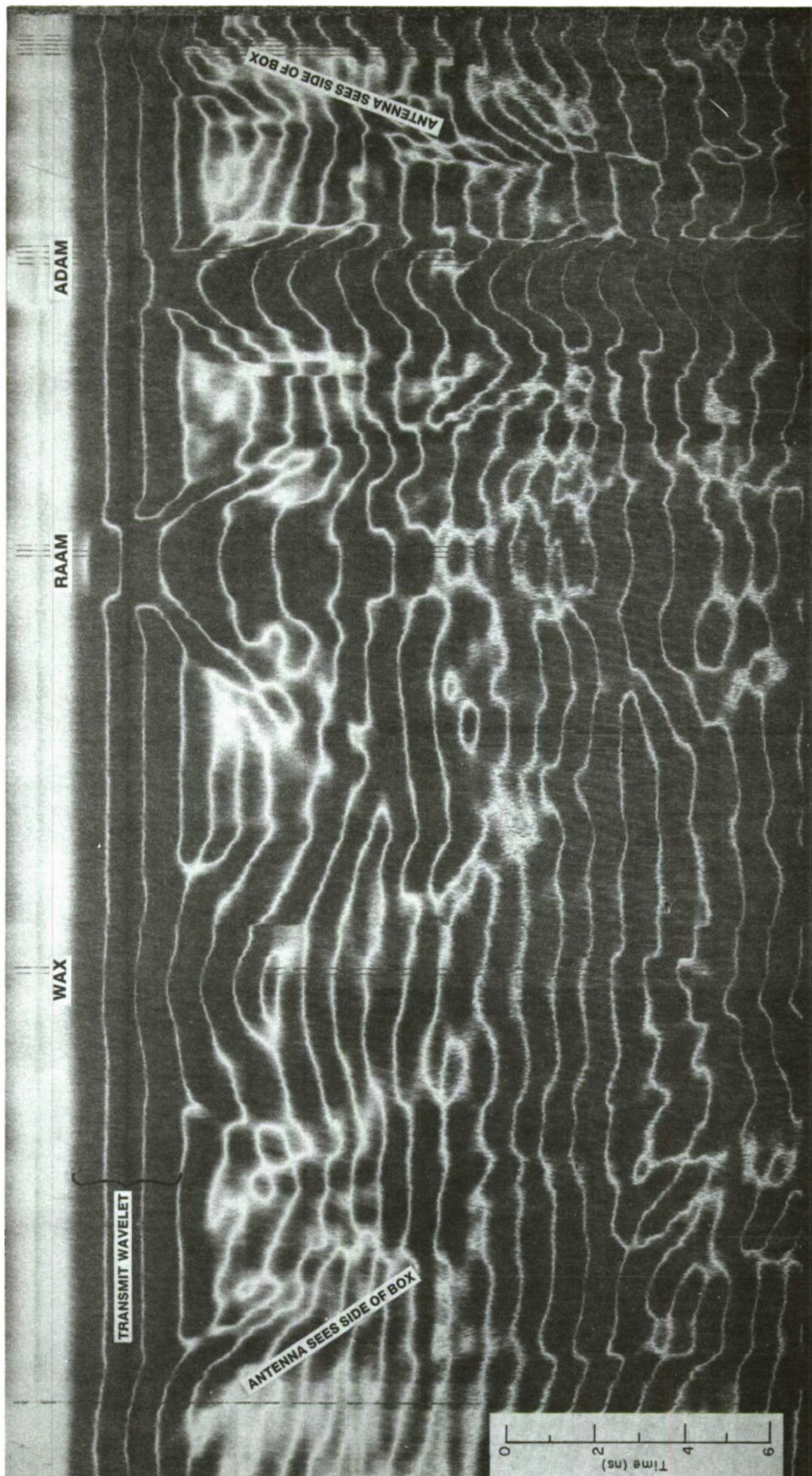


Figure A31.

Date: 10 Sept 82
Time: 1345

Tape Number: MB4
Tape Channel(s): 1

Approx. Tape Count: 6128-0388

Test Location: IEP cold storage room
Media Condition: 1 1/2 to 2 in. frozen silty sand,
w/surface thaw

Antenna Location: On surface
Antenna Model: 101C
Line of Survey: Centerline
Date: Unprocessed

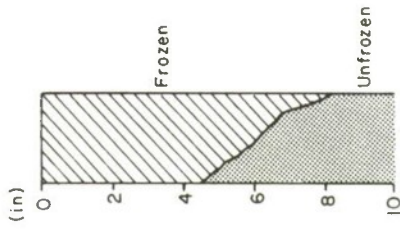
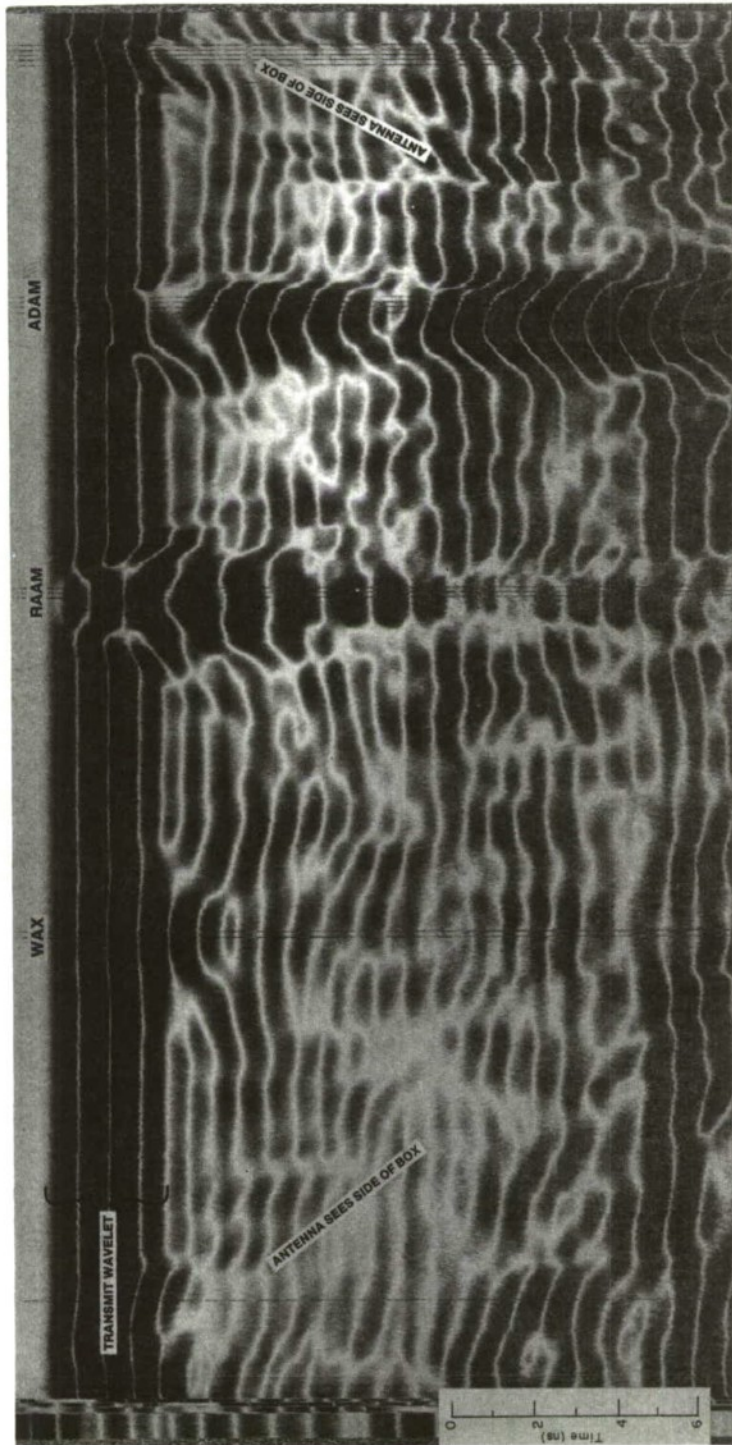


Figure A32.

Date: 13 Sept 82
 Time: 1110
 Tape Number: MB4
 Tape Channel(s): 1
 Approx. Tape Count: 0393-0505
 Test Location: IEF cold storage room
 Media Conditions: 4 to 8 in. frozen silty sand
 Antenna Location: Surface
 Antenna Model: 101C
 Line of Survey: Centerline
 Date: Unprocessed



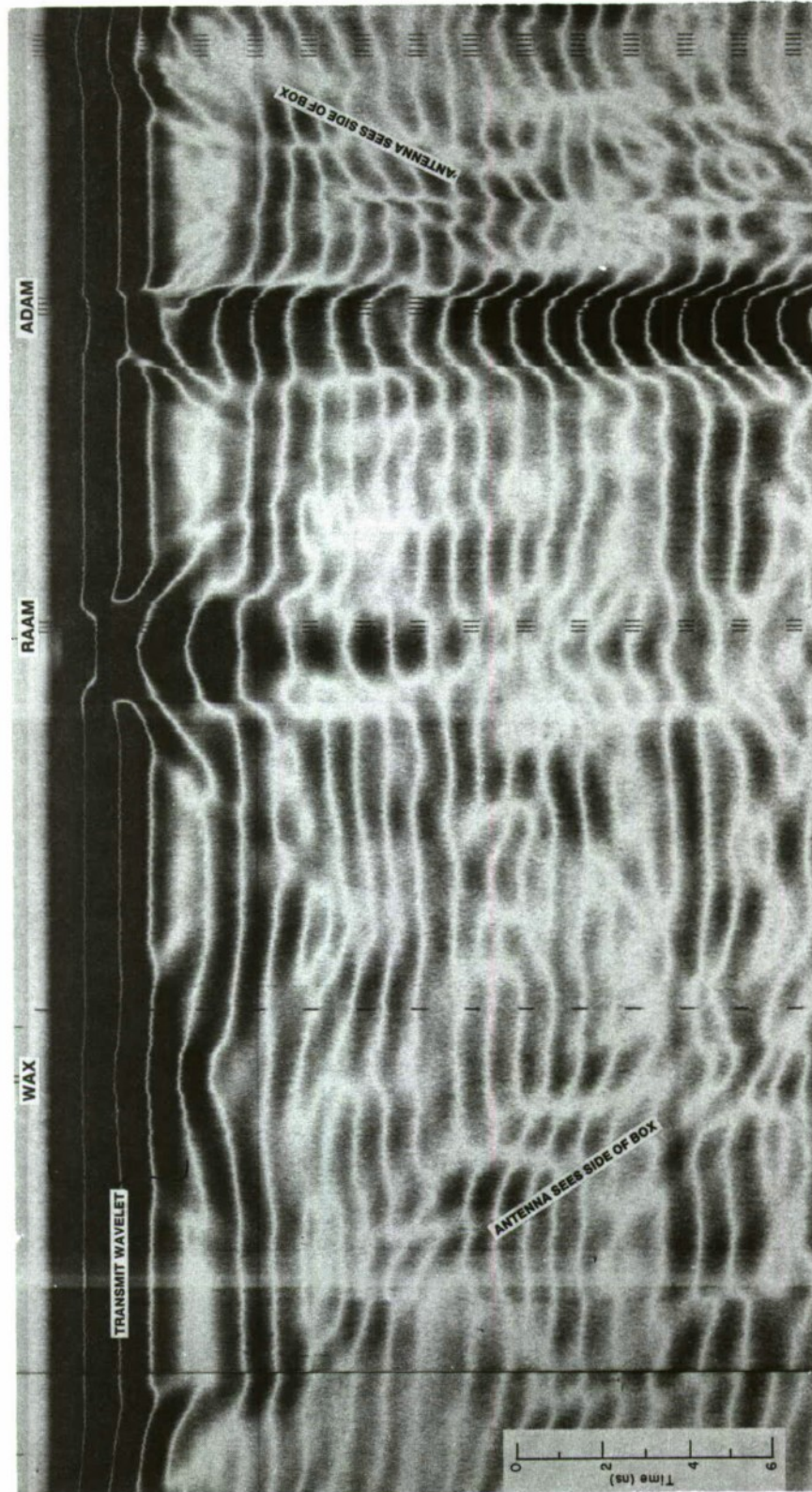
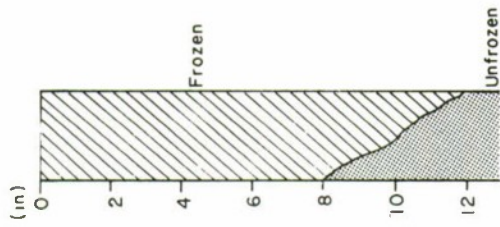


Figure A33.

Date: 15 Sept 82
 Time: 0845
 Tape Number: MB4
 Tape Channel: MB4
 Approx. Tape Count: 1558-1692
 Test Location: IEF cold storage room
 Media Conditions: 8 to 12 in. frozen silty sand
 Antenna Location: On surface
 Antenna Model: 101C
 Line of Survey: Centerline
 Date: Unprocessed

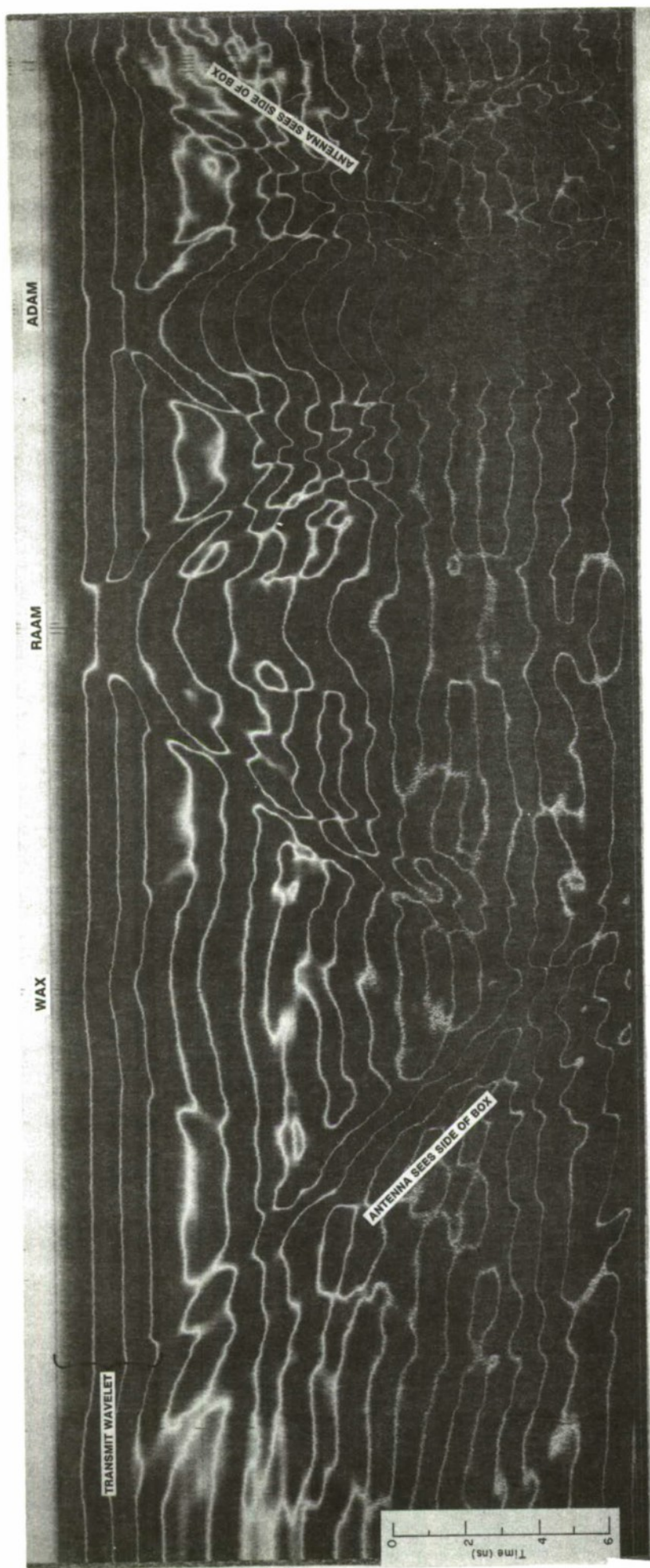
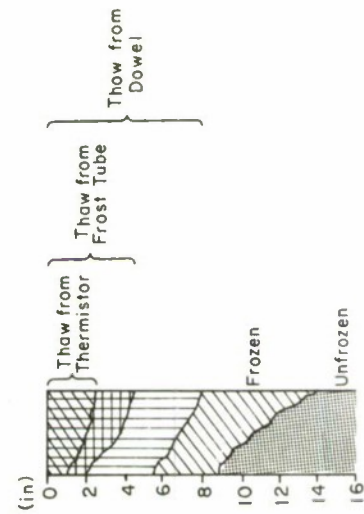


Figure A34.

Date: 16 Sept 82
 Time: 1114
 Tape Number: M85
 Tape Channel(s): 1
 Approx. Tape Count: 0813:1013
 Test Location: IEF cold storage room
 Media Conditions: 8 to 14 in. frozen silty sand
 w/1 to 6 in. thaw
 Antenna Location: Surface
 Antenna Model: 101C
 Line of Survey: Centarline
 Data: Unprocessed



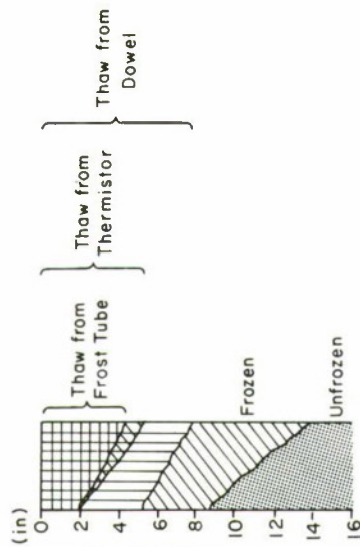
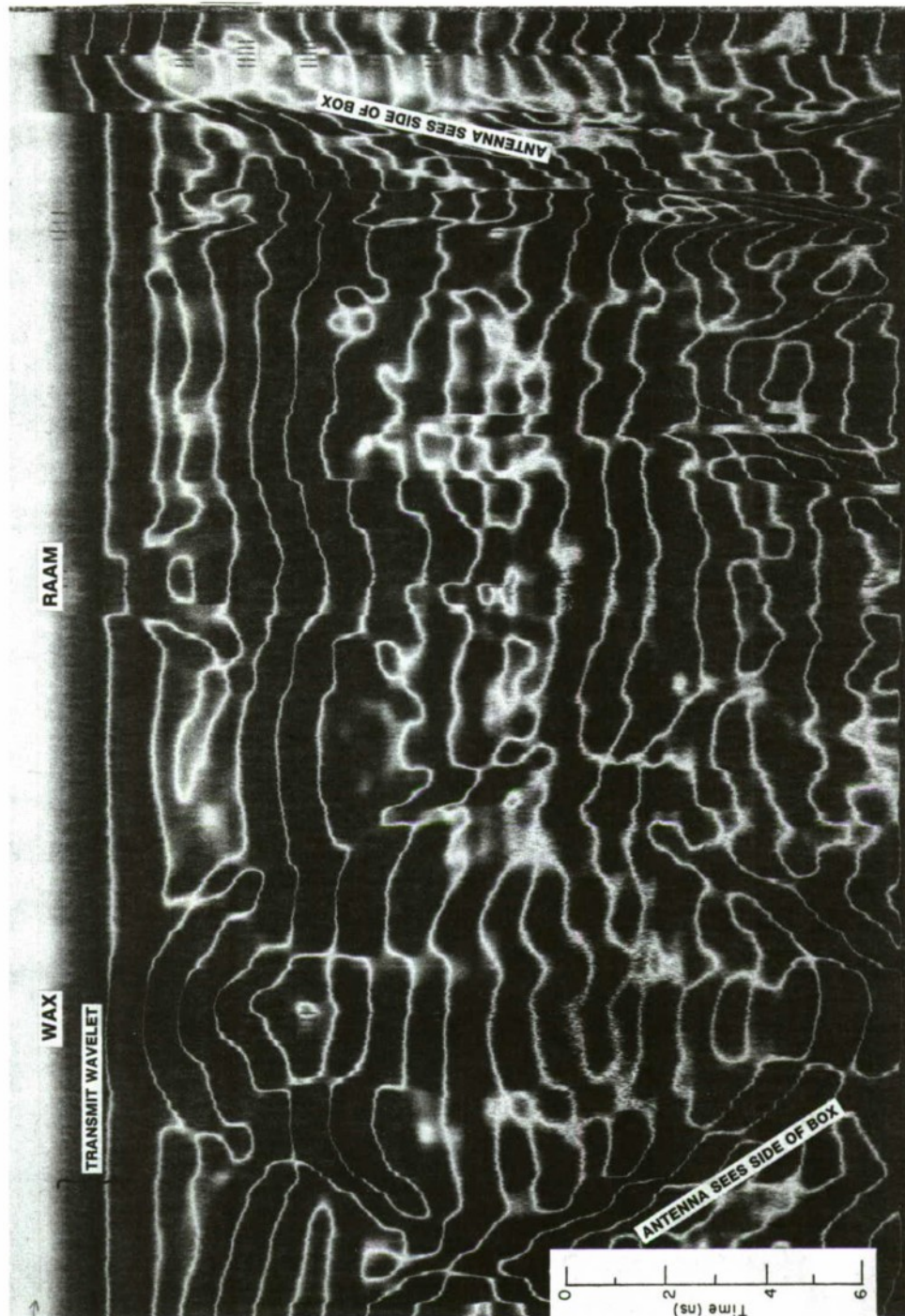


Figure A35.

Date: 15 Sept 82
 Time: - 1550
 Tape Number: MB5
 Tape Channel(s): 1
 Approx. Tape Count: 1041-1180
 Test Location: JEF cold storage room
 Media Conditions: 9 to 14 in. frozen silty
 sand—after wetting
 Antenna Location: Surface
 Antenna Model: 101C
 Line of Survey: Centerline
 Data: Unprocessed

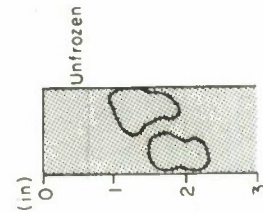
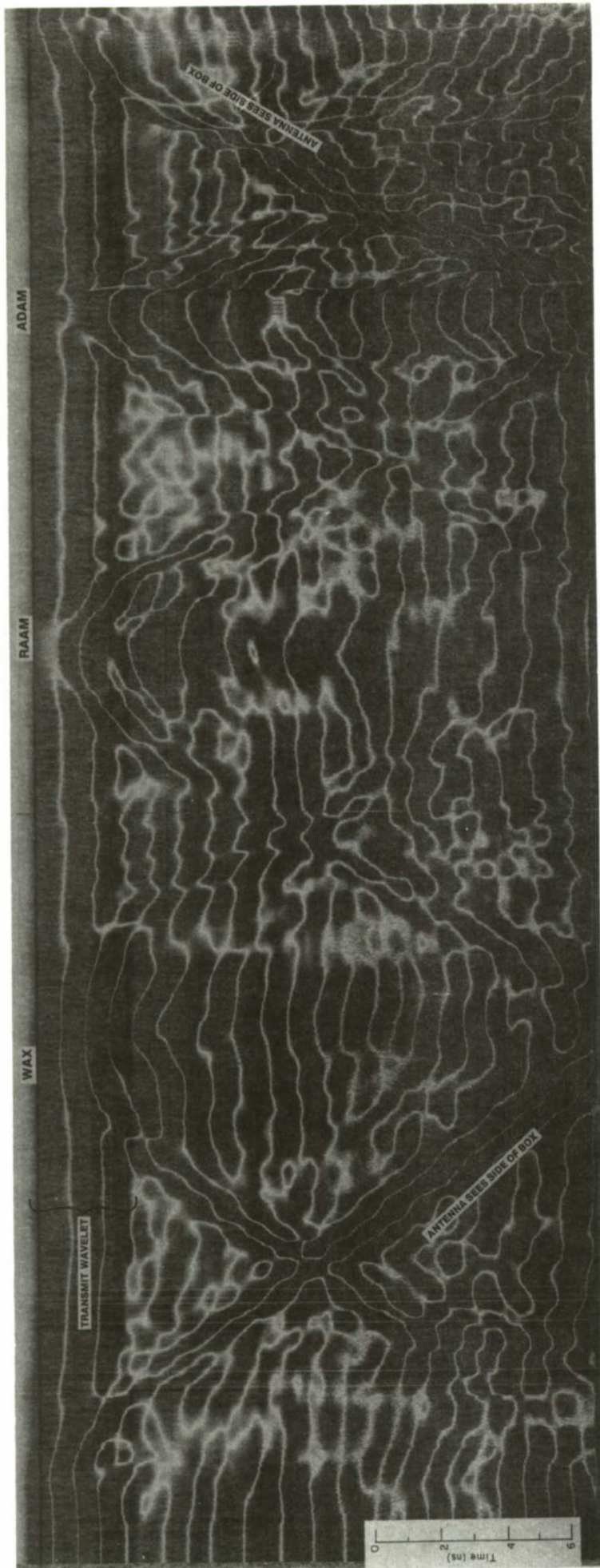


Figure A36.

Date: 29 Sept 82

Time: 1450

Tape Number: MB8

Tape Channel(s): 1, 4

Approx. Tape Count: 0701-0938

Test Location: IEP cold storage room

Media Conditions: Silty sand w/cobbles

Antenna Location: Surface

Antenna Model: 101C

Line of Survey: Centerline

Data: Unprocessed

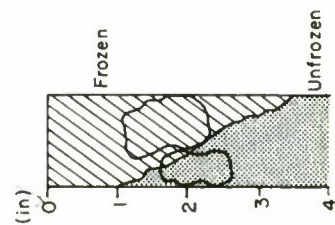
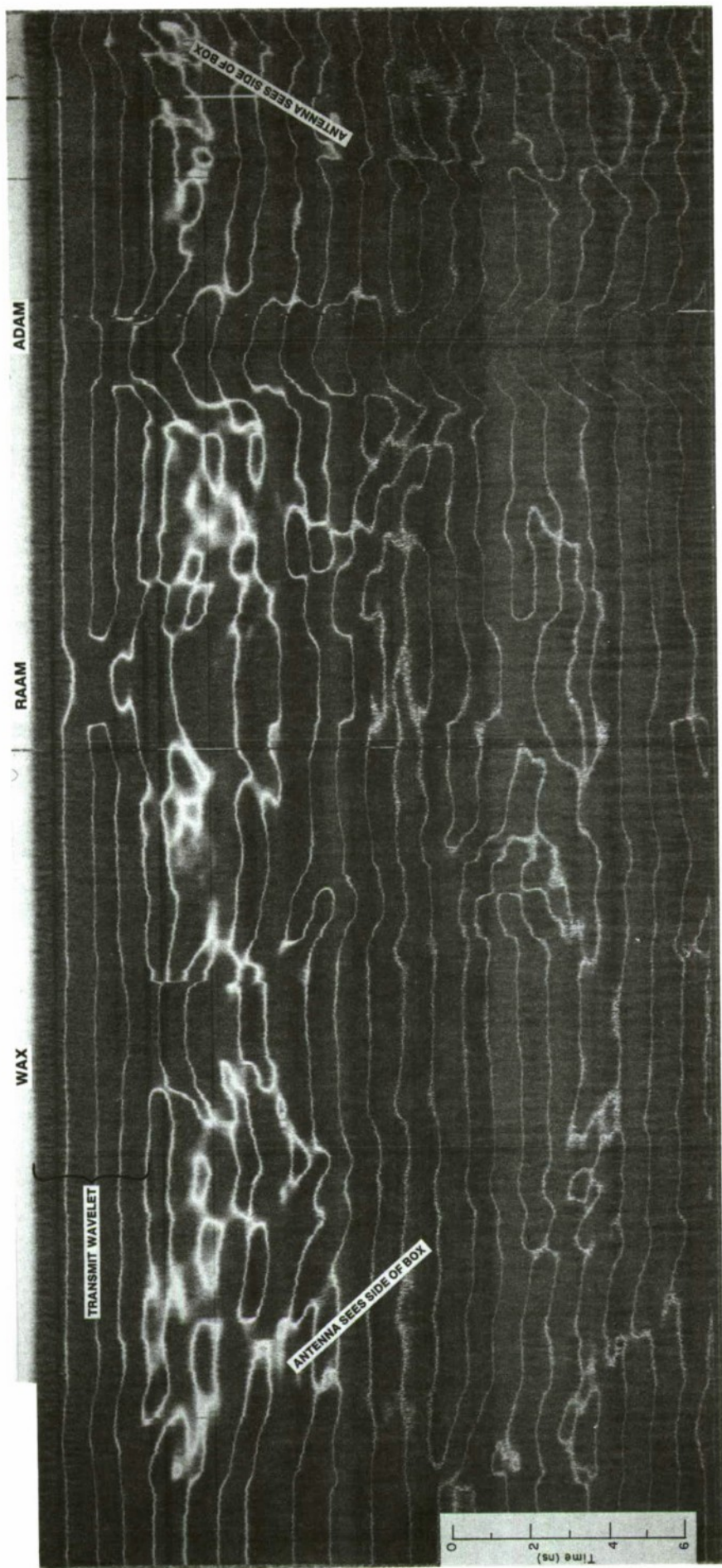


Figure A37.

Date: 30 Sept 82
 Time: -0845
 Tape Number: MB6
 Tape Channel(s):
 Approx. Tape Count: 1873-1803
 Test Location: IEF cold storage room
 Media Conditions: 1 to 3 1/4 in. frozen silty sand
 w/cobbles
 Antenna Location: Surface
 Antenna Model: 101C
 Line of Survey: Centerline
 Data: Unprocessed

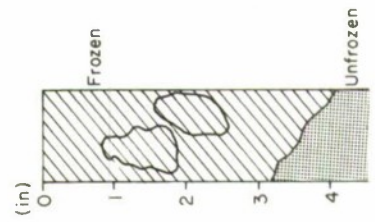
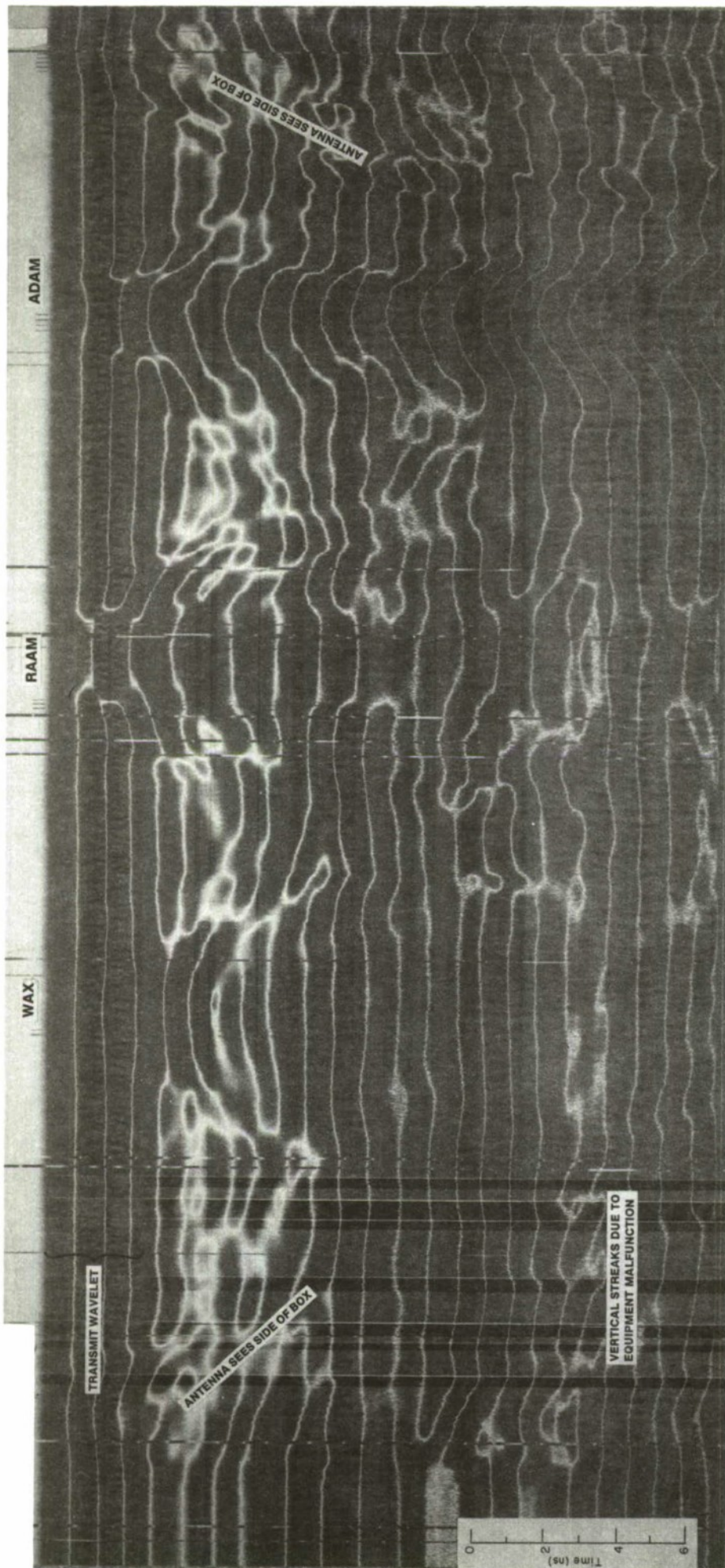


Figure A38.

Date: 30 Sept 82
 Time: 1345
 Tape Number: MB7
 Tape Channel(s):
 Approx. Tape Count: 0150-0438
 Test Location: IEF cold storage room
 Media Conditions: 3 to 4 in. frozen silty sand
 w/cobbles
 Antenna Location: Surface
 Antenna Model: 101C
 Line of Survey: Centerline
 Data: Unprocessed

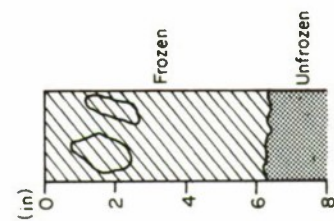
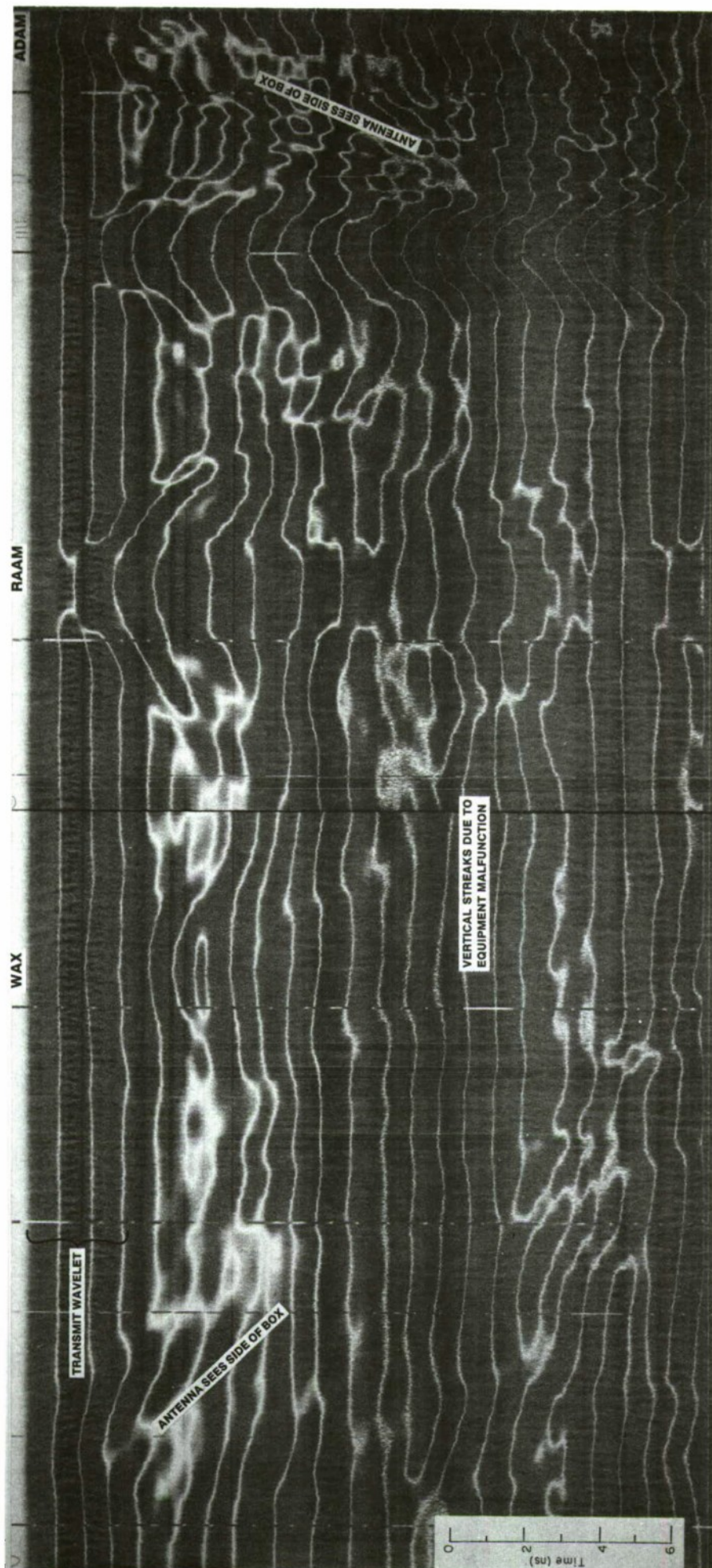


Figure A39.

Date: 1 Oct 82
 Time: 1300
 Type Number: 447
 Type Channel(s): 1, 4
 Approx. Tape Count: 1250-1378
 Test Location: EP cold storage room
 Media Conditions: 8 in. frozen silty sand w/cob-
 bles
 Antenna Location: On surface
 Antenna Model: 101C
 Line of Survey: Centerline
 Data: Unprocessed

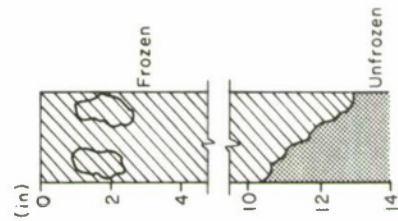
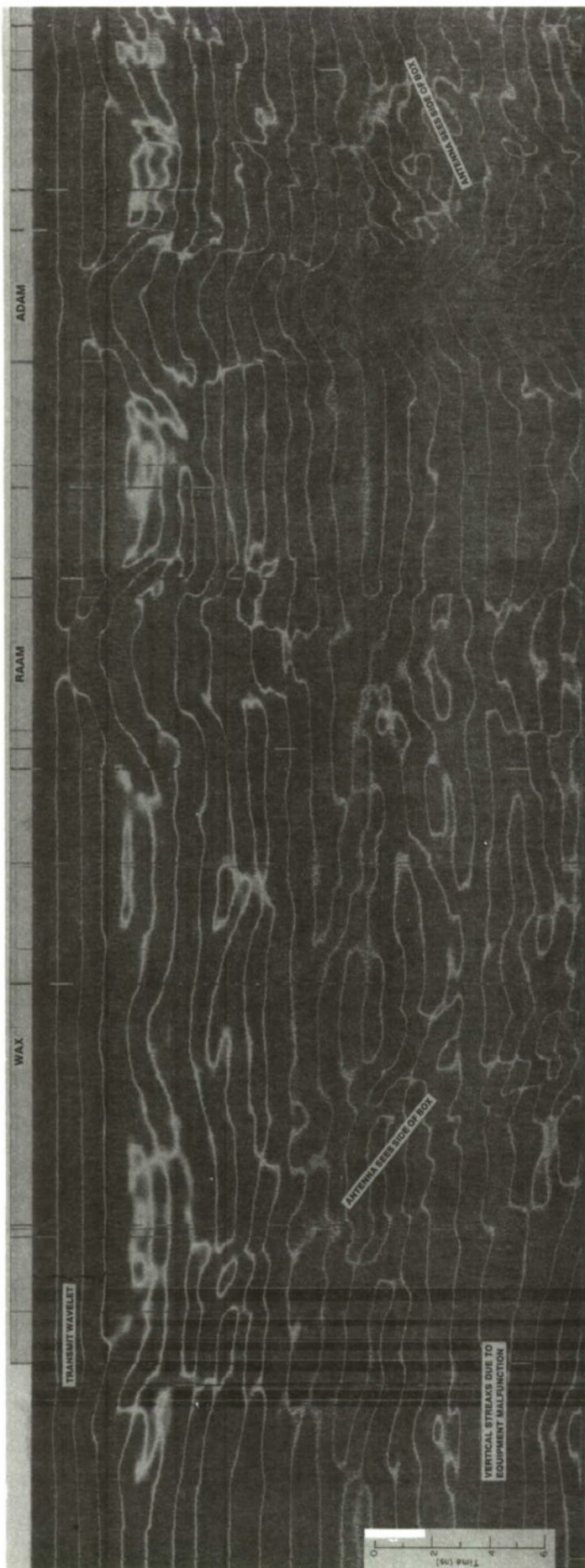


Figure A40.

Date: 5 Oct 82
 Time: 0823
 Tape Number: MB8
 Tape Channel(s): 1, 4
 Test Count: 1030-1230
 Test Location: IEF cold storage room
 Media Conditions: 10 to 13 in. frozen silty sand
 Antenna Location: On surface wicobles
 Antenna Model: 101C
 Line of Survey: Centerline
 Date: Unprocessed

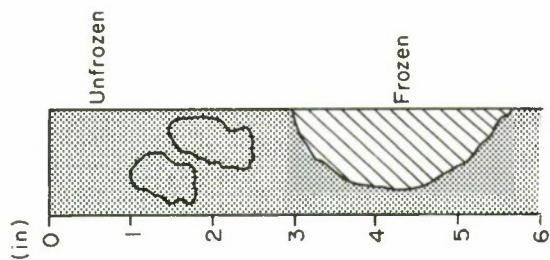
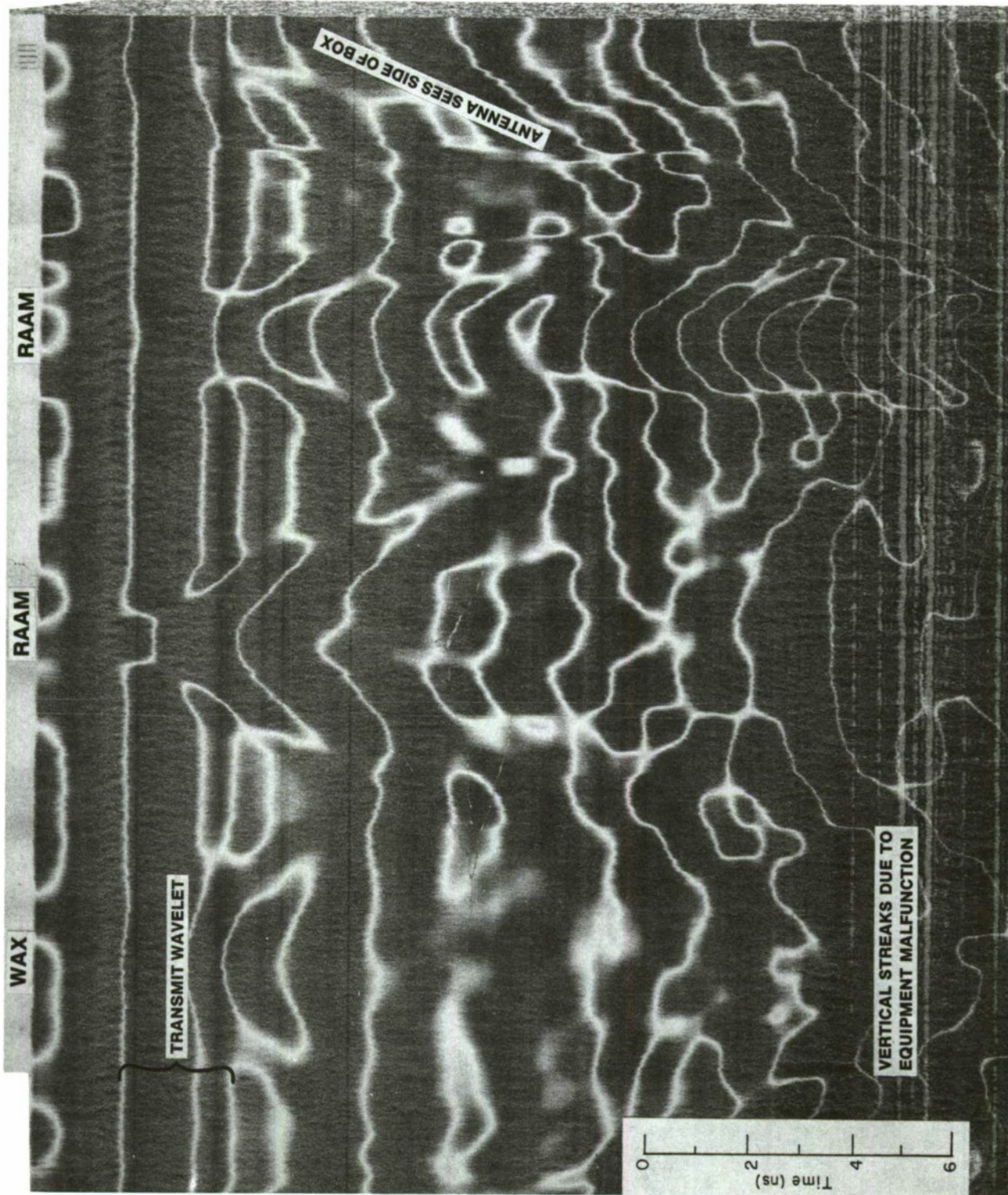


Figure A41.

Date: 5 Nov 82
 Time: 1529
 Tape Number: MB12
 Tape Channel(s): 1, 4
 Approx. Tape Count: 1045-1159
 Test Location: IEF cold storage room
 Media Conditions: 3 to 6 in. frozen elly sand
 w/cobbles; thaw to 3 in.
 Antenna Location: Surface
 Antenna Model: 3102
 Line of Survey: Centerline
 Date: Unprocessed

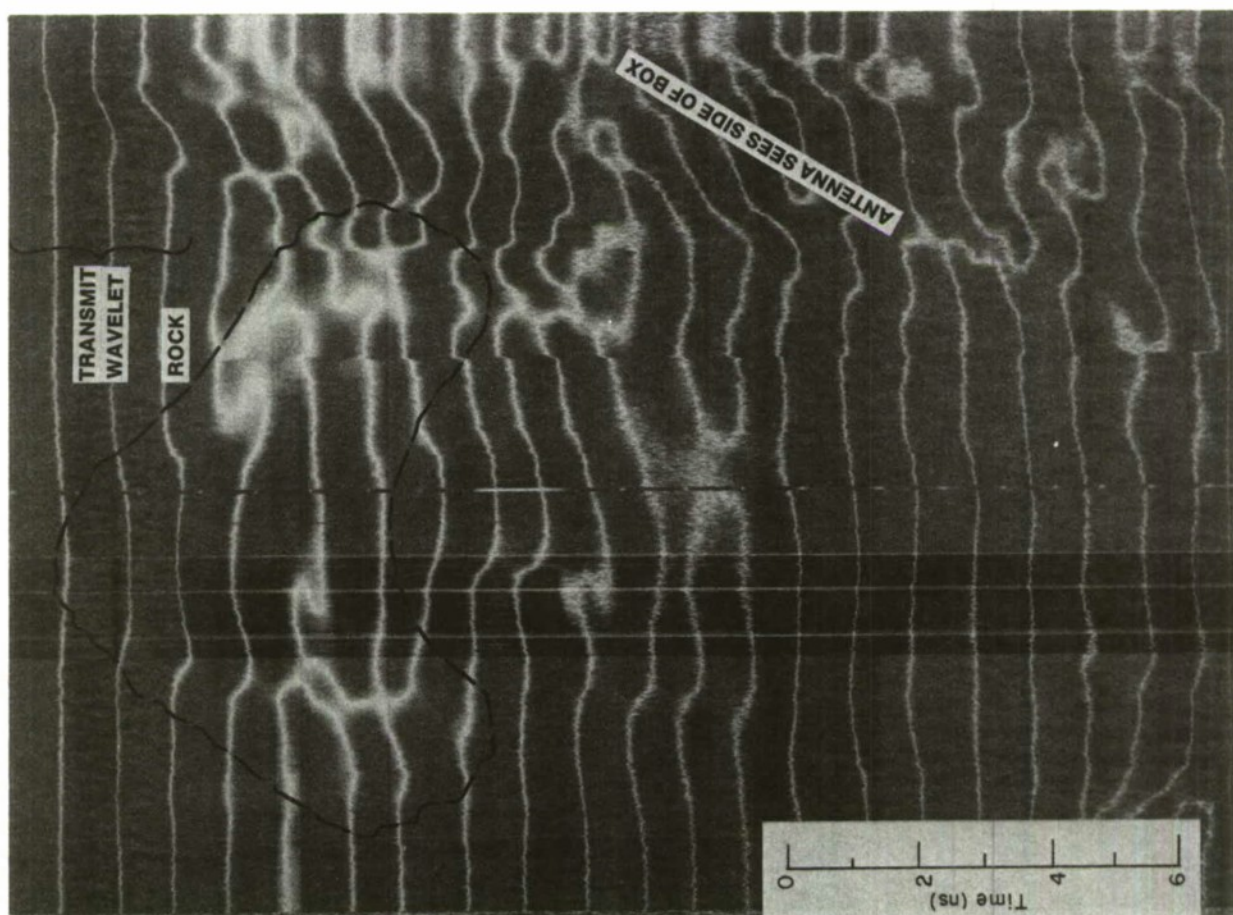
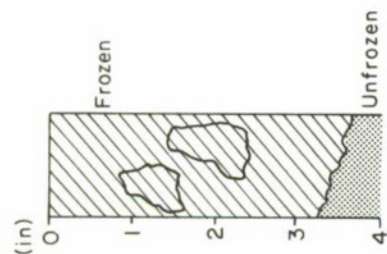


Figure A42.

Date: 29 Sept 82
 Time: 1500
 Tape Number: MB6
 Tape Channel(s): 1, 4
 Approx. Tape Count: 0938-1004
 Test Location: IEF cold storage room
 Media Conditions: Unfrozen silty sand w/cobbles
 Antenna Location: Surface
 Antenna Model: 101C
 Line of Survey: Over rock
 Data: Unprocessed

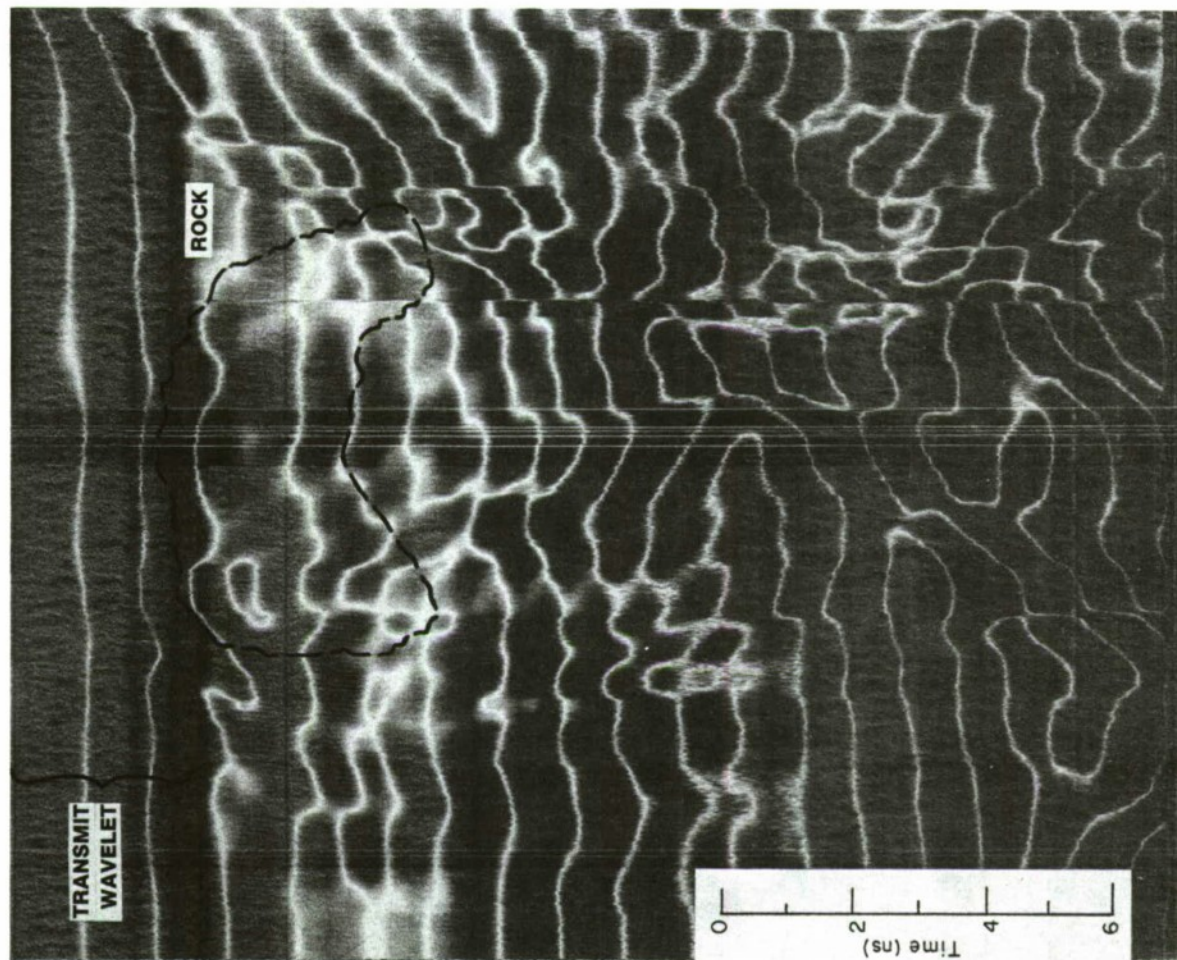
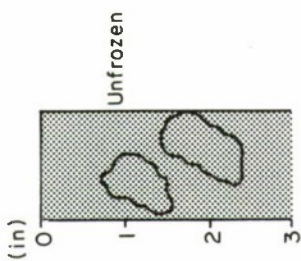


Figure A43.

Date: 30 Sept 82
 Time:
 Tape Number: MB7
 Tape Channel(s): 1, 4
 Approx. Tape Count: 0438-0514
 Test Location: IEF cold storage room
 Media Conditions: 3 to 4 in. frozen silty sand
 w/cobbles
 Antenna Location: Surface
 Antenna Model: 101C
 Line of Survey: Over rock
 Data: Unprocessed

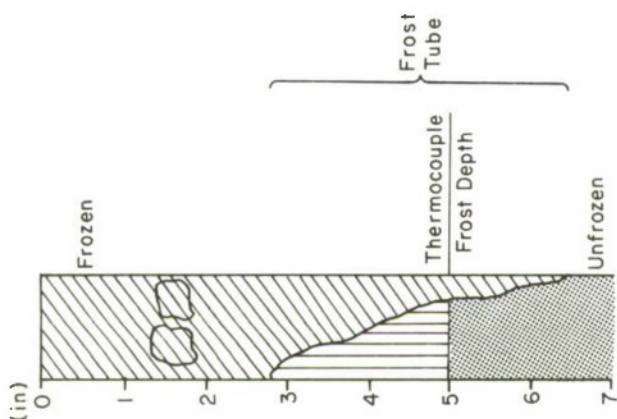
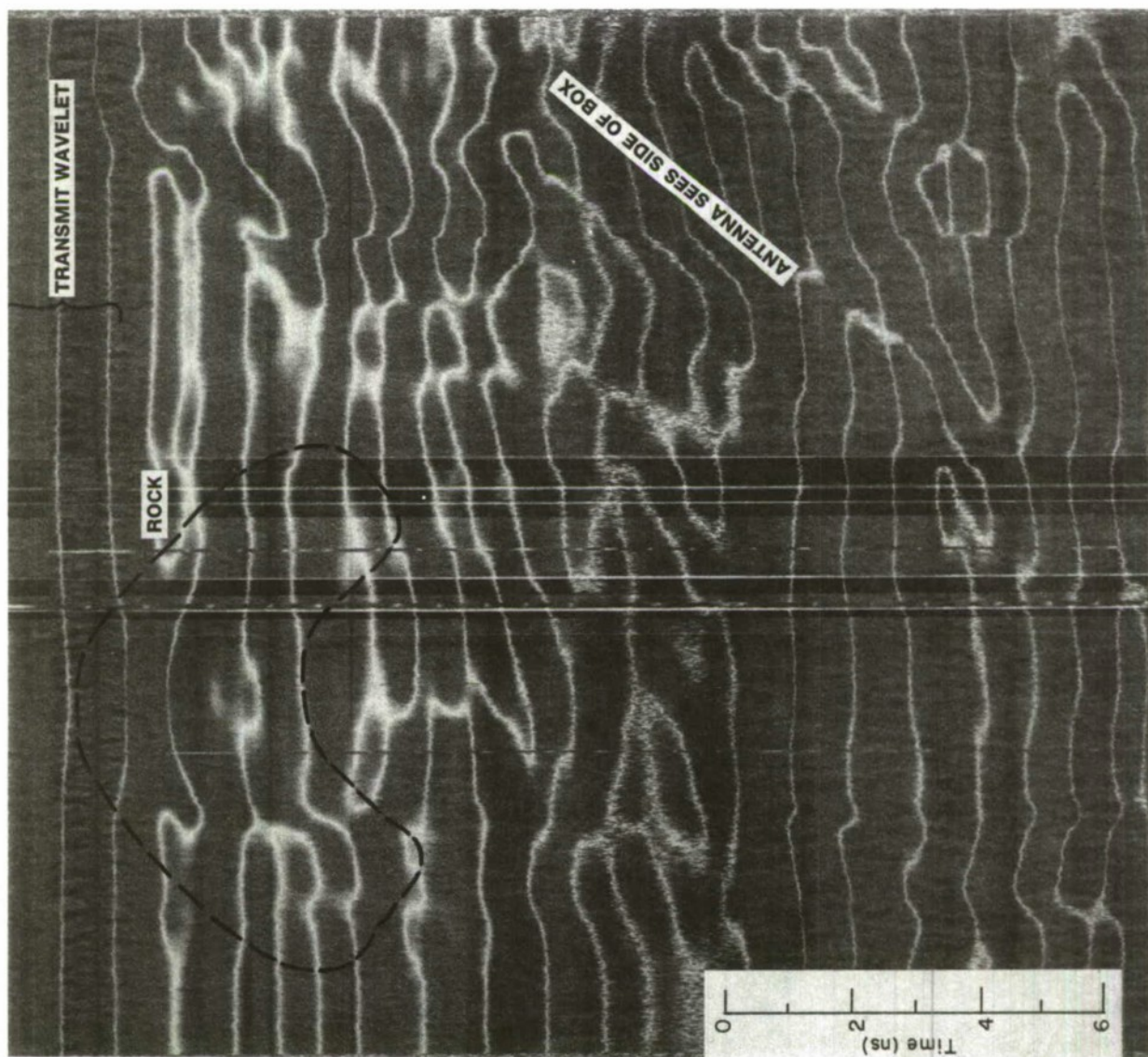


Figure A44.

Date: 1 Oct 82
 Time: 1306
 Tape Number: MB7
 Tape Channel(s): 1, 4
 Approx. Tape Count: 1378-1433
 Test Location: IEF cold storage room
 Media Conditions: 3 to 6 in. frozen silty sand
 w/cobbles
 Antenna Location: Surface
 Antenna Model: 101C
 Line of Survey: Over rock
 Data: Unprocessed



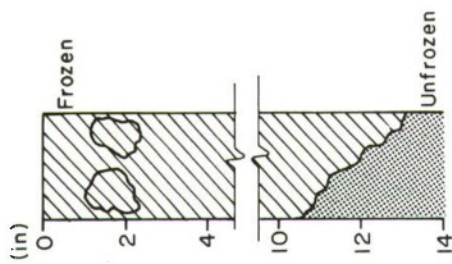
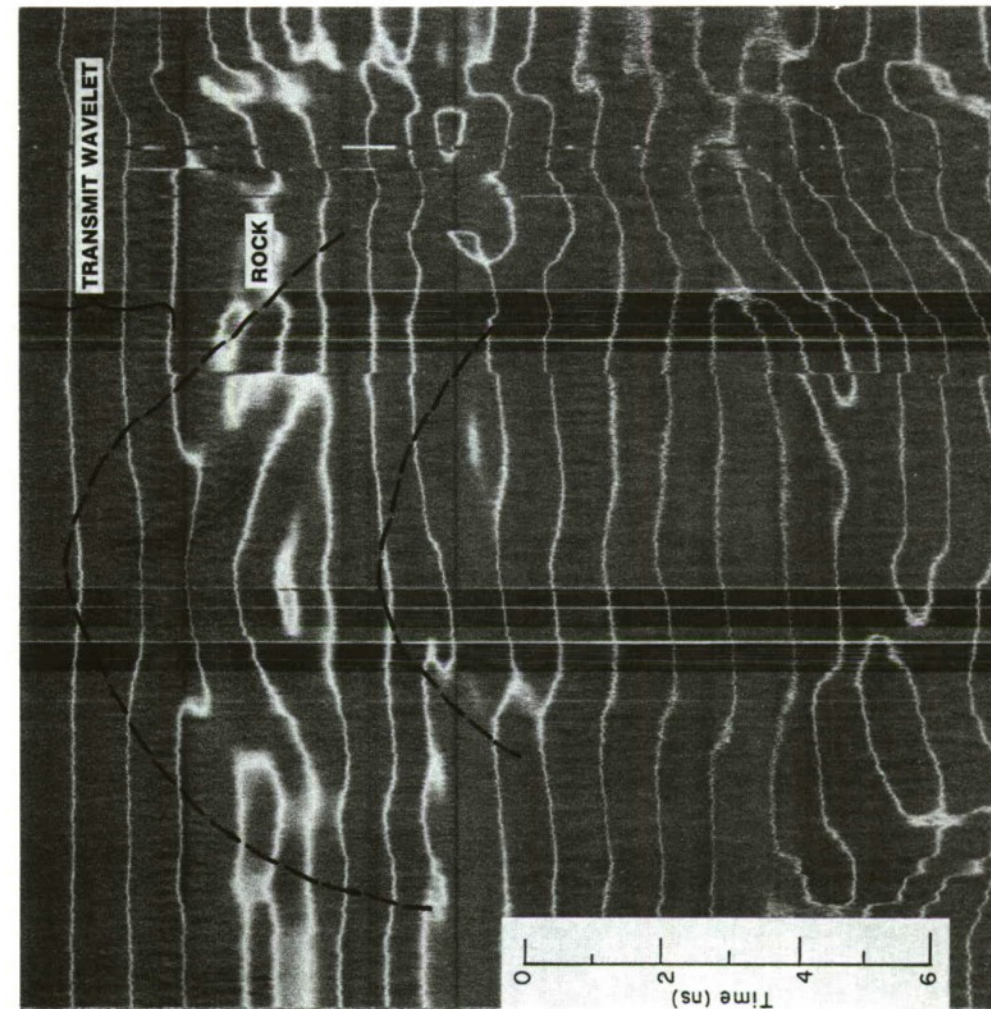
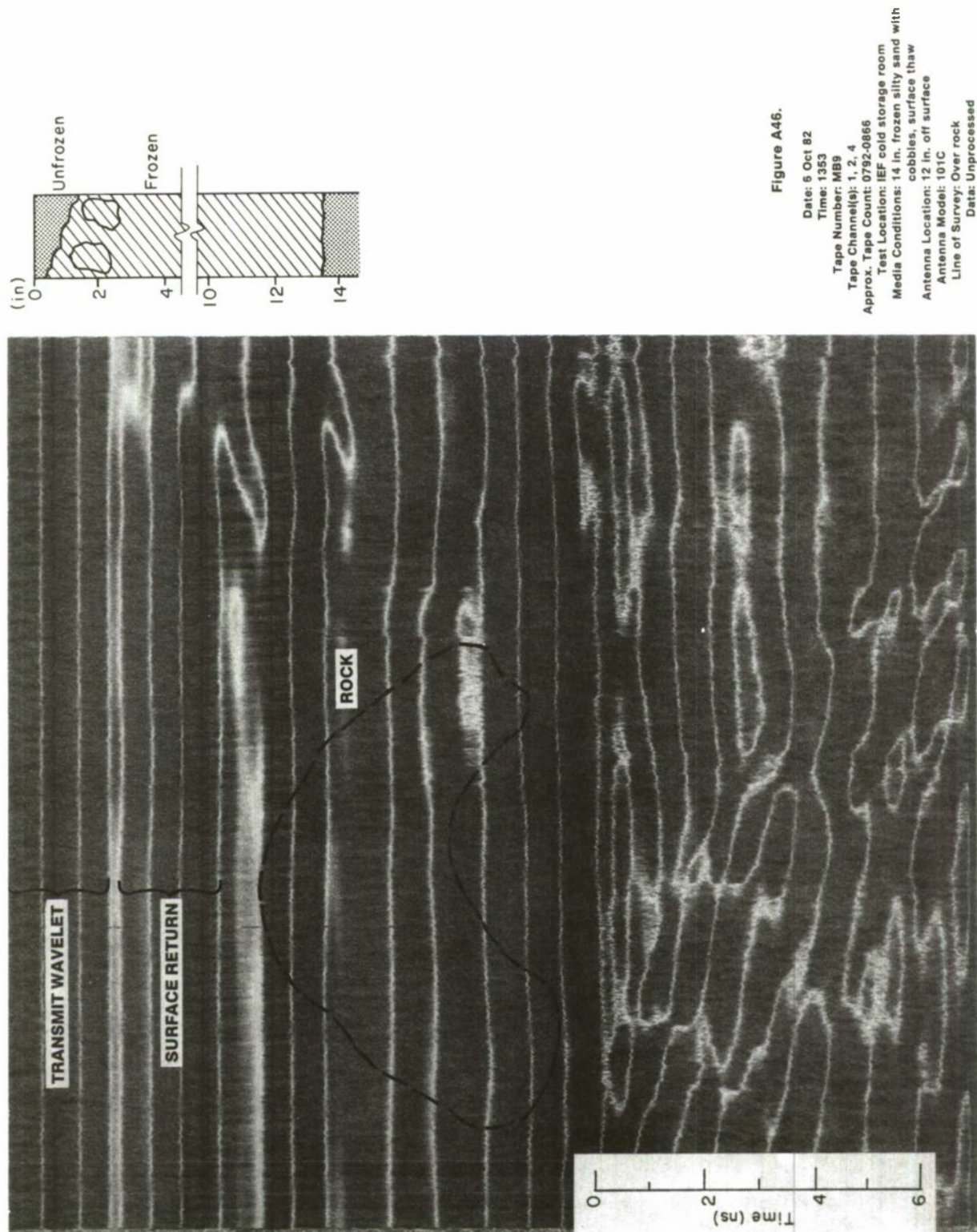


Figure A45.

Date: 5 Oct 82
 Time: 0928
 Tape Number: MB8
 Tape Channel(s): 1, 4
 Approx. Tape Count: 1230-1282
 Test Location: IEF cold storage room
 Media Conditions: 10 to 13 in. frozen silty sand
 w/cobbles
 Antenna Location: On surface
 Antenna Model: 101C
 Line of Survey: Over rock
 Data: Unprocessed



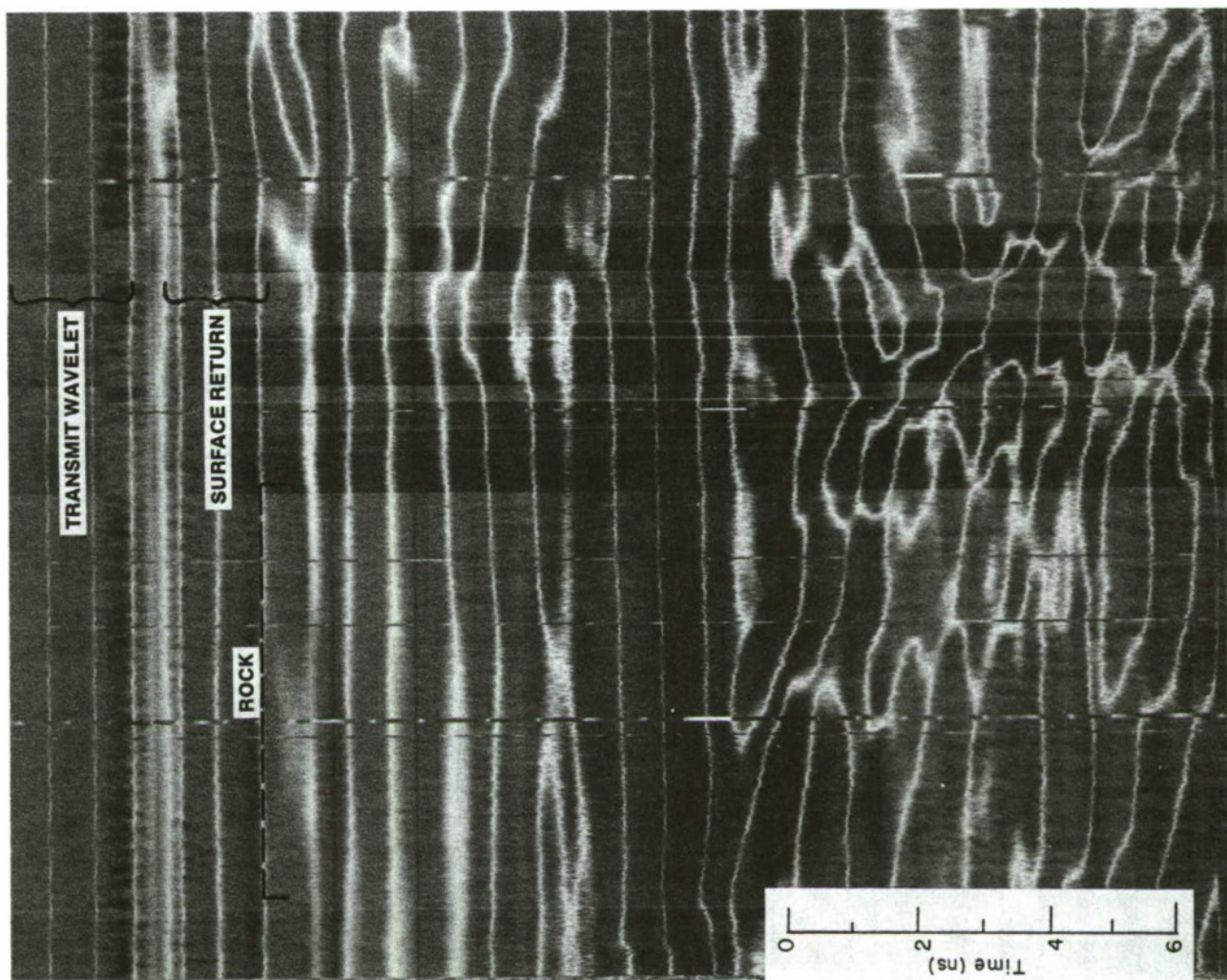
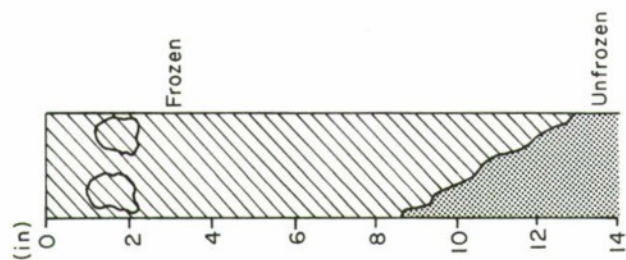


Figure A47.
 Date: 4 Oct 82
 Time: - 1251
 Tape Number: MB8
 Tape Channel(s): 1, 4
 Approx. Tape Count: 6662-0735
 Test Location: IEF cold storage room
 Media Conditions: 9 to 13 in. frozen silty sand w/cobbles
 Antenna Location: 12 in. above surface
 Antenna Model: 101C
 Line of Survey: Over rock
 Data: Unprocessed

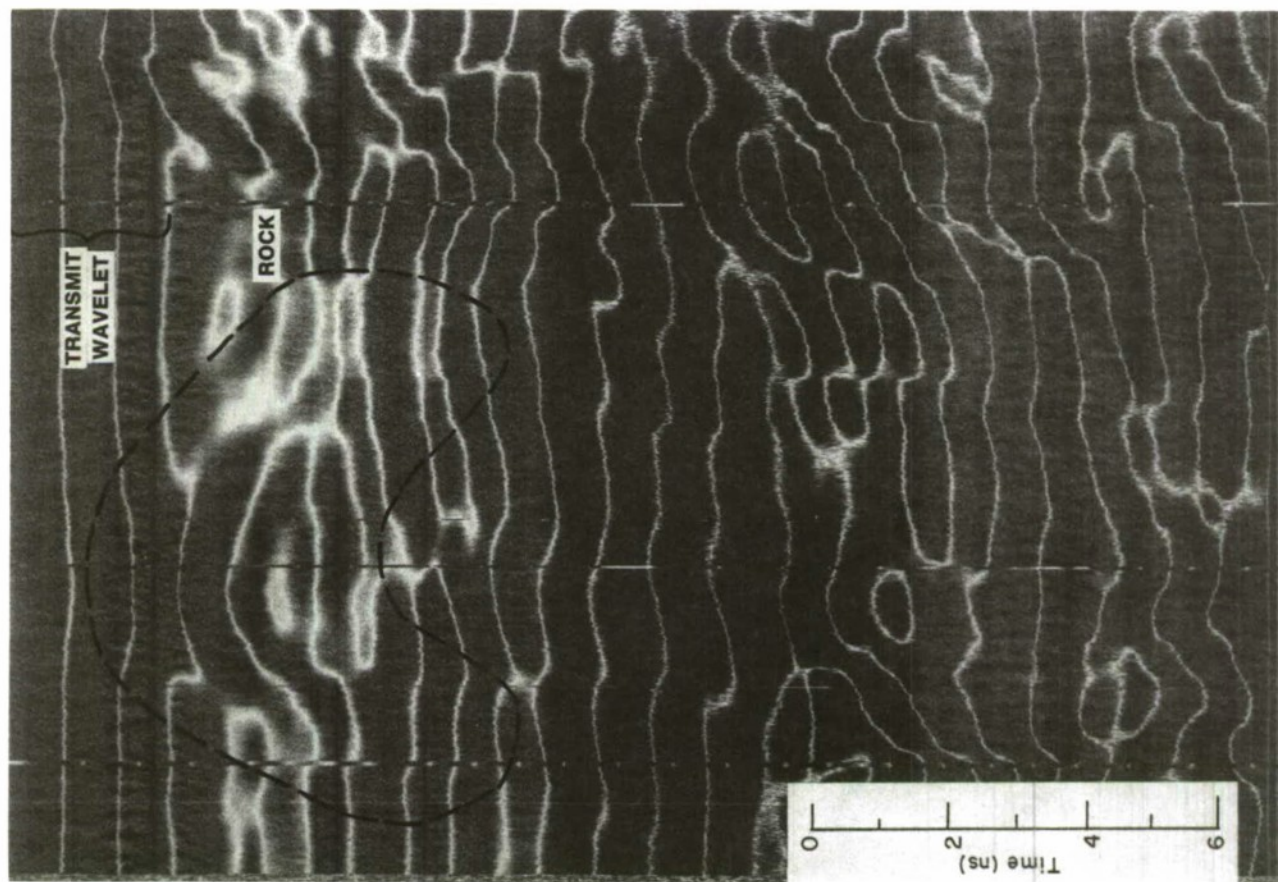
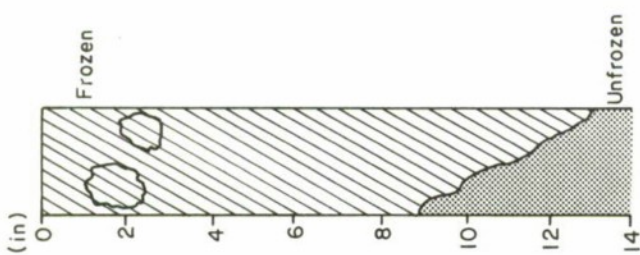


Figure A48.

Date: 4 Oct 82
 Time: ~ 1300
 Tape Number: MB8
 Tape Channel(s): 1, 4
 Approx. Tape Count: 0951-1014
 Test Location: IEF cold storage room
 Media Conditions: 9 to 13 in. frozen silty sand
 w/cobbles
 Antenna Location: Surface
 Antenna Model: 101C
 Line of Survey: Over rock
 Data: Unprocessed

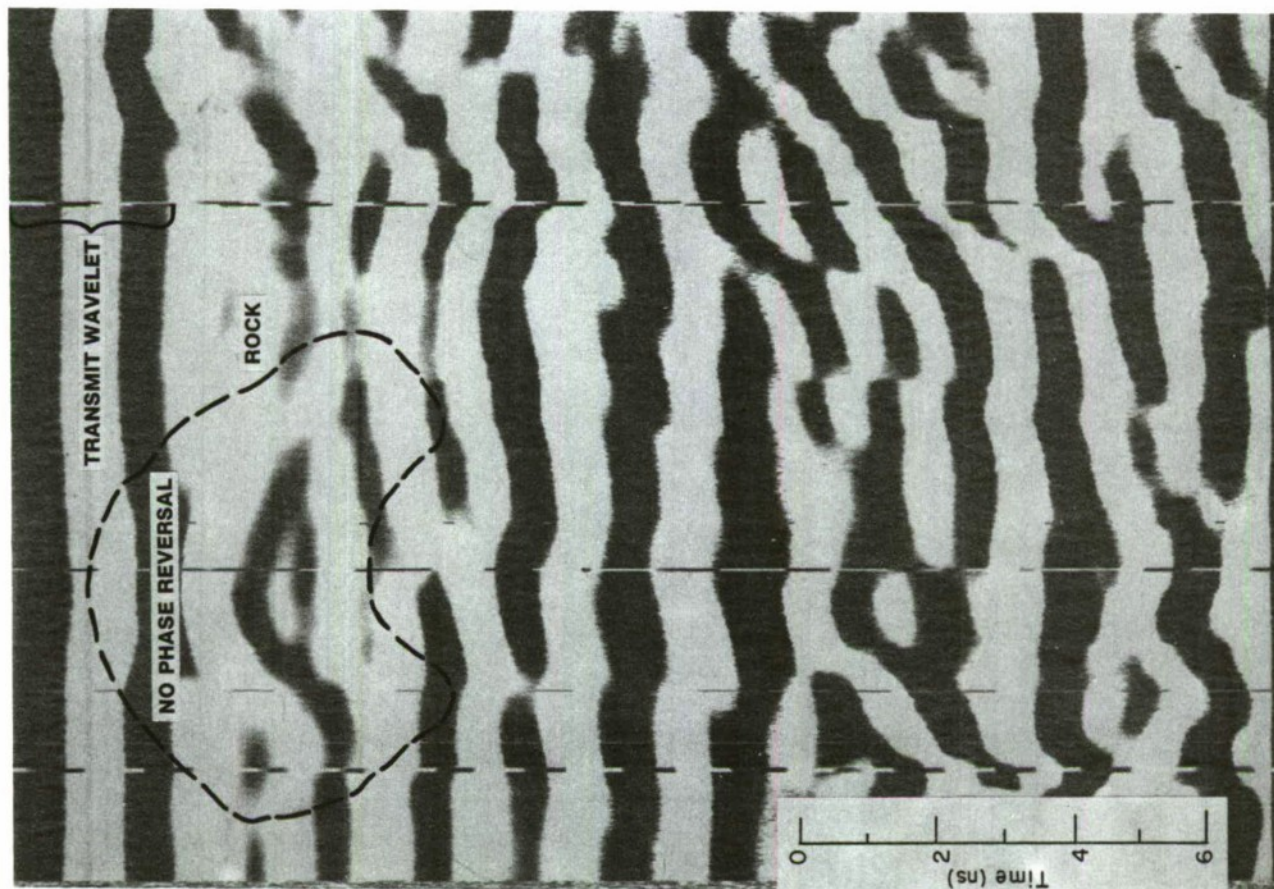
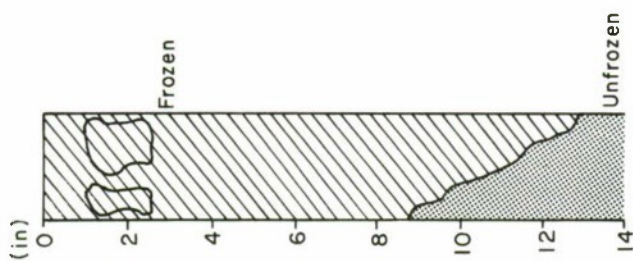


Figure A49.

Date: 4 Oct 82
 Time: ~1300
 Tape Number: M88
 Tape Channel(s): 1, 4
 Approx. Tape Count: 0961:1014
 Test Location: IEF cold storage room
 Media Conditions: 9 to 12 in. frozen silty sand
 w/cobbles
 Antenna Location: Surface
 Antenna Model: 101C
 Line of Survey: Over rock
 Data: Print "..."

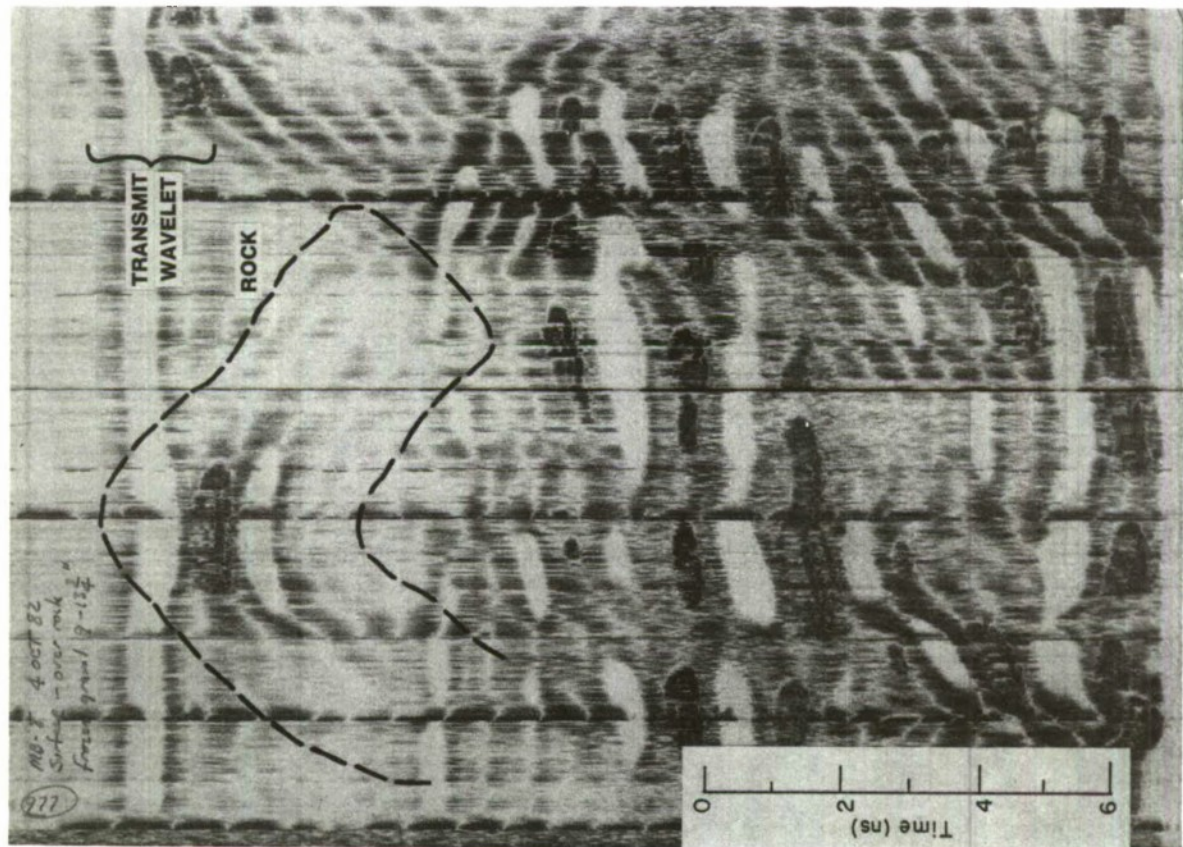
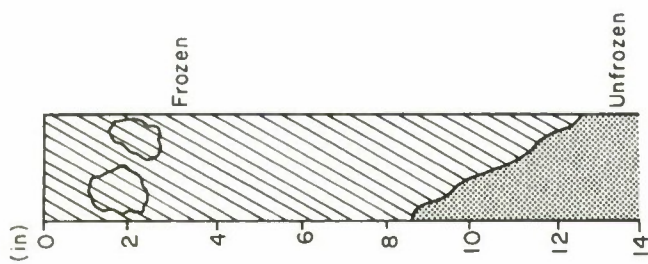


Figure A50.

Date: 4 Oct 82
 Time: ~ 1300
 Tape Number: MB8
 Tape Channel(s): 1, 4
 Approx. Tape Count: 0961-1014
 Test Location: IEF cold storage room
 Media Conditions: 9 to 12 in. frozen allly sand
 w/cobbles
 Antenna Location: Surface
 Antenna Model: 101C
 Line of Survey: Over rock
 Date: Program 2.3

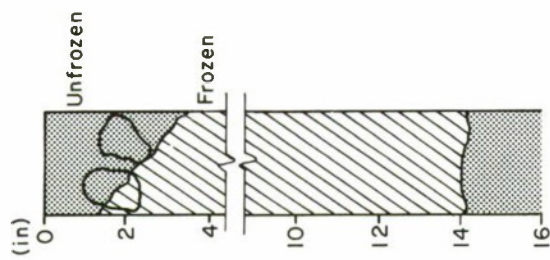
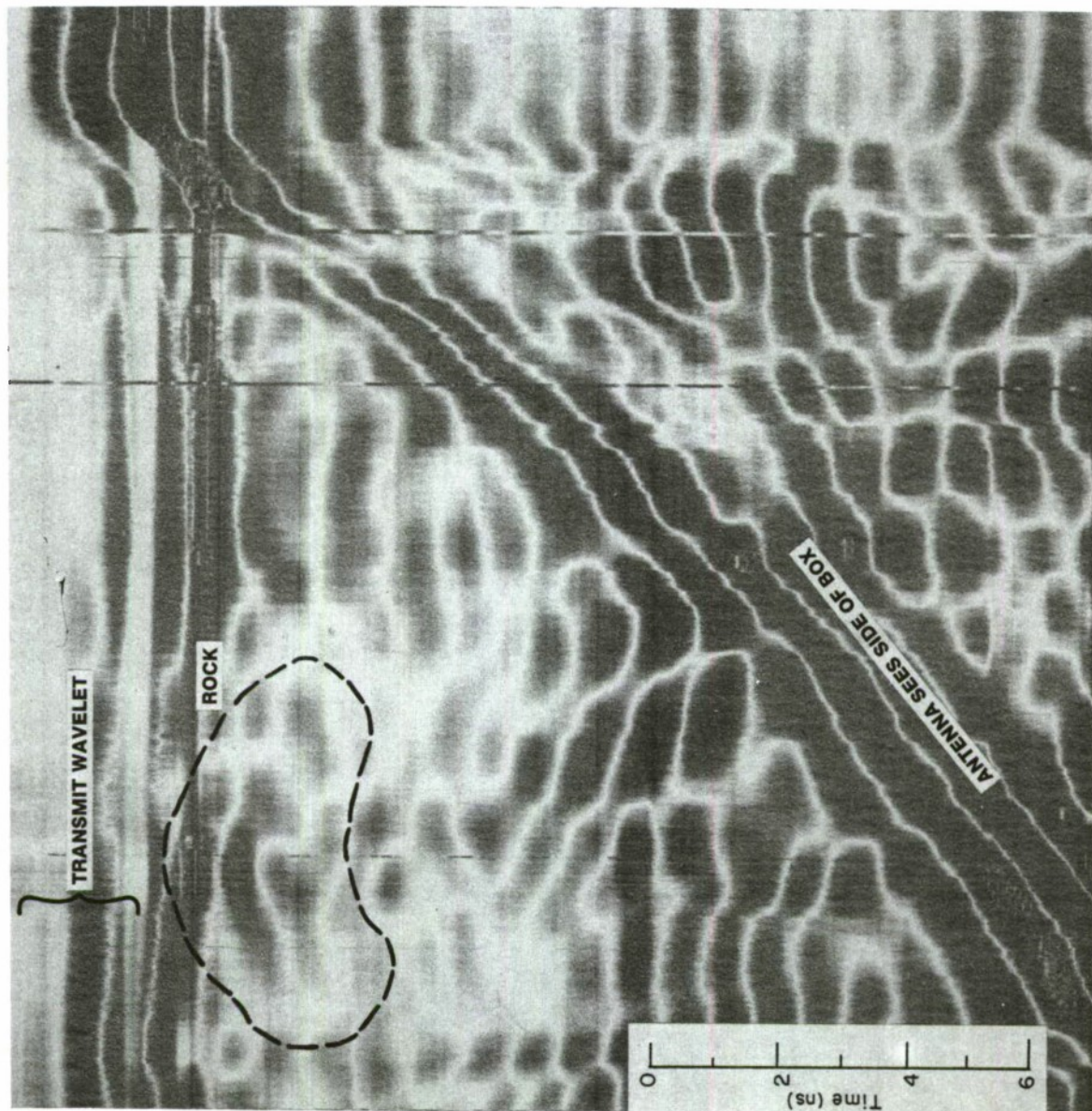


Figure A51.

Date: 8 Oct 82
 Time: 1400
 Tape Number: MB9
 Tape Channel(s):
 Approx. Tape Count: 1095-1147
 Test Location: IEF cold storage room
 Media Conditions: 14 in. frozen silty sand w/cob-
 bles, w/1 to 3 in. surface thaw
 Antenna Location: Surface
 Antenna Model: 101C
 Line of Survey: Over rock
 Date: Program 2-1



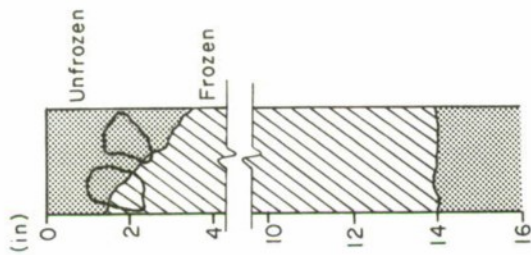
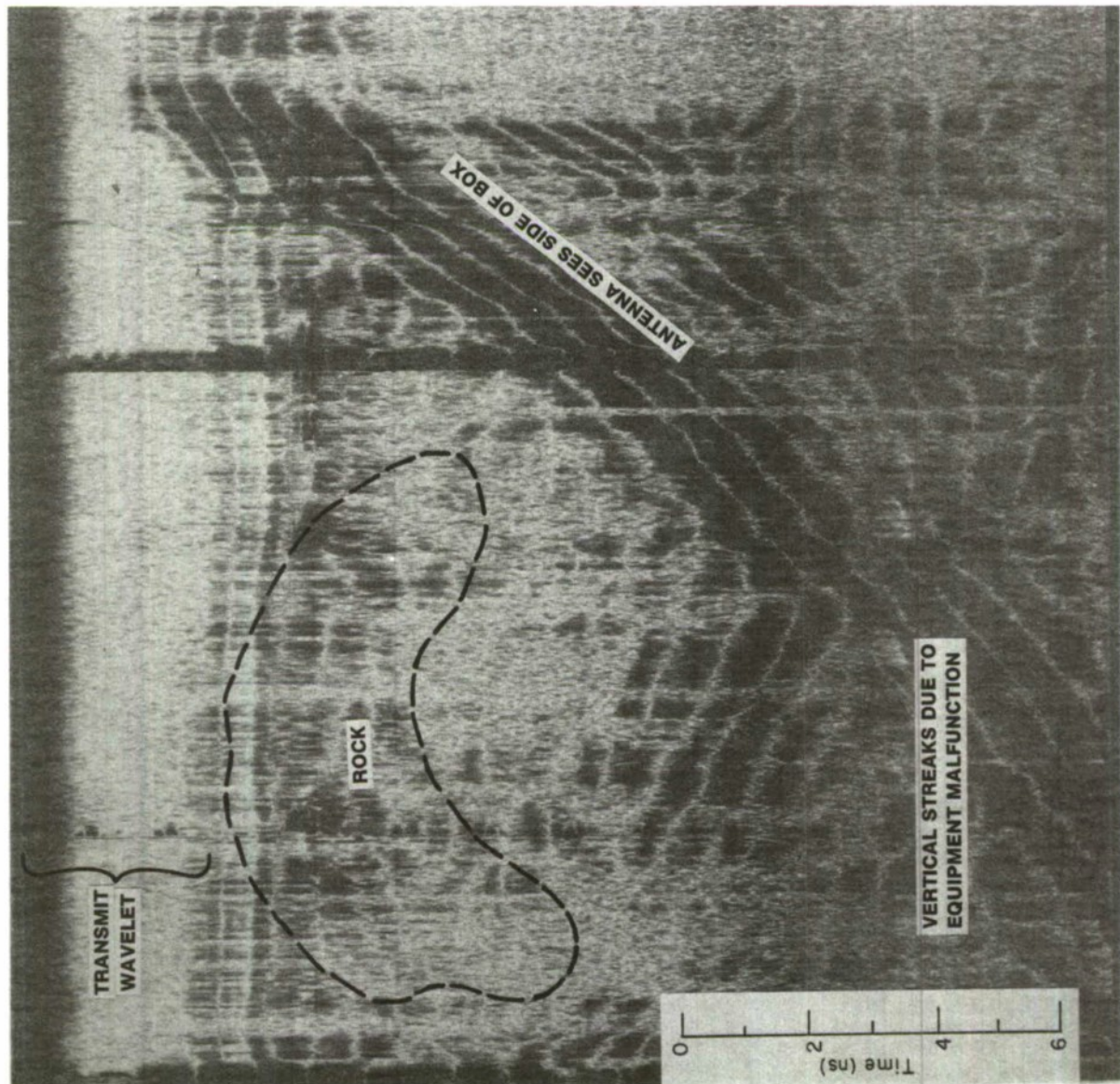


Figure A52.

Date: 6 Oct 82
 Time: 1400
 Tape Number: MB9
 Tape Channel(s): 1, 2, 4
 Approx. Tape Count: 1085-1147
 Test Location: IEF cold storage room
 Media Conditions: 14 in. frozen silty sand w/cob-
 bles; 1 to 3 in. surface thaw
 Antenna Location: Surface
 Antenna Model: 101C
 Line of Survey: Over rock
 Date: Program 2-3



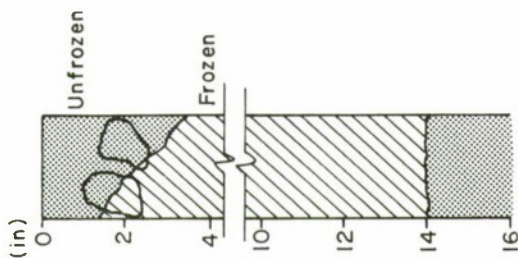
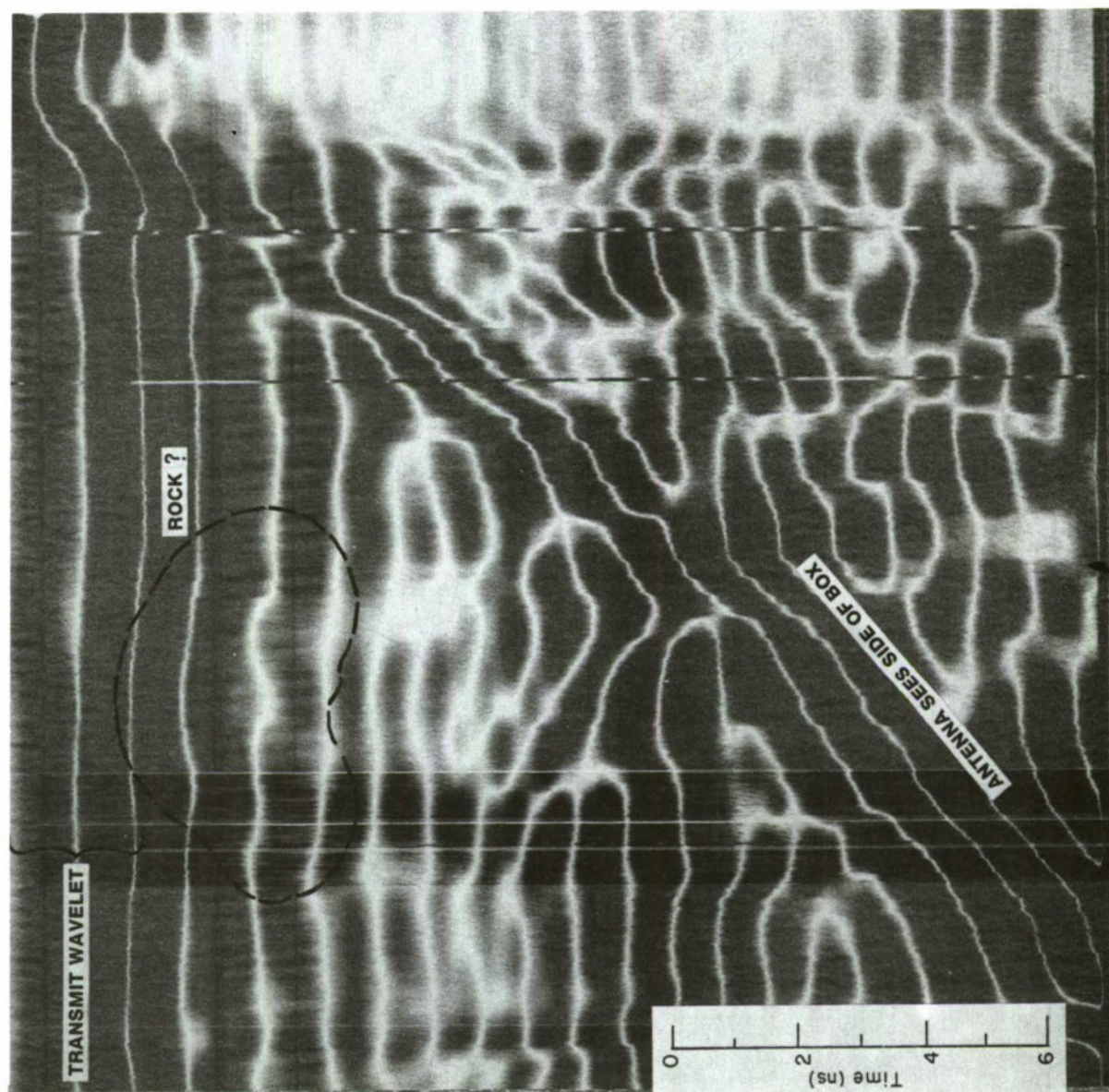


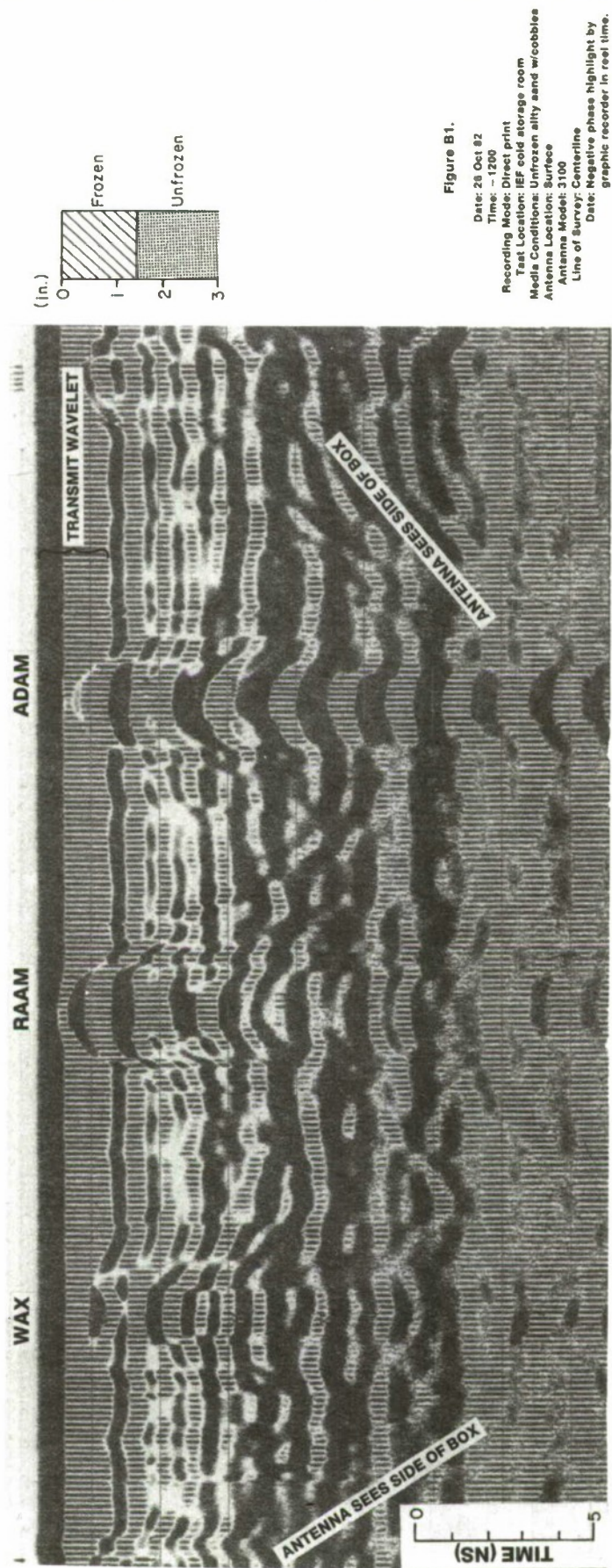
Figure A53.

Date: 6 Oct 82
 Time: 1400
 Tape Number: MB9
 Tape Channel(s):
 Approx. Tape Count: 1085-1147
 Test Location: IEF cold storage room
 Media Conditions: 14 in. frozen slity send w/cob-
 bles: 1 to 3 in. thaw
 Antenna Location: Surface
 Antenna Model: 101C
 Line of Survey: Over rock
 Date: Unprocessed



APPENDIX B: RADAR SCANS - PORTABLE EQUIPMENT

(See first page of Appendix A for explanation of information blocks.)



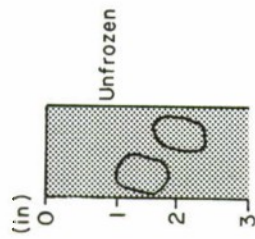
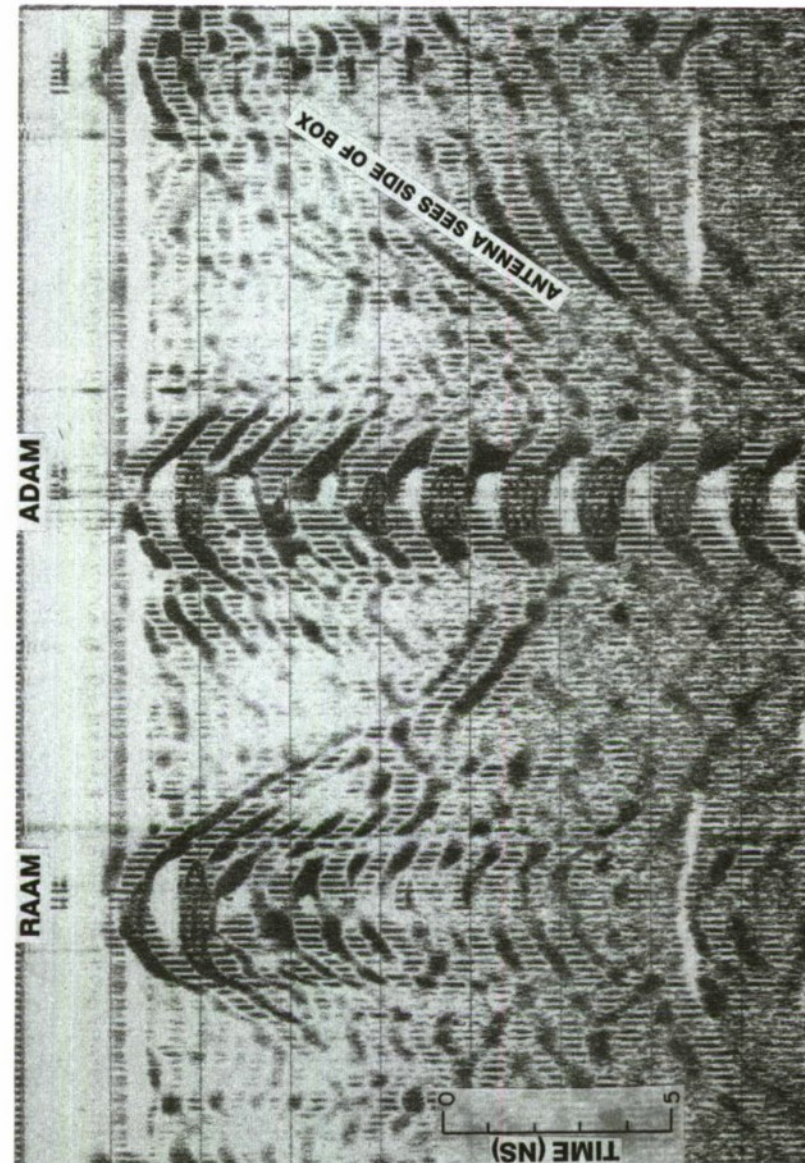


Figure B2.

Date: 26 Oct 82
 Time: ~ 1200
 Recording Mode: Direct print
 Test Location: IEF cold storage room
 Media Conditions: Unfrozen silty sand w/cobbles
 Antenna Location: Surface
 Antenna Model: 3100
 Line of Survey: Centerline
 Data: Positive phase highlight by
 graphic recorder. Processed in
 real time under program 27.

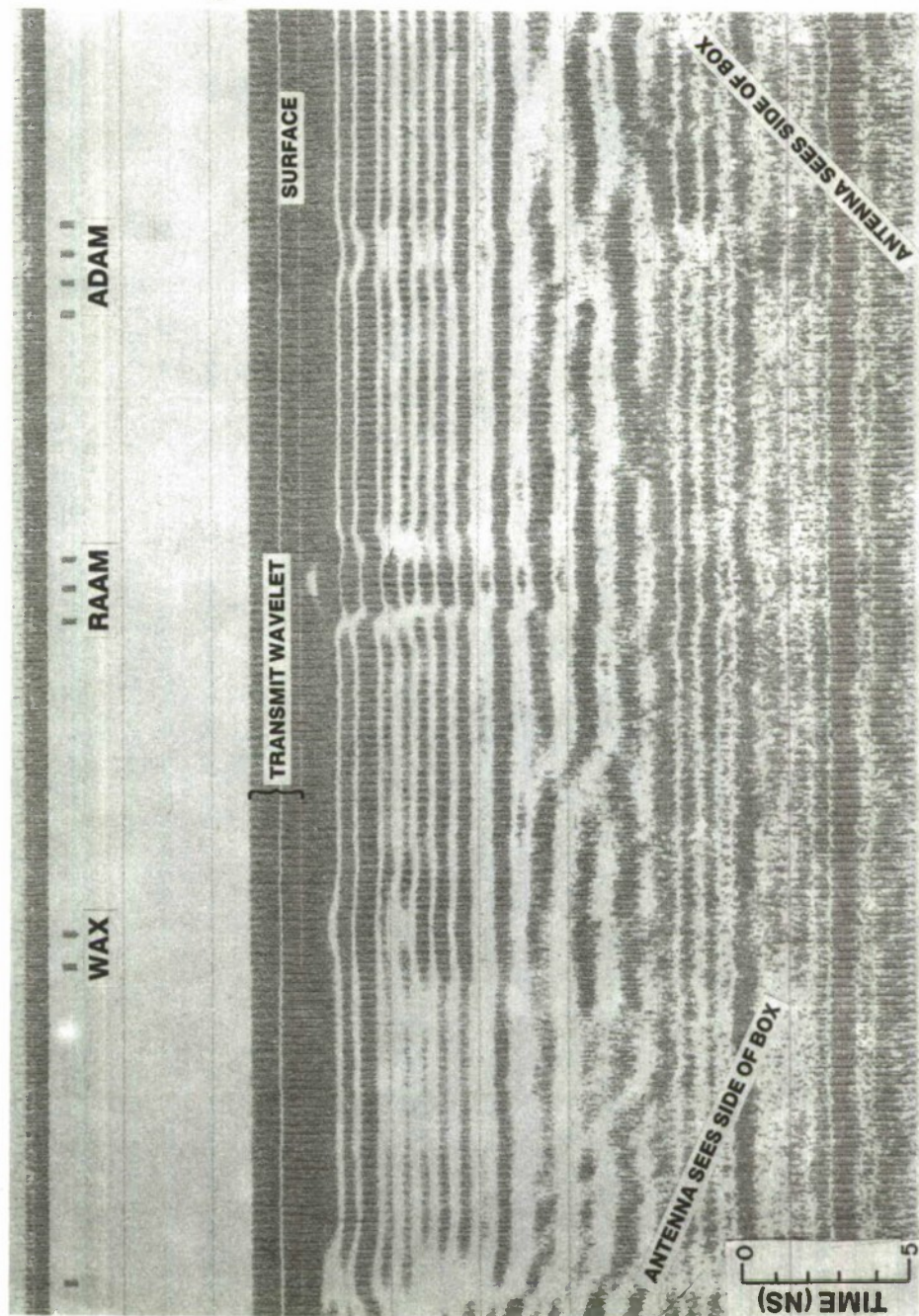
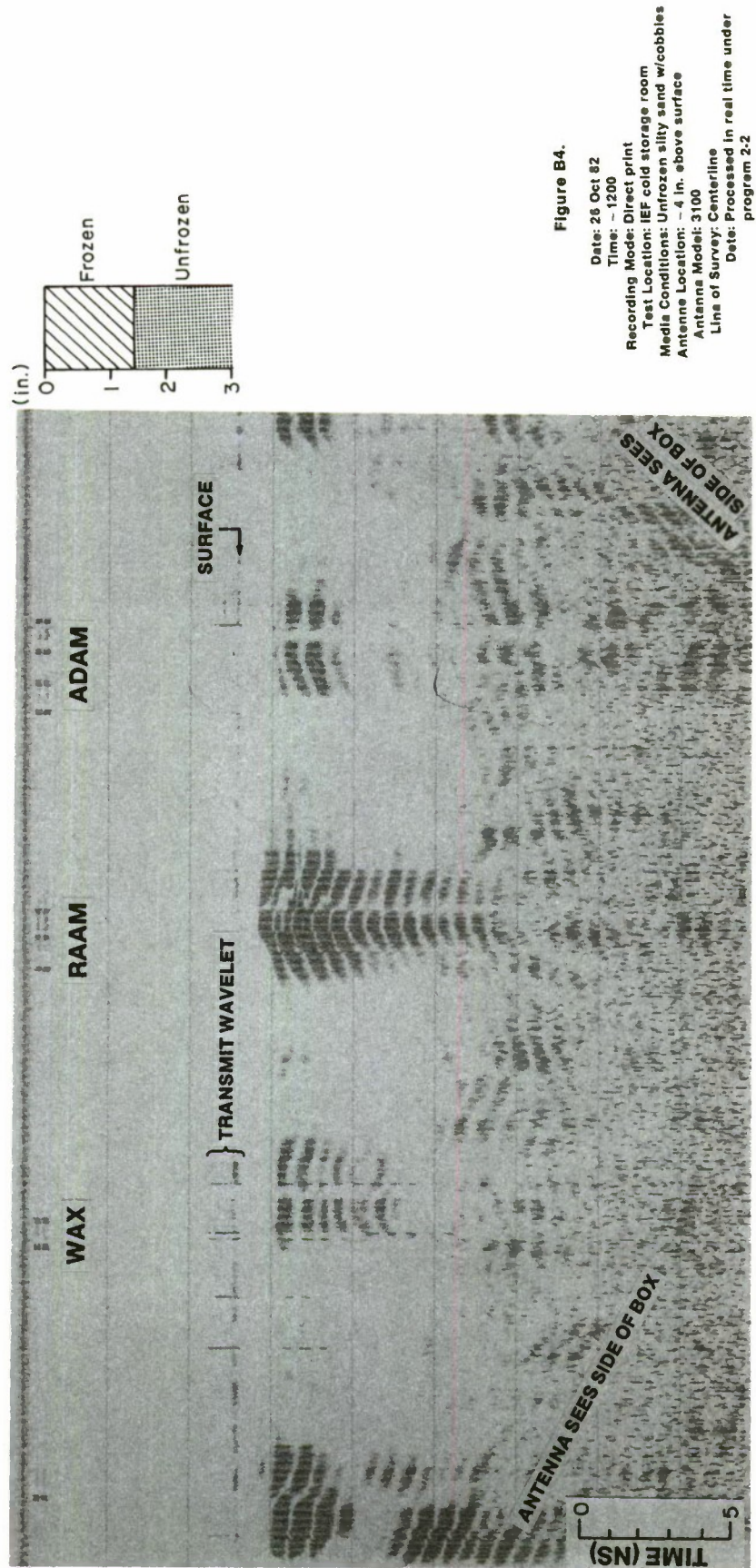


Figure B3.

Date: 28 Oct 82
 Time: ~ 1200
 Recording Mode: Direct print
 Test Location: IEF cold storage room
 Media Conditions: Unfrozen silty sand w/cobbles
 Antenna Location: ~ 4 in. above surface
 Antenna Model: 3100
 Line of Survey: Centerline
 Data: Raw data taken in real time



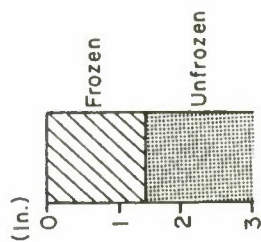
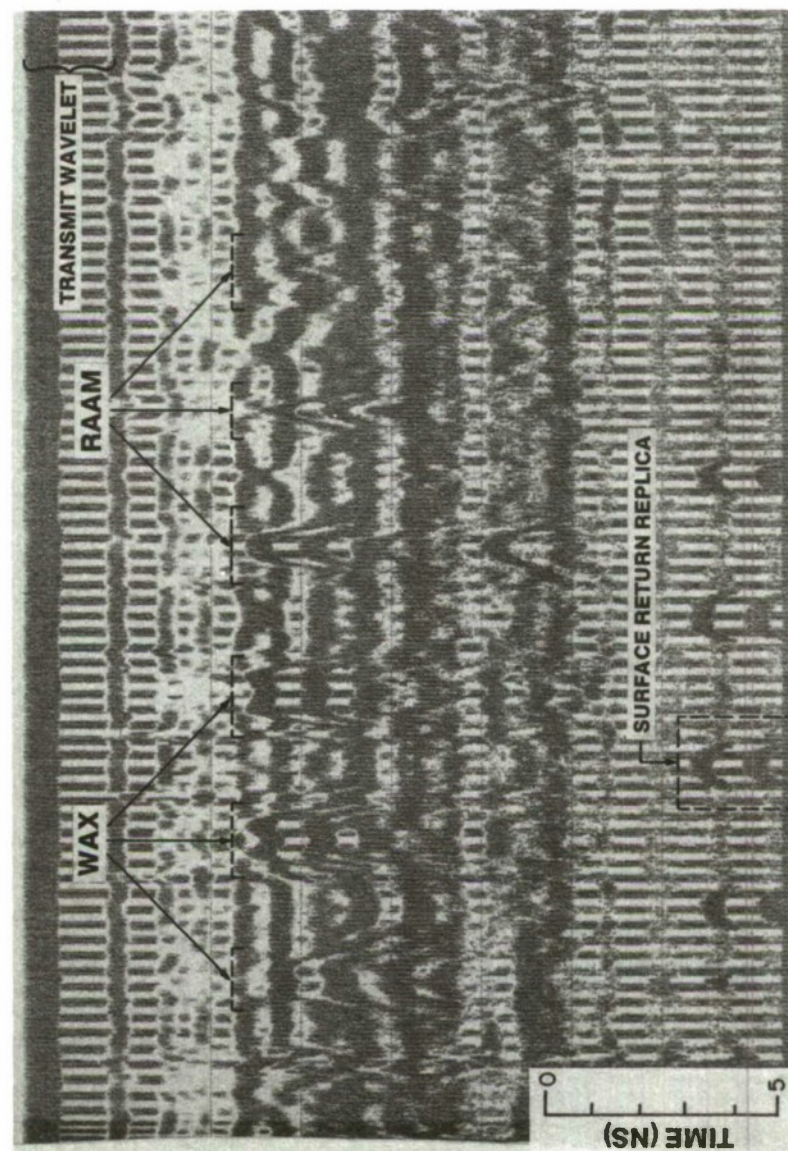


Figure B5.

Date: 26 Oct 82
 Time: ~ 1200
 Recording Mode: Direct print
 Test Location: IEF cold storage room
 Media Conditions: Unfrozen silty sand w/cobbles
 Antenna Location: Hand-held above surface
 Antenna Model: 3100
 Line of Survey: Sweeping across centerline
 Data: Negative phase highlight by
 graphic recorder in real time

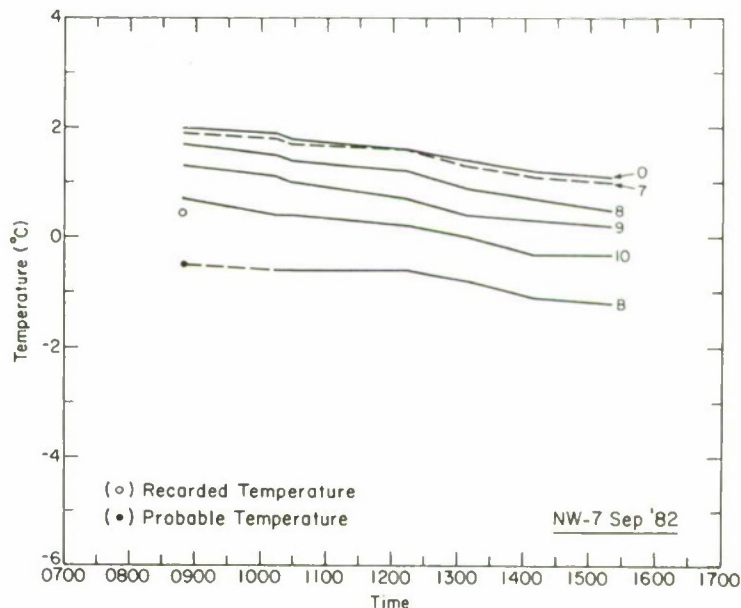
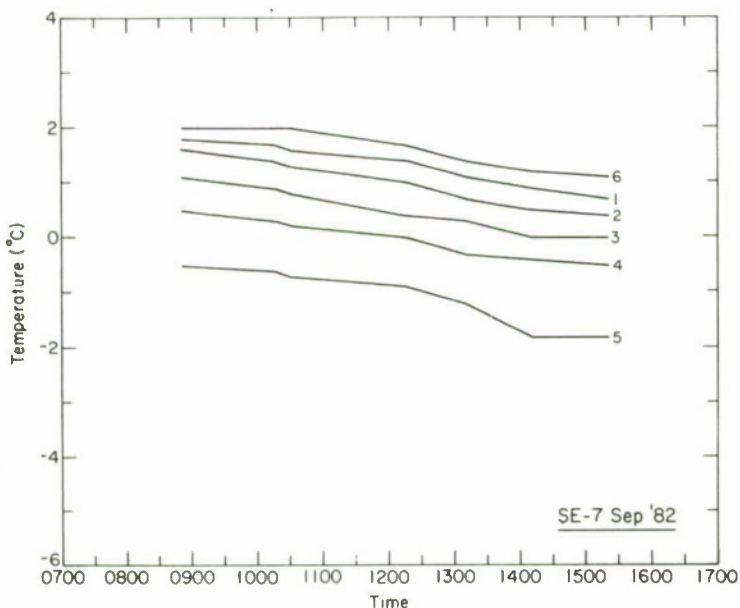
APPENDIX C:

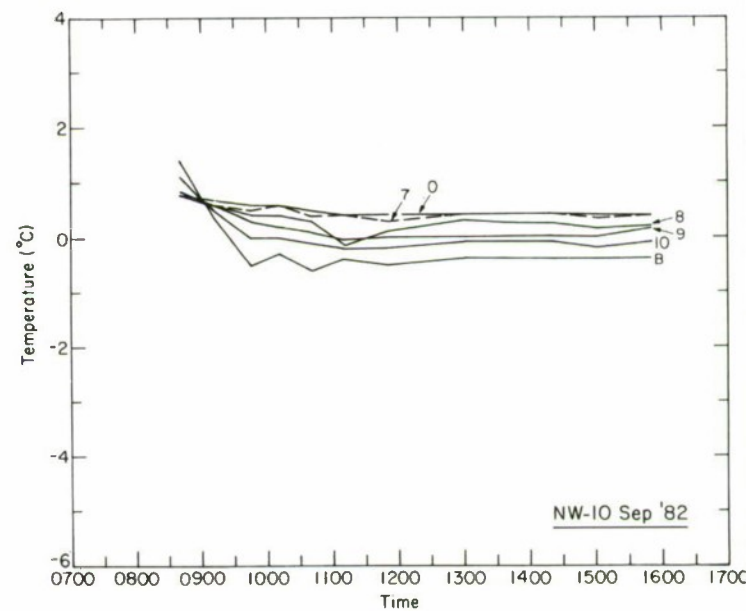
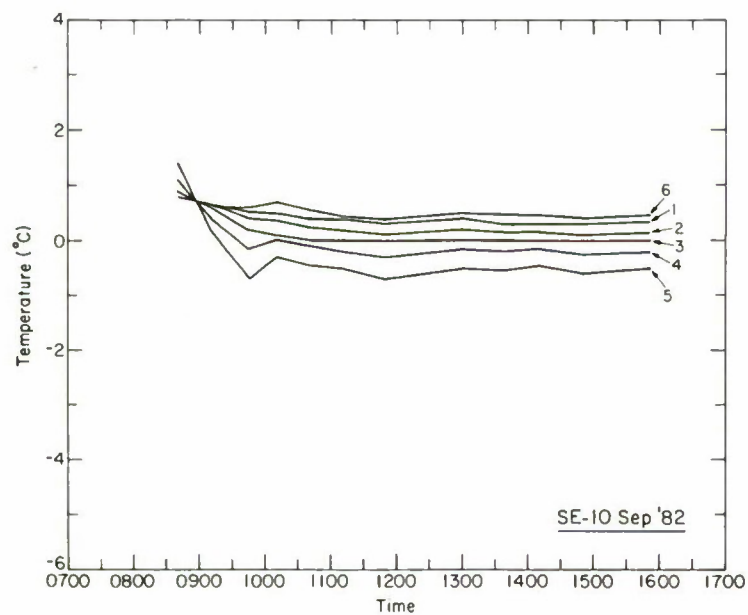
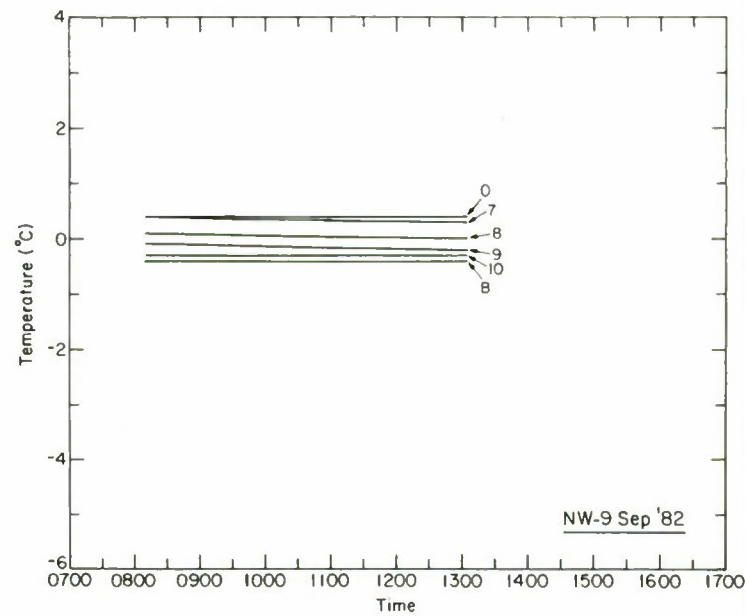
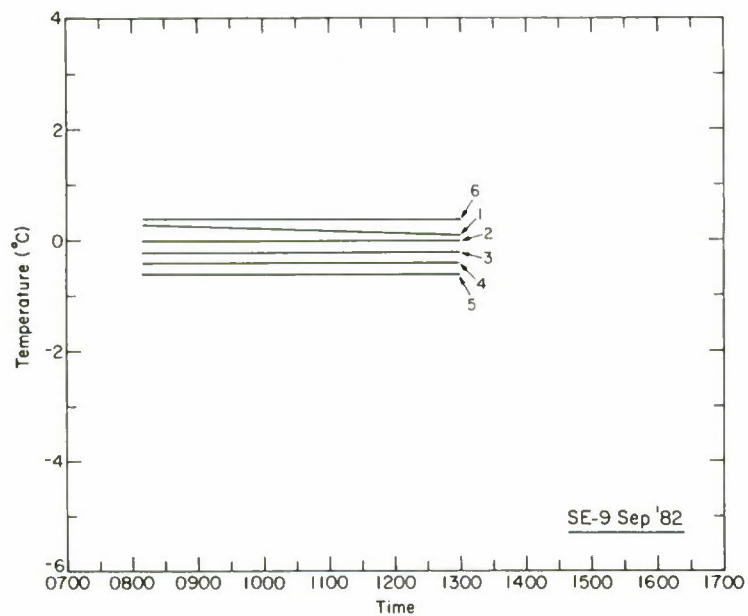
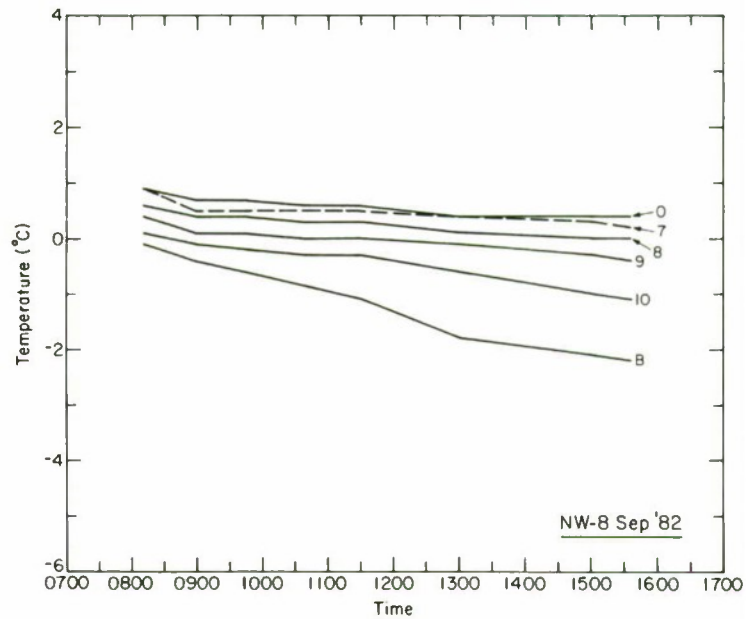
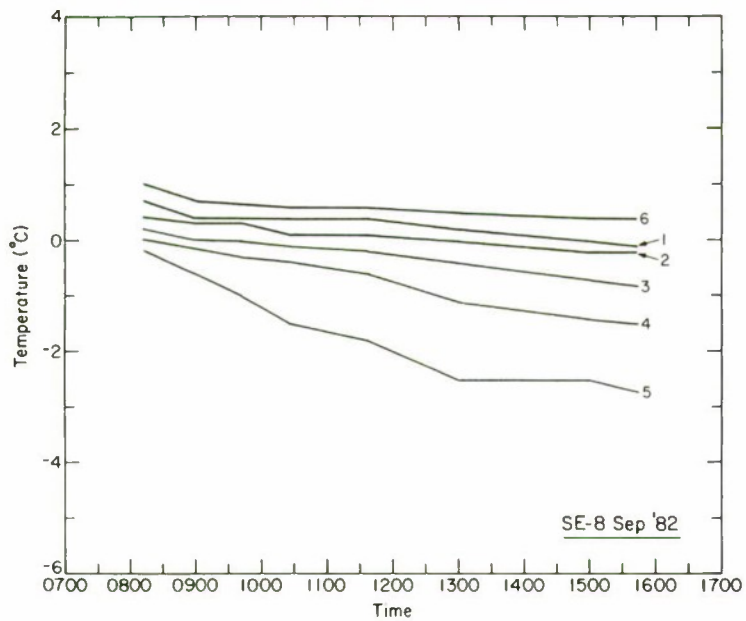
TEMPERATURES IN THE MEDIUM MEASURED BY THERMOCOUPLES

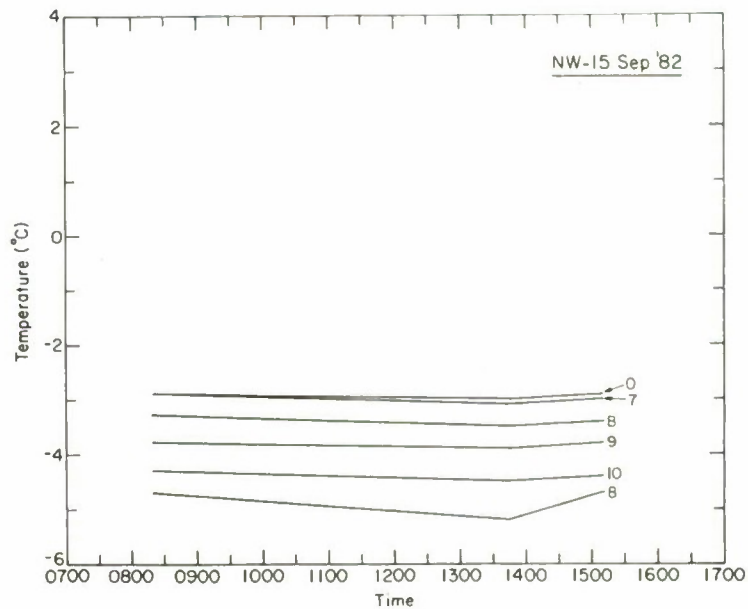
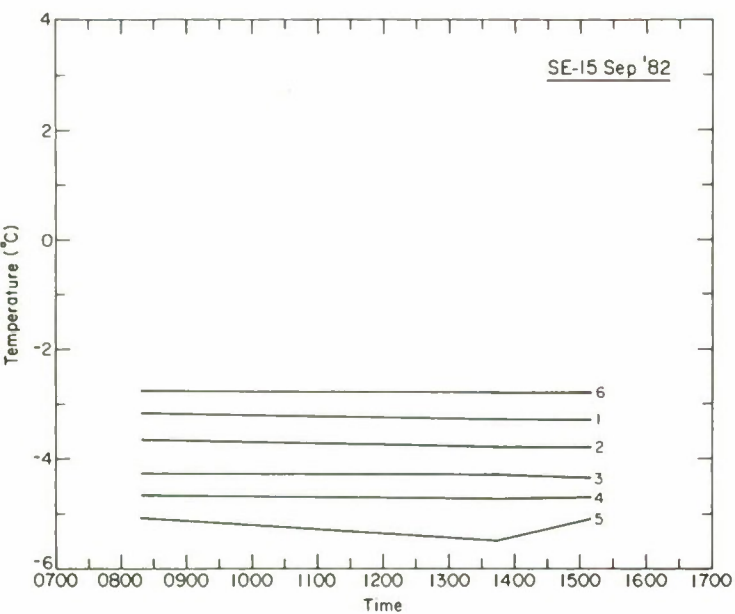
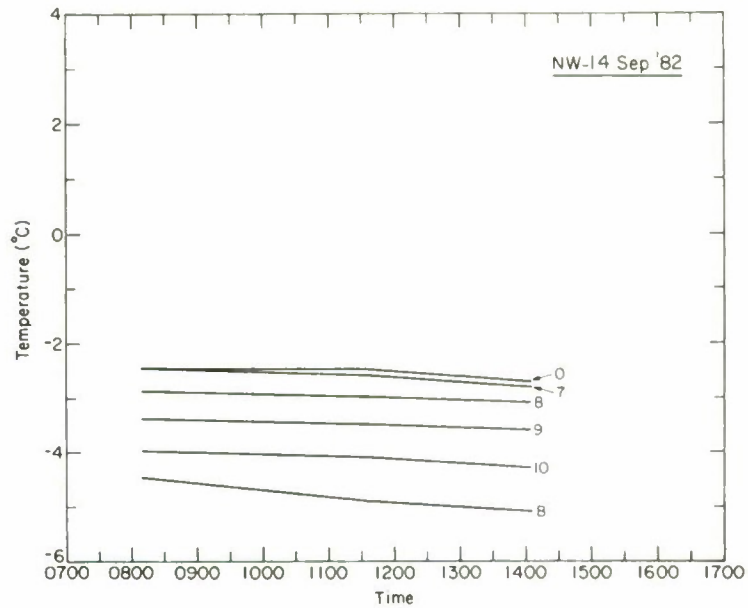
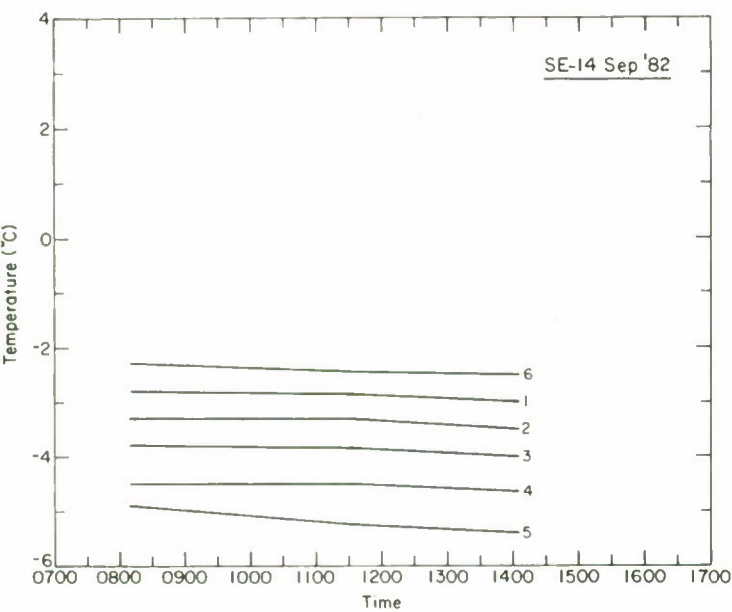
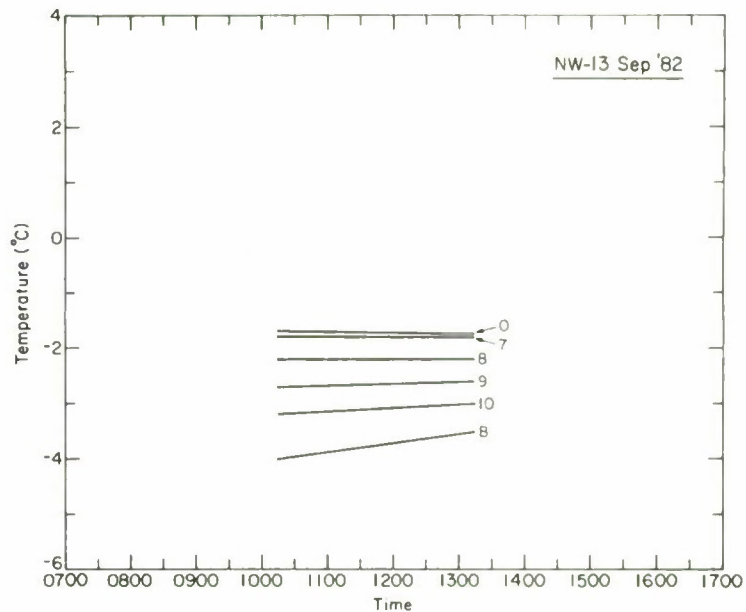
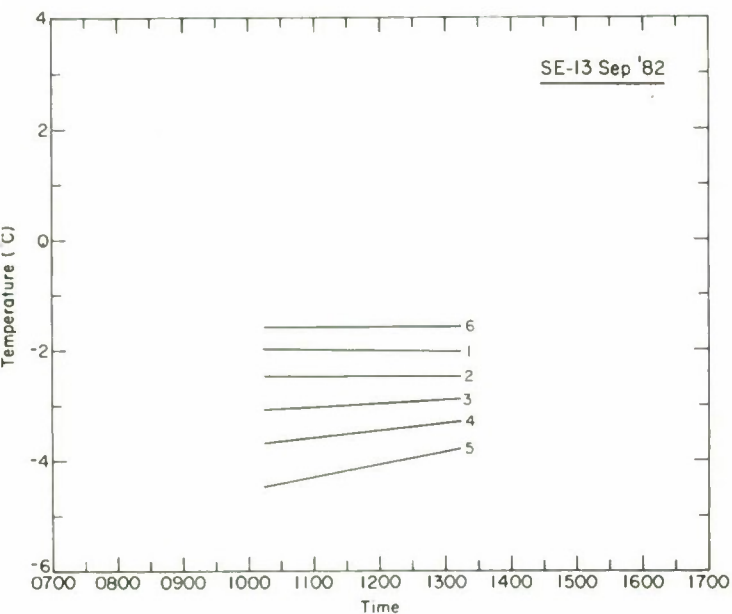
The graphs in this appendix are temperature records for the upper 12.7 cm of sand in the test box. Temperatures were taken with thermocouples at two locations (see Fig. 1 and 2) at 2.5-cm depth intervals down to a depth of 12.7 cm. Values below 0°C are taken to indicate frozen sand. See the Test Set-up and Procedures section.

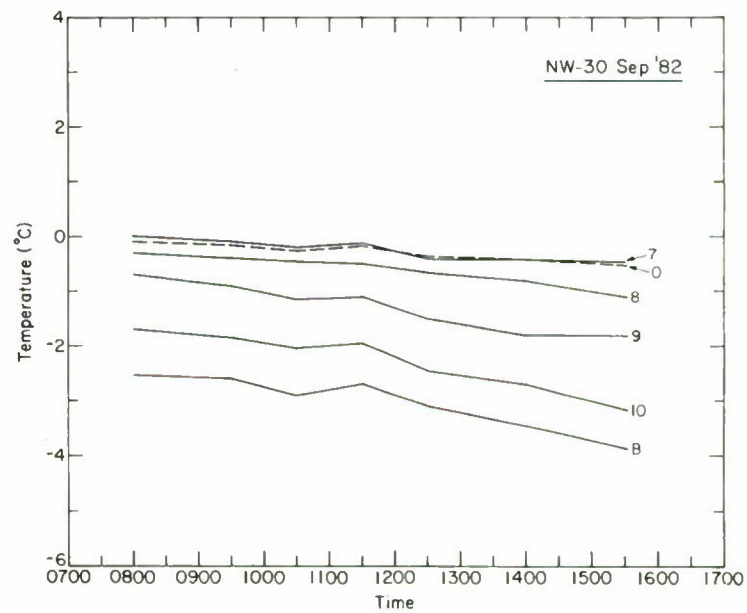
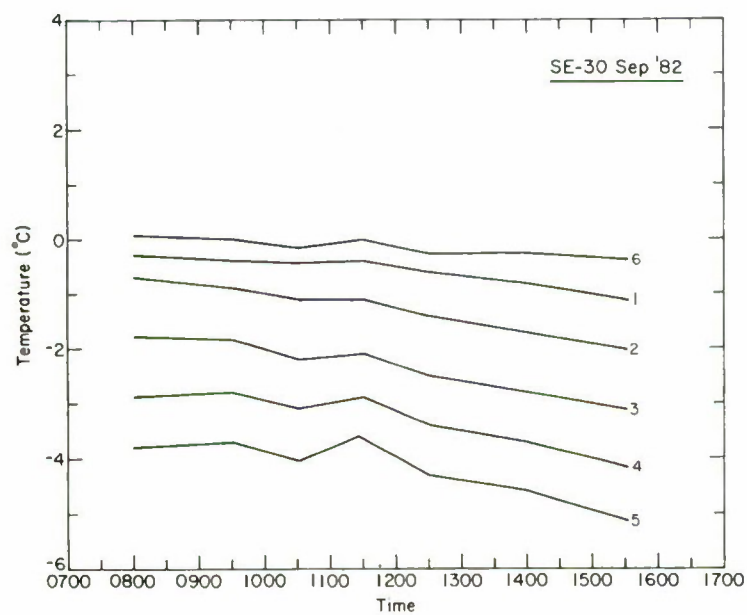
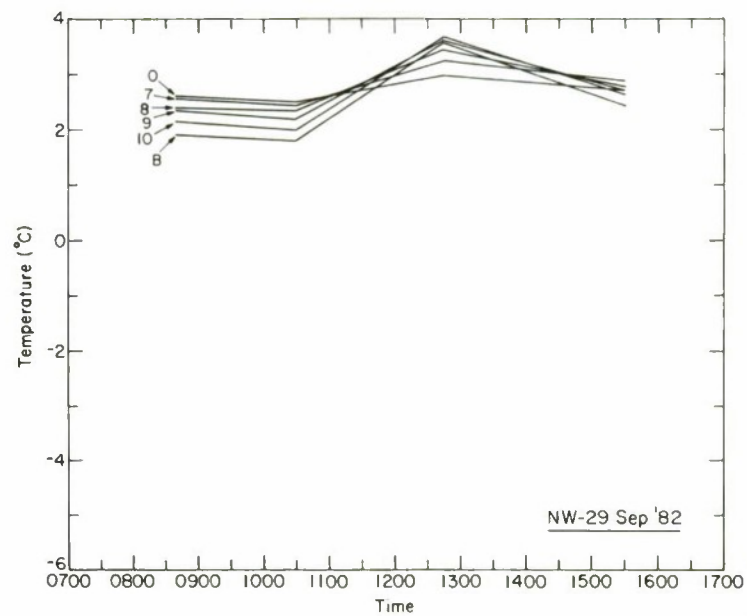
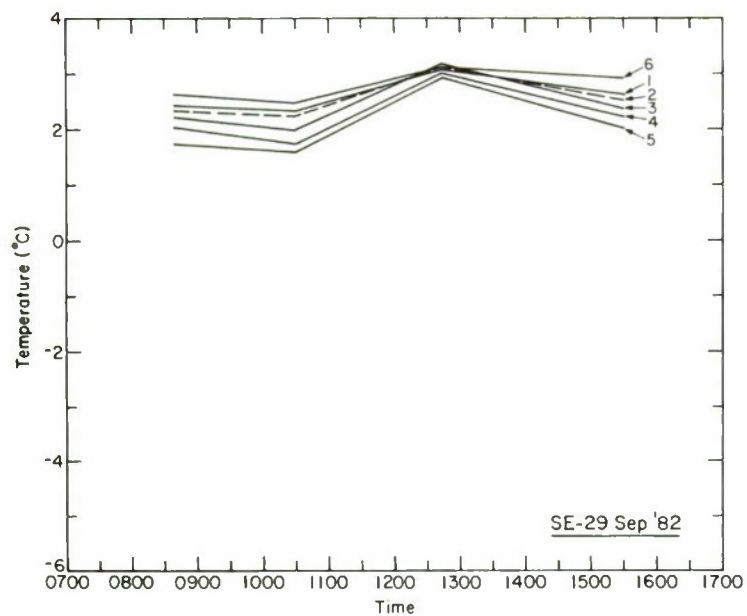
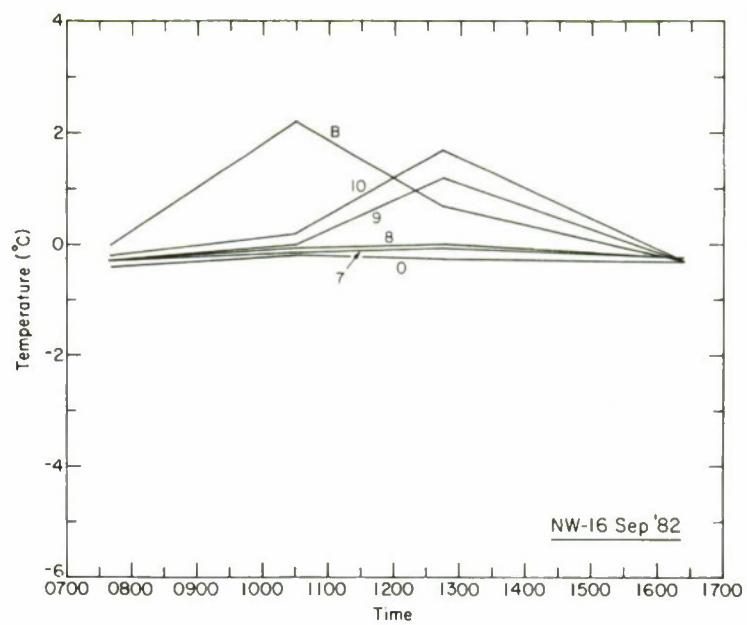
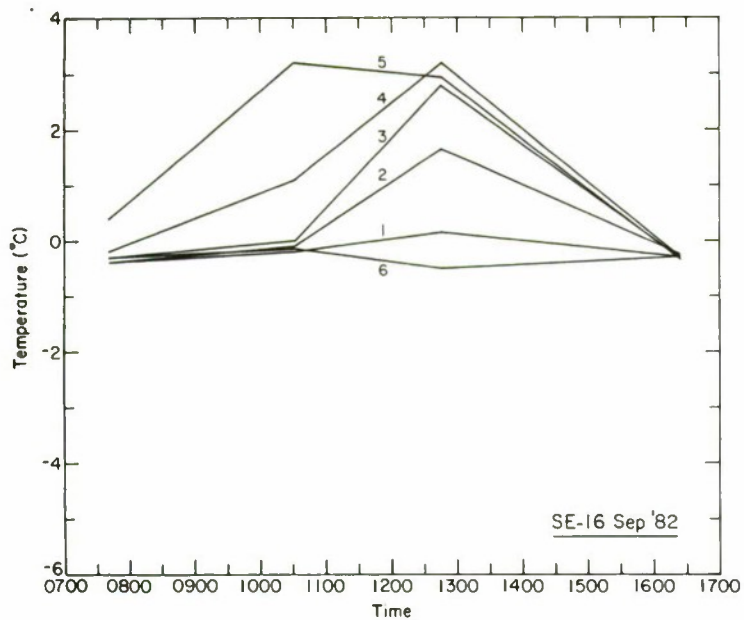
The thermocouple locations were as follows:

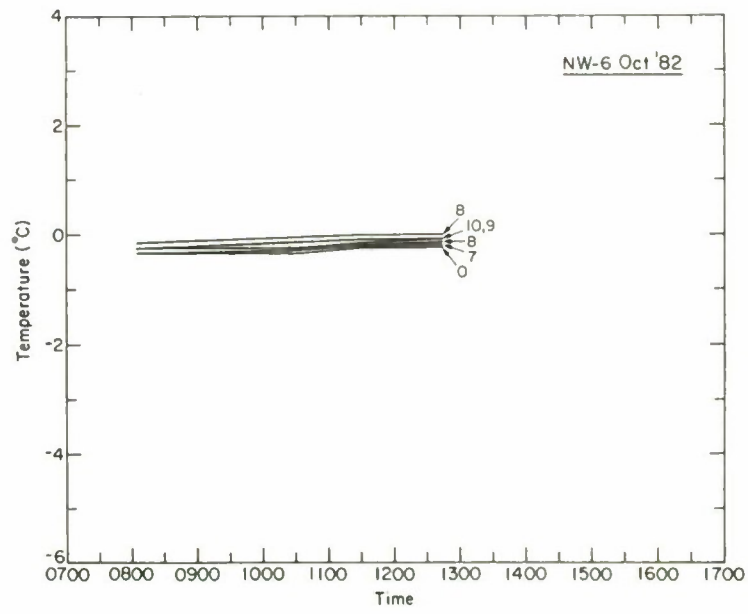
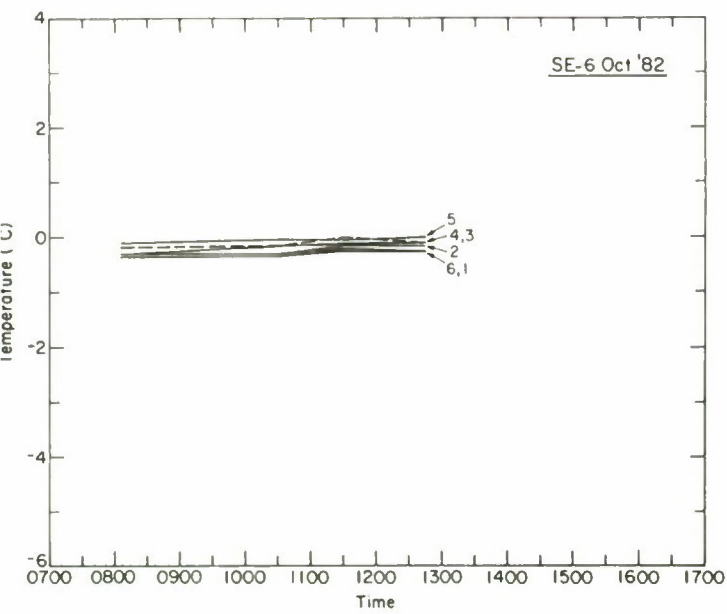
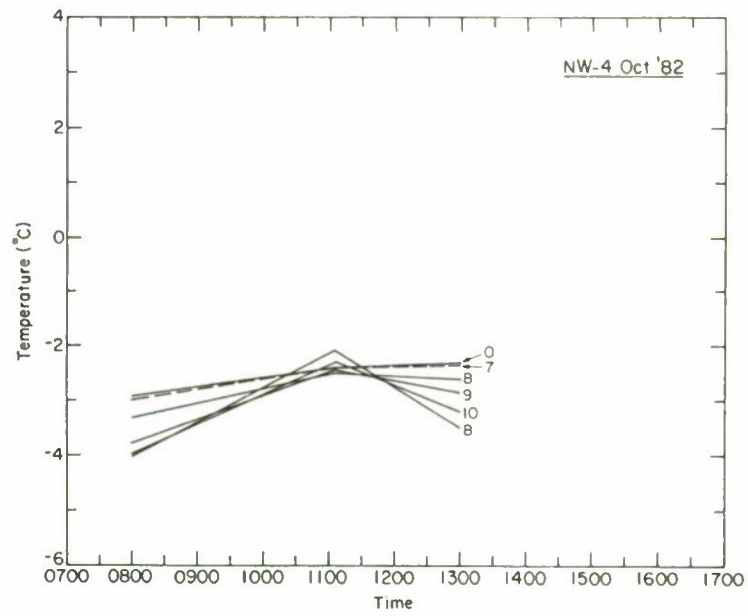
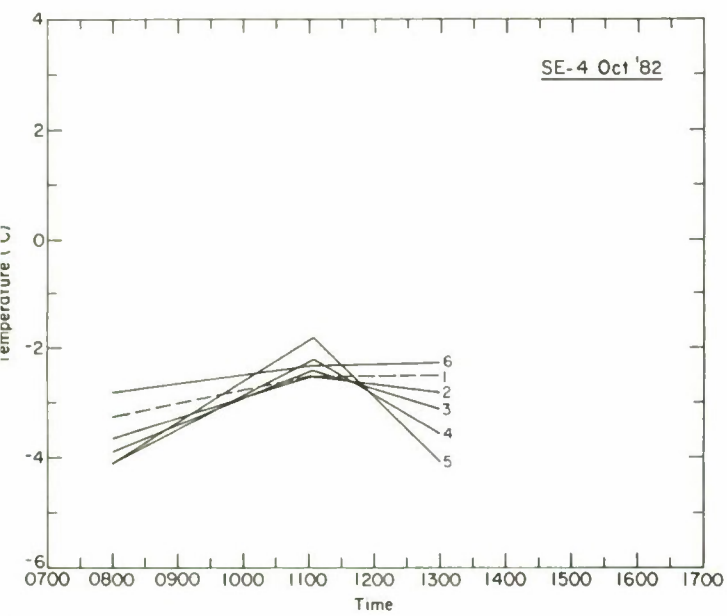
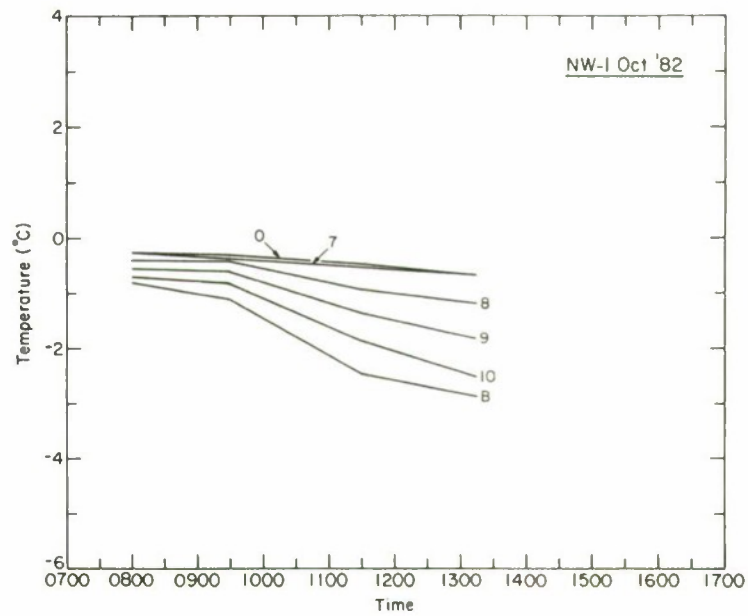
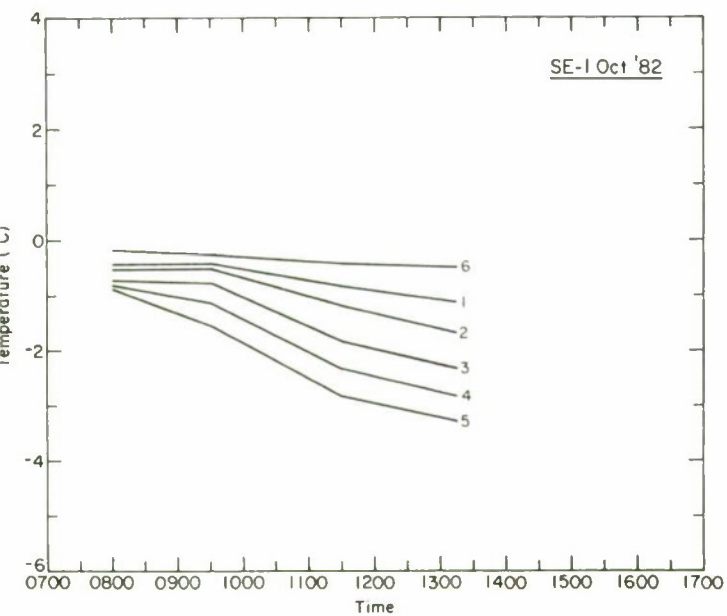
Thermocouple array position	Thermocouple number	Depth below the surface (cm)
Southeast	5	0-surface
	4	2.5
	3	5.0
	2	7.6
	1	10.2
	6	12.7
Northwest	B	0-surface
	10	2.5
	9	5.0
	8	7.6
	7	10.2
	0	12.7











APPENDIX D:

FROST DEPTH IN THE MEDIUM MEASURED BY FROST TUBES

The graphs in this appendix are depths of frost as determined by frost tube measurements. The locations of the frost tubes (Fig. 1 and 2) were as follows: no. 1 in the northeast corner, no. 2 in the northwest corner, no. 3 in the southwest corner, and no. 4 in the southeast corner. Where no data are plotted on a graph for a particular frost tube there was no frost indicated by the frost tube at that location. Only one reading was made on 10 September. Dowel measurements for 16 September will not correspond to frost tube measurements for reasons discussed in the Test Set-up and Procedures section. A brief discussion of the function of the frost tube can also be found in that section. A more in-depth discussion may be found in Ricard (1976).

